A thermodynamically consistent time integration scheme for non-linear thermo-electro-mechanics

M. Franke[◇1], R. Ortigosa[†2], J. Martínez-Frutos[†3], A. J. Gil[‡4], P. Betsch[◇]

† *Computational Mechanics and Scientific Computing Group,*
Technical University of Cartagena, Campus Muralla del Mar, 30202, Cartagena (Murcia), Spain
‡*Zienkiewicz Centre for Computational Engineering, College of Engineering*
Swansea University, Bay Campus, SA1 8EN, United Kingdom
◇*Institute of Mechanics, Karlsruhe Institute of Technology, 76131 Karlsruhe, Germany*

Abstract

The aim of this paper is the design of a new one-step implicit and thermodynamically consistent Energy-Momentum (EM) preserving time integration scheme for the simulation of thermo-electro-elastic processes undergoing large deformations. The time integration scheme takes advantage of the notion of polyconvexity and of a new tensor cross product algebra. These two ingredients are shown to be crucial for the design of so-called discrete derivatives fundamental for the calculation of the second Piola-Kirchhoff stress tensor, the entropy and the electric field. In particular, the exploitation of polyconvexity and the tensor cross product, enable the derivation of comparatively simple formulas for the discrete derivatives. This is in sharp contrast to much more elaborate discrete derivatives which are one of the main downsides of classical EM time integration schemes. The newly proposed scheme inherits the advantages of EM schemes recently published in the context of thermo-elasticity and electro-mechanics, whilst extending to the more generic case of nonlinear thermo-electro-mechanics. Furthermore, the manuscript delves into suitable convexity/concavity restrictions that thermo-electro-mechanical strain energy functions must comply with in order to yield physically and mathematically admissible solutions. Finally, a series of numerical examples will be presented in order to demonstrate robustness and numerical stability properties of the new EM scheme.

Keywords: finite element method, nonlinear thermo-electro-elastodynamics, energy-momentum scheme, tensor cross product, polyconvexity, dielectric elastomers, electro active polymers.

1. Introduction

Dielectric Elastomers (DEs) are a class of Electro Active Polymers (EAPs) that have demonstrated remarkable electrically induced actuation properties [22, 23, 33, 34]. These materials are particularly sensitive to changes of the thermal field, a property which often remains unconsidered [5, 13, 15, 19, 41, 45]. Nonetheless, a thermodynamically consistent framework for the simulation of EAPs under non-isothermal conditions was postulated in Reference [42]. In this connection, numerical studies have been recently published [26], considering thermo-visco-elastic behaviour of the material, excluding inertial effects.

The numerical simulation of these materials [19, 30, 31, 44–46] relies on the definition of a suitable constitutive model. In the purely isothermal case, it is customary to propose a frame-

---

[1]Corresponding author: marlon.franke@kit.edu@kit
[2]Corresponding author: r.ortigosa@swansea.ac.uk
[3]Corresponding author: jesus.martinez@upct.es
[4]Corresponding author: a.j.gil@swansea.ac.uk

indifferent representation of the enthalpy function, depending upon the deformation and the electric field. Other authors prefer to propose a constitutive model based on the invariant representation of the internal energy, depending upon the deformation and the electric displacement field. Motivated by the possible loss of ellipticity [1, 24] of the enthalpy function, Gil and Ortigosa [19, 30, 31] advocated for the use of the internal energy function for the definition of constitutive models in nonlinear electro-mechanics. In essence, the authors postulated a definition of the internal energy convex with respect to an extended set of arguments, namely the deformation gradient tensor $\boldsymbol{F}$, its co-factor $\boldsymbol{H}$, its Jacobian J, the Lagrangian electric displacement field $\boldsymbol{D}_0$ with $\boldsymbol{d} = \boldsymbol{F}\boldsymbol{D}_0$ and proved that this definition satisfies the ellipticity condition unconditionally. In the absence of electric effects, where the two last arguments vanish, the proposed definition coincides with the well-established concept of polyconvexity [1, 3, 4, 38, 43]. In the context of thermo-mechanics, Shilhavy [39] postulated the concept of polyconvexity by augmenting the multi-variable convex nature of the strain energy with respect to the entropy field in the deformed configuration. Recently, the authors in [11, 18] exploited the concept of polyconvex thermo-mechanics in the case of fast solid dynamics.

With regard to the finite element modelling of DEs, several formulations are available: most authors prefer a two-field formulation where the unknown fields are displacements and electric potential (scalar field) [15, 26, 41, 46]. This formulation is specially amenable when the preferred thermo-dynamical potential encapsulating the constitutive response of the material is the enthalpy function (depending upon the electric field). However, in our case, motivated by material stability considerations, we advocate for the internal energy function, which depends upon the electric displacement field. In this case, the two-field formulation requires to make use of the relation between both thermo-dynamical potentials through a Legendre transformation per Gauss point in order to obtain the later as a function of the electric field. This yields a possibly nonlinear equation per Gauss point solvable by means of the Newton-Raphson method. Alternative formulations, as the one presented in this paper, include the electric displacement field as an unknown. This formulation, pursued already in [17, 29], yields a three-field formulation whose computational effort depends on the continuity across finite elements of the additional vector field. In particular, the use of discontinuous interpolation for the electric displacement field permits to statically condense out these extra degrees of freedom, resulting in a formulation with a computational effort similar to that of classical two-field formulation. More sophisticated finite element formulations for the simulation of DEs can be found in [17], where additionally, strain measures and their conjugates are included as unknown fields. Use of discontinuous interpolations across elements of these, compliant with the *inf-sup* or LBB condition [12], permit to obtain computationally competitive formulations.

Although DEs, and in general, polymeric materials, exhibit temperature fluctuations due to the application of high electric fields, these are typically neglected, assuming an isothermal response. However, these thermal fluctuations can severely influence the deformation of the material and their dielectric properties. For instance, depending on the thermal expansion coefficient of the material, up to 5% volumetric changes have been reported in these materials [27]. In addition, a dielectric constant increase by more than 20 can be induced through heating in DEs [42].

Some authors [26, 27, 42] have incorporated thermal effects into the constitutive response of the material. In particular, above works considered the general case where the temperature field can induce not only changes in the deformation of the material (thermo-mechanical coupling) but also in the electric displacement field (thermo-electrical coupling). Furthermore, Reference [26] permitted the consideration of field dependent material properties by incorporating a dependency of the heat capacity and mechanical material parameters with respect to temperature and electric field. In the previous works [26, 27, 42], the entire isothermal electro-mechanical energy density is multiplied by a function depending upon the temperature field. Experimental evidence reveals that this model is suitable for the description of the constitutive response of DEs. In the

context of thermo-elasticity (i.e. electrical physics not considered), more simplified constitutive models [16] consider a more decoupled response where the total energy density of the material is additively decomposed into a purely isothermal part (depending upon strain), a purely thermal term (depending upon the temperature field exclusively) and a coupled term coupling the volumetric part of the deformation and the temperature field. In this work, we advocate for the latter model, extending it to the field of thermo-electro-mechanics. A simplification of this model lies in the fact that it does not contemplate interactions between the temperature field and the isothermal electro-mechanical contribution (thermo-electric coupling is ignored). It is important to emphasise that the EM scheme proposed on this paper does not restrict to a particular type of constitutive model, and although its stability properties have been tested by using the latter type of simplified consitutive models, the more realistic constitutive models previously described [26, 27, 42], which do contemplate the possibility for thermo-electric coupling, can be considered.

The advantage of EM time integration schemes is that they consistently reproduce the conservation properties such as total linear and angular momenta and total energy of the continuum system for the temporal discrete case. In particular, the term consistency in connection with EM schemes implies their ability to correctly preserve or dissipate the total energy of a system in agreement with the first laws of thermodynamics [7, 16, 21, 25]. The idea of EM schemes is to replace the exact partial derivatives of the strain energy (or other energy forms) with respect to its arguments with their carefully designed algorithmic counterparts, well known as discrete derivatives [7, 16, 20, 25, 29, 36, 40], which are formulated in compliance with the so-called directionality property [20].

In recent publications of the authors [7, 16] novel EM schemes are proposed in the context of nonlinear elasticity and thermo-elasticity. In particular in [7, 16] both the concept of polyconvexity [1–4, 37] and the use of a novel tensor cross product pioneered by de Boer [14] and re-discovered in the context of nonlinear continuum mechanics by Bonet et al. [8–10] have been employed and facilitate the design of the EM schemes. In essence, in [16] the consideration of four discrete derivatives which are used to form algorithmic versions of the second Piola-Kirchoff stress tensor and the entropy of the system. In addition to the discrete derivative with respect to the temperature, three further discrete derivatives are presented, which represent the algorithmic counterparts of the work conjugates of the right Cauchy-Green deformation tensor, its co-factor and its determinant. This strategy leads to simplified expressions of the algorithmic second Piola-Kirchoff stress tensor and entropy, when comparing against those obtained following the classical approach [20]. Furthermore, the work [7] was extended to multiphysics scenarios, such as thermo-elasticity [32] and to nonlinear electro-mechanics [17, 29]. The aim of the current paper is the development of a new polyconvexity inspired EM scheme for non-isothermal long-term simulations of DEs, assessing its superiority in terms of long-term stability with respect to other classical time integrators.

The paper is structured as follows: Section 2 briefly introduces some basic kinematics and the initial boundary value problem for thermo-electro-elastodynamics. Section 3 delves into mathematical requirements inherent to constitutive models in nonlinear thermo-electro-mechanics. In Section 4 the weak form of the whole system and conservation properties for the continuous system are presented. In Section 5 an one-step implicit EM time integrator scheme is introduced in order to obtain the semi-discrete system. The spatial discretization with the finite element method is shown in Section 6. Section 7 provides some static/time independent and some dynamic/time dependent numerical examples in order to validate the conservation properties and robustness of the proposed EM scheme. In Section 8 concluding remarks are drawn. Eventually Appendix A, Appendix B and Appendix C outline the definition of the discrete derivative expressions featuring in the proposed time integrator in Section 5.

2. Nonlinear continuum thermo-electro-mechanics

In the current section some basic kinematic relations and the initial boundary value problem (IBVP) for nonlinear continuum thermo-electro-elastodynamics are introduced.

2.1. Kinematics

Let $\mathcal{B}_0 \subset \mathbb{R}^3$ be an open, bounded and connected domain which represents the reference configuration of an elastic body. The deformation of the body $\mathcal{B}_0$ is defined through the mapping $\boldsymbol{\phi} : \mathcal{B}_0 \times [0, T] \to \mathbb{R}^3$, which is assumed to be sufficiently smooth, bijective and orientation preserving, and with $T \in \mathbb{R}^+$ the final time, namely $t \in [0, T]$. The mapping $\boldsymbol{\phi}$ links a material particle from the reference configuration $\boldsymbol{X} \in \mathcal{B}_0$ to a particle in the deformed configuration $\boldsymbol{x} \in \mathcal{B}$ according to $\boldsymbol{x} = \boldsymbol{\phi}(\boldsymbol{X}, t)$ and $\mathcal{B}(t) = \boldsymbol{\phi}(\mathcal{B}_0, t)$ (refer to Figure 1). Associated with the mapping $\boldsymbol{\phi}$, the deformation gradient $\boldsymbol{F}$ is defined as

$$\boldsymbol{F} : \mathcal{B}_0 \times [0, T] \to \mathbb{R}^{3\times 3}, \quad \boldsymbol{F} = \boldsymbol{\nabla}_0 \boldsymbol{\phi}(\boldsymbol{X}, t),$$

where $\boldsymbol{\nabla}_0$ represents the gradient with respect to the material coordinates $\boldsymbol{X}$. Associated with $\boldsymbol{F}$, its co-factor $\boldsymbol{H}$ and its Jacobian J are defined as

$$\boldsymbol{H} = (\det \boldsymbol{F}) \boldsymbol{F}^{-T} = \frac{1}{2} \boldsymbol{F} \times \boldsymbol{F}; \qquad J = \det \boldsymbol{F} = \frac{1}{6} (\boldsymbol{F} \times \boldsymbol{F}) : \boldsymbol{F}, \tag{1}$$

with $(\boldsymbol{A} \times \boldsymbol{B})_{iI} = \mathcal{E}_{ijk} \mathcal{E}_{IJK} A_{jJ} B_{kK}$, $\forall \boldsymbol{A}, \boldsymbol{B} \in \mathbb{R}^{3\times 3}$, where $\mathcal{E}_{ijk}$ (or $\mathcal{E}_{IJK}$) symbolises the third order alternating tensor components[5].
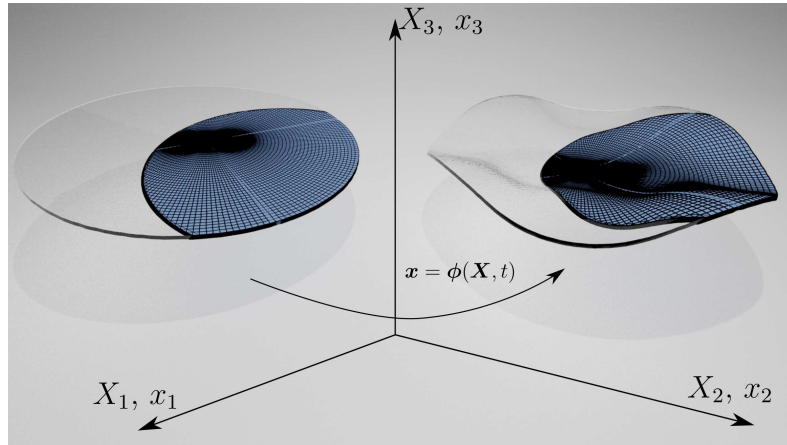
Figure 1: The mapping $\boldsymbol{\phi}$ relating points from the material configuration $\boldsymbol{X} \in \mathcal{B}_0$ with those in the deformed configuration $\boldsymbol{x} \in \mathcal{B}$.

2.2. Elastodynamics

The initial boundary value problem for elastodynamics is given by

$$\begin{aligned}
\rho_0 \dot{\boldsymbol{v}} - \mathrm{DIV}\,(\boldsymbol{F}\boldsymbol{S}) - \boldsymbol{f}_0 &= \boldsymbol{0}; && \text{in } \mathcal{B}_0 \times [0, T]\,; \\
(\boldsymbol{F}\boldsymbol{S})\,\boldsymbol{N} &= \boldsymbol{t}_0; && \text{on } \partial_t \mathcal{B}_0 \times [0, T]\,; \\
\boldsymbol{\phi}|_{t=0} &= \boldsymbol{\phi}_0; && \text{in } \mathcal{B}_0\,; \\
\dot{\boldsymbol{\phi}}\Big|_{t=0} &= \dot{\boldsymbol{\phi}}_0; && \text{in } \mathcal{B}_0\,; \\
\boldsymbol{\phi} &= \bar{\boldsymbol{\phi}}; && \text{on } \partial_\phi \mathcal{B}_0 \times [0, T]\,.
\end{aligned} \tag{2}$$

---

[5]The use of repeated indices implies summation, unless otherwise stated. In addition, lower case and capital case indices $\{i, j, k\}$ and $\{I, J, K\}$ will be used to represent the deformed and reference configurations, respectively.

Therein $(\mathrm{DIV}(\boldsymbol{A}))_i = \partial_{X_I} A_{iI}$ and $(\dot{\bullet}) := \frac{d(\bullet)}{dt}$ denotes differentiation with respect to time. Furthermore, in (2) $\rho_0 : \mathcal{B}_0 \to \mathbb{R}^+$ denotes the mass density of the continuum body with respect to the reference configuration, $\boldsymbol{v} : \mathcal{B}_0 \times [0, T] \to \mathbb{R}^3$ the velocity field, $\boldsymbol{f}_0$ represents a body force per unit undeformed volume $\mathcal{B}_0$ and $\boldsymbol{t}_0$, the traction force per unit undeformed area applied on $\partial_t \mathcal{B}_0 \subset \partial \mathcal{B}_0$ where $\partial_t \mathcal{B}_0 \cup \partial_\phi \mathcal{B}_0 = \partial \mathcal{B}_0$ and $\partial_t \mathcal{B}_0 \cap \partial_\phi \mathcal{B}_0 = \emptyset$. Local conservation of angular momentum leads to symmetry of the second Piola-Kirchhoff stress tensor $\boldsymbol{S}$, such that $\boldsymbol{S} = \boldsymbol{S}^T$.

2.3. Electrostatics

In the electrostatics case considered, the local form of Gauss's law can be written in a Lagrangian setting as

$$
\begin{aligned}
\mathrm{DIV}\boldsymbol{D}_0 - \rho_0^e &= 0; & &\text{in } \mathcal{B}_0 \times [0, T] \\
\boldsymbol{D}_0 \cdot \boldsymbol{N} &= -\omega_0^e; & &\text{on } \partial_\omega \mathcal{B}_0 \times [0, T].
\end{aligned}
\tag{3}
$$

Therein $\boldsymbol{D}_0$ is the Lagrangian electric displacement vector, ρ_0^e represents an electric volume charge per unit of undeformed volume $\mathcal{B}_0$ and ω_0^e, the electric surface charge per unit of undeformed area $\partial_\omega \mathcal{B}_0 \subset \partial \mathcal{B}_0$. Furthermore, Faraday's law can be written in a Lagrangian setting as

$$
\begin{aligned}
\boldsymbol{E}_0 &= -\boldsymbol{\nabla}_0 \varphi; & &\text{in } \mathcal{B}_0 \times [0, T]; \\
\varphi &= \bar{\varphi}; & &\text{on } \partial_\varphi \mathcal{B}_0 \times [0, T].
\end{aligned}
\tag{4}
$$

In the above (4) $\boldsymbol{E}_0$ is the Lagrangian electric field vector and φ, the scalar electric potential. Furthermore, $\partial_\varphi \mathcal{B}_0 \subset \partial \mathcal{B}_0$ represents the part of the boundary where essential electric potential boundary conditions are applied such that $\partial_\omega \mathcal{B}_0 \cup \partial_\varphi \mathcal{B}_0 = \partial \mathcal{B}_0$ and $\partial_\omega \mathcal{B}_0 \cap \partial_\varphi \mathcal{B}_0 = \emptyset$.

2.4. Thermodynamics

The IBVP for thermodynamics can be stated as

$$
\begin{aligned}
\theta \dot{\eta} + \mathrm{DIV}\boldsymbol{Q} - R_\theta &= 0; & &\text{in } \mathcal{B}_0 \times [0, T]; \\
\boldsymbol{Q} \cdot \boldsymbol{N} &= -Q_\theta; & &\text{on } \partial_Q \mathcal{B}_0 \times [0, T]; \\
\theta|_{t=0} &= \theta_0; & &\text{in } \mathcal{B}_0; \\
\theta &= \bar{\theta}; & &\text{on } \partial_\theta \mathcal{B}_0 \times [0, T].
\end{aligned}
\tag{5}
$$

Therein θ denotes the absolute temperature field, η the entropy density and $\boldsymbol{Q}$ heat flux per unit undeformed volume $\mathcal{B}_0$, respectively. Furthermore, R_θ and Q_θ represent a heat source per unit undeformed volume $\mathcal{B}_0$ and the rate of heat transfer across the unit undeformed area applied on $\partial_Q \mathcal{B}_0 \subset \partial \mathcal{B}_0$, respectively. With $(5)_d$ essential temperature boundary conditions are applied on $\partial_\theta \mathcal{B}_0 \subset \partial \mathcal{B}_0$. The boundaries in (5) need to satisfy $\partial_Q \mathcal{B}_0 \cup \partial_\theta \mathcal{B}_0 = \partial \mathcal{B}_0$ and $\partial_Q \mathcal{B}_0 \cap \partial_\theta \mathcal{B}_0 = \emptyset$, respectively. With the aim of simplifying the time discretisation of (5), the authors in [32] proposed an alternative but equivalent re-expression at the continuum level to that in (5) as

$$
\begin{aligned}
\frac{d}{dt}(\theta \eta) - \dot{\theta} \eta + \mathrm{DIV}\boldsymbol{Q} - R_\theta &= 0; & &\text{in } \mathcal{B}_0 \times [0, T]; \\
\boldsymbol{Q} \cdot \boldsymbol{N} &= -Q_\theta; & &\text{on } \partial_Q \mathcal{B}_0 \times [0, T]; \\
\theta|_{t=0} &= \theta_0; & &\text{in } \mathcal{B}_0; \\
\theta &= \bar{\theta}; & &\text{on } \partial_\theta \mathcal{B}_0 \times [0, T].
\end{aligned}
\tag{6}
$$

In this work we will advocate for (6) in order to derive the new EM time integrator in the context of thermo-electro-mechanics.

3. Constitutive equations in nonlinear thermo-electro-elasticity

In this section the consideration is supplemented by means of suitable constitutive laws in thermo-electro-elasticity. In this connection some notions on constitutive laws are presented.

3.1. The energy density function

In the following we will present the specific form of the energy density function encapsulating the constitutive coupled thermo-electro-mechanical response of the continuum $\mathcal{B}_0$, paying special attention to the mathematical/physical constraints that energy density function needs to comply with.

In this work, we consider a simplified constitutive model where the purely isothermal electro-mechanical contribution does not interact with the temperature field, i.e. no thermo-electrical coupling is considered. The more generic case including the latter effect is described in Remark 3.

3.1.1. The enthalpy function

It is costumary to define the coupled thermo-electro-mechanical response of the solid $\mathcal{B}_0$ in terms of an invariant-based representation of the enthalpy Ψ per unit undeformed volume, defined as

$$\Psi = \Psi(\boldsymbol{F}, \boldsymbol{E}_0, \theta) : \mathbb{R}^{3 \times 3} \times \mathbb{R}^3 \times \mathbb{R}^+ \to \mathbb{R}. \tag{7}$$

The requirement of objectivity implies that Ψ should be expressable in terms of the right Cauchy-Green deformation tensor, namely

$$\Psi(\boldsymbol{F}, \boldsymbol{E}_0, \theta) = \widetilde{\Psi}(\boldsymbol{C}, \boldsymbol{E}_0, \theta); \qquad \boldsymbol{C} = \boldsymbol{F}^T \boldsymbol{F}. \tag{8}$$

The second law of thermodynamics in the absence of internal state variables leads to[6]

$$D\widetilde{\Psi}[\delta \boldsymbol{F}] = \boldsymbol{S} : \frac{1}{2} D\boldsymbol{C}[\delta \boldsymbol{F}]; \qquad D\widetilde{\Psi}[\delta \boldsymbol{E}_0] = -\boldsymbol{D}_0 \cdot \delta \boldsymbol{E}_0; \qquad D\widetilde{\Psi}[\delta \theta] = -\eta \delta \theta, \tag{9}$$

where the second Piola-Kirchhoff stress tensor $\boldsymbol{S}$, the Lagrangian electric displacement field $\boldsymbol{D}_0$ and the material entropy η are defined in terms of the derivatives of $\widetilde{\Psi}(\boldsymbol{C}, \boldsymbol{E}_0, \theta)$, namely

$$\boldsymbol{S} = 2\partial_{\boldsymbol{C}}\widetilde{\Psi}; \qquad \boldsymbol{D}_0 = -\partial_{\boldsymbol{E}_0}\widetilde{\Psi}; \qquad \eta = -\partial_\theta \widetilde{\Psi}. \tag{10}$$

More generally, we will consider energy density functions $\widetilde{\Psi}(\boldsymbol{C}, \boldsymbol{E}_0, \theta)$ which admit an equivalent extended representation in terms of the symmetric kinematic measures $\{\boldsymbol{C}, \boldsymbol{G}, C\}$, with $\boldsymbol{G}$ and C being the co-factor and determinant of $\boldsymbol{C}$, namely

$$\Psi(\boldsymbol{F}, \boldsymbol{E}_0, \theta) = \widetilde{\Psi}(\boldsymbol{C}, \boldsymbol{E}_0, \theta) = \widehat{\Psi}(\boldsymbol{C}, \boldsymbol{G}, C, \boldsymbol{E}_0, \theta), \tag{11}$$

with

$$\boldsymbol{G} = (\det \boldsymbol{C})\boldsymbol{C}^{-1} = \frac{1}{2}\boldsymbol{C} \times \boldsymbol{C}; \qquad C = \det \boldsymbol{C} = \frac{1}{6}(\boldsymbol{C} \times \boldsymbol{C}) : \boldsymbol{C}. \tag{12}$$

Proceeding as in (9) but making use of the chain rule and the definitions of $\boldsymbol{C}$ and C in (12), it is possible to relate $\boldsymbol{S}$, $\boldsymbol{D}_0$ and the entropy field η with the derivatives of the extended representation $\widehat{\Psi}(\boldsymbol{C}, \boldsymbol{G}, C, \boldsymbol{E}_0, \theta)$ as

$$\boldsymbol{S} = 2\partial_{\boldsymbol{C}}\widehat{\Psi} + 2\partial_{\boldsymbol{G}}\widehat{\Psi} \times \boldsymbol{C} + 2\partial_C\widehat{\Psi}\boldsymbol{G}; \qquad \boldsymbol{D}_0 = -\partial_{\boldsymbol{E}_0}\widehat{\Psi}; \qquad \eta = -\partial_\theta \widehat{\Psi}. \tag{13}$$

In this work it is assumed that the enthalpy function $\Psi(\boldsymbol{F}, \boldsymbol{E}_0, \theta)$ satisfies the following conditions

$$(\boldsymbol{u} \otimes \boldsymbol{V}) : \partial^2_{\boldsymbol{FF}}\Psi : (\boldsymbol{u} \otimes \boldsymbol{V}) > 0; \qquad \boldsymbol{V} \cdot (\partial^2_{\boldsymbol{E}_0\boldsymbol{E}_0}\Psi)\boldsymbol{V} < 0; \qquad \partial^2_{\theta\theta}\Psi < 0, \tag{14}$$

$\forall \boldsymbol{u}, \boldsymbol{V} \in \mathbb{R}^3$. The first two conditions in (14) ensure that material stability is guaranteed [28], namely, perturbations according to the following ansatz $\Delta\boldsymbol{\phi} = \boldsymbol{u}\mathcal{G}(\boldsymbol{X} \cdot \boldsymbol{V} - c_\alpha t)$ and $\Delta\varphi =$

---

[6]$Df(x)[y]$ represents the directional derivative of $f(x)$ with respect to y, namely $Df(x)[y] = \lim_{\varepsilon \to 0} f(x + \varepsilon y)$.

$b\mathcal{F}(\boldsymbol{X} \cdot \boldsymbol{V} - c_\alpha t)$ admit real solutions for the speed of propagation c_α of the perturbations (cf. [37]). Therein $\boldsymbol{u}$ and b denote the polarization vector/scalar, $\mathcal{G}$ and $\mathcal{F}$ denote the traveling wave ansatz for fields $\boldsymbol{\phi}$ and φ, respectively and $\boldsymbol{V}$ denotes the referential direction of wave propagation. Finally, the last condition $(14)_c$ permits to guarantee that the heat capacity of the material is positive (see Remark 1 below).

3.1.2. Volumetric-deviatoric constitutive model

Condition $(14)_c$, namely, concavity of the enthalpy function with respect to the temperature field θ, permits to establish a one-to-one and invertible relationship between the latter and the material entropy η through the following Legendre transformation

$$\widehat{U}(\boldsymbol{C}, \boldsymbol{G}, C, \boldsymbol{E}_0, \eta) = \sup_\theta \{\widehat{\Psi}(\boldsymbol{C}, \boldsymbol{G}, C, \boldsymbol{E}_0, \theta) + \eta\theta\}. \tag{15}$$

Notice that the function $\widehat{U}(\boldsymbol{C}, \boldsymbol{G}, C, \boldsymbol{E}_0, \eta)$ in (15) can be re-expressed as a function of θ as

$$\hat{U}(\boldsymbol{C}, \boldsymbol{G}, C, \boldsymbol{E}_0, \theta) = \widehat{U}(\boldsymbol{C}, \boldsymbol{G}, C, \boldsymbol{E}_0, \eta(\boldsymbol{C}, \boldsymbol{G}, C, \theta, \boldsymbol{E}_0)). \tag{16}$$

Calorimetry principles permit to experimentally measure the change of internal energy as a function of the temperature, yielding

$$\partial_\theta \hat{U} = c_{\boldsymbol{C}, \boldsymbol{E}_0}(\theta), \tag{17}$$

with $c_{\boldsymbol{C}, \boldsymbol{E}_0}(\theta)$ the heat capacity at constant strain and electric field. In the sequel, a constant heat capacity will be assumed for simplicity, denoting it as c_0. Notice that (17) can be conveniently re-written as

$$\partial_\theta \hat{U} = \partial_\eta \widehat{U}\, \partial_\theta \eta = \theta \partial_\theta \eta = c_{\boldsymbol{C}, \boldsymbol{E}_0}(\theta) = c_0 \Rightarrow \partial_\theta \eta = \frac{c_0}{\theta}. \tag{18}$$

Integration of (18) twice with respect to the temperature field (see Reference [32]) yields

$$\widehat{\Psi}(\boldsymbol{C}, \boldsymbol{G}, C, \boldsymbol{E}_0, \theta) = \widehat{\Psi}_{em}(\boldsymbol{C}, \boldsymbol{G}, C, \boldsymbol{E}_0) - \eta_R(\boldsymbol{C}, \boldsymbol{G}, C)(\theta - \theta_R) + \widehat{\Psi}_\theta(\theta);$$
$$\widehat{\Psi}_\theta(\theta) = c_0 \left(\theta - \theta_R - \theta \ln \frac{\theta}{\theta_R}\right), \tag{19}$$

where $\eta_R(\boldsymbol{C}, \boldsymbol{G}, C, \boldsymbol{E}_0)$ represents the reference entropy, depending exclusively upon the deformation. In this paper, we consider a volumetric-type thermo-mechanical coupling. Hence, $\eta_R := \eta_R(\boldsymbol{C}, \boldsymbol{G}, C)$ is particularised to depend exclusively upon C, namely $\eta_R = \widehat{\eta}_R(C)$. Specifically, $\widehat{\eta}_R(C)$ will adopt in this paper the following expression (cf. [16])

$$\widehat{\eta}_R(C) = 3\beta e\,(C - 1), \tag{20}$$

with β and e (positive) material parameters. Therefore, the final additive form of $\widehat{\Psi}(\boldsymbol{C}, \boldsymbol{G}, C, \boldsymbol{E}_0, \theta)$ is (cf. [16])

$$\widehat{\Psi}(\boldsymbol{C}, \boldsymbol{G}, C, \boldsymbol{E}_0, \theta) = \widehat{\Psi}_{em}(\boldsymbol{C}, \boldsymbol{G}, C, \boldsymbol{E}_0) + \widehat{\Psi}_{tm}(C, \theta) + \widehat{\Psi}_\theta(\theta); \qquad \widehat{\Psi}_{tm}(C, \theta) = -\widehat{\eta}_R(C)(\theta - \theta_R). \tag{21}$$

Remark 1. *The specific form of the purely thermal function $\widehat{\Psi}_\theta(\theta)$ in (19) and (20) yields*

$$\partial^2_{\theta\theta} \widehat{\Psi}(\theta) = \partial^2_{\theta\theta} \widehat{\Psi}_\theta(\theta) = -c_0. \tag{22}$$

Therefore, the concavity of the enthalpy function $\widehat{\Psi}(\boldsymbol{C}, \boldsymbol{G}, C, \boldsymbol{E}_0, \theta)$ in (14) entails the physical requirement of the specific heat capacity c_0 being a positive number.

Remark 2. *In this work we consider the thermo-mechanical contribution defined in* (19) *and* (20), *recast here for convenience, i.e.*

$$\Psi_{tm}(J,\theta) = -\eta_R(J)\,(\theta - \theta_R)\,; \qquad \eta_R(J) = 3\beta e(J^2 - 1). \tag{23}$$

The previous energetic contribution can be compared against that in Reference [42], defined as

$$\Psi_{tm}^V(J,\theta) = -3\alpha\kappa_0\frac{J^\xi - 1}{\xi}, \tag{24}$$

where κ_0 represents the bulk modulus in the origin of deformations (i.e. $\boldsymbol{F} = \boldsymbol{I}$, with $\boldsymbol{I}$ the second order identity tensor), α, the thermal expansion coefficient and ξ, a dimensionless constant material parameter. In above expression (24) *we have used the superscript V to differentiate it from that in* (23). *The volumetric stress generated by both energetic contributions is defined as*

$$\boldsymbol{P}_{tm} = \partial_J\Psi_{tm}\boldsymbol{H} = -6\beta eJ\boldsymbol{H}; \qquad \boldsymbol{P}_{tm}^V = \partial_J\Psi_{tm}^V\boldsymbol{H} = -3\alpha\kappa_0 J^{\xi-1}\boldsymbol{H}. \tag{25}$$

Evaluation of both expressions $\boldsymbol{P}_{tm}$ and $\boldsymbol{P}_{tm}^V$ in (25) *in the origin ($\boldsymbol{H} = \boldsymbol{I}$ and $J = 1$) permits to relate the coefficients β and e featuring in the thermo-mechanical contribution chosen in this work with the thermal expansion coefficient α as*

$$\beta e = \frac{\alpha\kappa_0}{2}. \tag{26}$$

3.1.3. The internal energy function

The definition of enthalpy density functions $\widehat{\Psi}(\boldsymbol{C}, \boldsymbol{G}, C, \boldsymbol{E}_0, \theta)$ as in (21) *ab-initio* complying simultaneously with the convexity and concavity conditions in (14) is a non-trivial endeavor. Instead, a more amenable energy function, denoted as $\widehat{W}(\boldsymbol{C}, \boldsymbol{G}, C, \boldsymbol{D}_0, \theta)$, depending upon $\boldsymbol{D}_0$ instead of $\boldsymbol{E}_0$, is introduced in order to facilitate the fulfillment of the convexity/concavity constraints on $\widehat{\Psi}(\boldsymbol{C}, \boldsymbol{G}, C, \boldsymbol{E}_0, \theta)$. For the specific volumetric-deviatoric thermo-electro-mechanical model considered in the previous section, $\widehat{W}(\boldsymbol{C}, \boldsymbol{G}, C, \boldsymbol{D}_0, \theta)$ adopts a similar decomposition as $\widehat{\Psi}(\boldsymbol{C}, \boldsymbol{G}, C, \boldsymbol{E}_0, \theta)$ in (21), namely

$$\widehat{W}(\boldsymbol{C}, \boldsymbol{G}, C, \boldsymbol{D}_0, \theta) = \widehat{W}_{em}(\boldsymbol{C}, \boldsymbol{G}, C, \boldsymbol{D}_0) + \widehat{W}_{tm}(C, \theta) + \widehat{W}_\theta(\theta);$$
$$\widehat{W}_{tm}(C, \theta) = \widehat{\Psi}_{tm}(C, \theta); \qquad \widehat{W}_\theta(\theta) = \widehat{\Psi}_\theta(\theta)\,, \tag{27}$$

where the coupled isothermal electro-mechanical contributions $\widehat{\Psi}_{em}(\boldsymbol{C}, \boldsymbol{G}, C, \boldsymbol{E}_0)$ in equation (21) and $\widehat{W}_{em}(\boldsymbol{C}, \boldsymbol{G}, C, \boldsymbol{D}_0)$ above are related through the following Legendre transformation[7], i.e.

$$\widehat{\Psi}_{em}(\boldsymbol{C}, \boldsymbol{G}, C, \boldsymbol{E}_0) = \min_{\boldsymbol{D}_0}\{\widehat{W}_{em}(\boldsymbol{C}, \boldsymbol{G}, C, \boldsymbol{D}_0) - \boldsymbol{E}_0 \cdot \boldsymbol{D}_0\}. \tag{28}$$

A possible example for $\widehat{W}_{em}(\boldsymbol{C}, \boldsymbol{G}, C, \boldsymbol{D}_0)$, widely used by the authors in [19, 31] is

$$\widehat{W}_{em}(\boldsymbol{C}, \boldsymbol{G}, C, \boldsymbol{D}_0) = \frac{\mu_1}{2}\mathrm{tr}(\boldsymbol{C}) + \frac{\mu_2}{2}\mathrm{tr}(\boldsymbol{G}) - (\mu_1 + 2\mu_2)\log C^{1/2} + \frac{\lambda}{2}\left(C^{1/2} - 1\right)^2$$
$$+ \frac{1}{2\varepsilon_1}II_{\boldsymbol{D}_0} + \frac{1}{2\varepsilon_2}\boldsymbol{D}_0 \cdot \boldsymbol{C}\boldsymbol{D}_0, \tag{29}$$

---

[7]Note that this Legendre transformation can only exist provided that $\widehat{W}(\boldsymbol{C}, \boldsymbol{G}, C, \boldsymbol{D}_0, \theta)$ is convex with respect to $\boldsymbol{D}_0$, which will be the case for the energy proposed in this paper.

where $II_{\boldsymbol{a}} = \boldsymbol{a} \cdot \boldsymbol{a}$, $\forall \mathbf{a} \in \mathbb{R}^3$, $II_{\boldsymbol{A}} = \boldsymbol{A} : \boldsymbol{A}$ and $\{\mu_1, \mu_2, \lambda\}$ are positive material parameters related to the shear and bulk moduli of the material in the origin (when $\boldsymbol{\nabla}_0 \boldsymbol{\phi} = \boldsymbol{I}$, $\boldsymbol{D}_0 = \boldsymbol{0}$ and $\theta = \theta_R$), namely $\{\mu_R, \lambda_R\}$ as

$$\mu_R = \mu_1 + \mu_2; \qquad \lambda_R = \lambda + 2\mu_2. \tag{30}$$

Furthermore, ε_1 and ε_2 are electric permittivity parameters. Crucially, notice that $\widehat{W}_{em}(\boldsymbol{C}, \boldsymbol{G}, C, \boldsymbol{D}_0)$ is polyconvex in the isothermal electro-mechanical context, namely, it can be written as a convex multi-variable energy function, i.e.

$$\widehat{W}_{em}(\boldsymbol{C}, \boldsymbol{G}, C, \boldsymbol{D}_0) = \hat{W}_{em}(\boldsymbol{\mathcal{V}}); \qquad \boldsymbol{\mathcal{V}} = \{\boldsymbol{F}, \boldsymbol{H}, J, \boldsymbol{D}_0, \boldsymbol{d}\}; \qquad \boldsymbol{d} = \boldsymbol{F}\boldsymbol{D}_0, \tag{31}$$

with $\hat{W}_{em}(\boldsymbol{\mathcal{V}})$ as

$$\hat{W}_{em}(\boldsymbol{\mathcal{V}}) = \frac{\mu_1}{2} II_{\boldsymbol{F}} + \frac{\mu_2}{2} II_{\boldsymbol{H}} - (\mu_1 + 2\mu_2) \log J + \frac{\lambda}{2} (J-1)^2 + \frac{1}{2\varepsilon_1} II_{\boldsymbol{D}_0} + \frac{1}{2\varepsilon_2} II_{\boldsymbol{d}}, \tag{32}$$

It is easy to verify that $\hat{W}_{em}(\boldsymbol{\mathcal{V}})$ (32) is indeed polyconvex, namely, the following condition is satisfied[8]

$$\delta \boldsymbol{\mathcal{V}} : [\mathbb{H}_{\hat{W}_{em}}] : \delta \boldsymbol{\mathcal{V}} > 0, \ \forall \delta \boldsymbol{\mathcal{V}}, \tag{33}$$

where $[\mathbb{H}_{\hat{W}_{em}}]$ denotes the (positive definite) Hessian operator of $\hat{W}_{em}(\boldsymbol{\mathcal{V}})$, namely

$$[\mathbb{H}_{\hat{W}_{em}}] = \begin{bmatrix} \partial^2_{\boldsymbol{F}\boldsymbol{F}} \hat{W}_{em} & \partial^2_{\boldsymbol{F}\boldsymbol{H}} \hat{W}_{em} & \partial^2_{\boldsymbol{F}J} \hat{W}_{em} & \partial^2_{\boldsymbol{F}\boldsymbol{D}_0} \hat{W}_{em} & \partial^2_{\boldsymbol{F}\boldsymbol{d}} \hat{W}_{em} \\ \partial^2_{\boldsymbol{H}\boldsymbol{F}} \hat{W}_{em} & \partial^2_{\boldsymbol{H}\boldsymbol{H}} \hat{W}_{em} & \partial^2_{\boldsymbol{H}J} \hat{W}_{em} & \partial^2_{\boldsymbol{H}\boldsymbol{D}_0} \hat{W}_{em} & \partial^2_{\boldsymbol{H}\boldsymbol{d}} \hat{W}_{em} \\ \partial^2_{J\boldsymbol{F}} \hat{W}_{em} & \partial^2_{J\boldsymbol{H}} \hat{W}_{em} & \partial^2_{JJ} \hat{W}_{em} & \partial^2_{J\boldsymbol{D}_0} \hat{W}_{em} & \partial^2_{J\boldsymbol{d}} \hat{W}_{em} \\ \partial^2_{\boldsymbol{D}_0\boldsymbol{F}} \hat{W}_{em} & \partial^2_{\boldsymbol{D}_0\boldsymbol{H}} \hat{W}_{em} & \partial^2_{\boldsymbol{D}_0 J} \hat{W}_{em} & \partial^2_{\boldsymbol{D}_0\boldsymbol{D}_0} \hat{W}_{em} & \partial^2_{\boldsymbol{D}_0\boldsymbol{d}} \hat{W}_{em} \\ \partial^2_{\boldsymbol{d}\boldsymbol{F}} \hat{W}_{em} & \partial^2_{\boldsymbol{d}\boldsymbol{H}} \hat{W}_{em} & \partial^2_{\boldsymbol{d}J} \hat{W}_{em} & \partial^2_{\boldsymbol{d}\boldsymbol{D}_0} \hat{W}_{em} & \partial^2_{\boldsymbol{d}\boldsymbol{d}} \hat{W}_{em} \end{bmatrix}. \tag{34}$$

Unfortunately, the term $\widehat{W}_{tm}(C, \theta)$ in (27) is not convex with respect to J, namely

$$\hat{W}_{tm}(J, \theta) = \widehat{W}_{tm}(C, \theta); \qquad \partial^2_{JJ} \hat{W}_{tm} \not> 0, \quad \forall J, \forall \theta > 0. \tag{35}$$

However, the purely isothermal part $\widehat{W}_{em}(\boldsymbol{C}, \boldsymbol{G}, C, \boldsymbol{D}_0) = \hat{W}_{em}(\boldsymbol{\mathcal{V}})$ in equation (29) also depends on J. Therefore, it is the positiveness of the second derivative of both contributions $\hat{W}_{em}(\boldsymbol{\mathcal{V}})$ and $\hat{W}_{tm}(J, \theta)$ (for a fixed temperature) together that needs to be checked in order to verify when polyconvexity with respect to $\boldsymbol{\mathcal{V}}$ of the complete function $\widehat{W}(\boldsymbol{C}, \boldsymbol{G}, C, \boldsymbol{D}_0, \theta) = \hat{W}(\boldsymbol{\mathcal{V}}, \theta)$ is compromised. The latter yields

$$\partial^2 \hat{W}_{JJ} = \partial^2_{JJ}\left(\hat{W}_{em} + \hat{W}_{tm}\right) = \frac{\mu_1 + 2\mu_2}{J^2} + \lambda - 6\beta e (\theta - \theta_R). \tag{36}$$

The critical value of θ beyond which $\partial^2_{JJ} \hat{W} > 0$ is compromised can be obtained then from (36), yielding

$$\theta_{cr} = \theta_R \left(1 + \frac{\frac{\mu_1 + 2\mu_2}{J^2} + \lambda}{6\beta e \theta_R}\right). \tag{37}$$

Therefore, provided that the temperature field θ never exceeds the bound in equation (37), the complete energy function $\widehat{W}(\boldsymbol{C}, \boldsymbol{G}, C, \boldsymbol{D}_0, \theta) = \hat{W}(\boldsymbol{\mathcal{V}}, \theta)$ in (29) would be polyconvex with respect to $\boldsymbol{\mathcal{V}}$, namely

$$\delta \boldsymbol{\mathcal{V}} : [\mathbb{H}_{\hat{W}}] : \delta \boldsymbol{\mathcal{V}} > 0, \ \forall \delta \boldsymbol{\mathcal{V}}. \tag{38}$$

---

[8]Equation (33) can be understood as the vectorised product between a 25×25 matrix $[\mathbb{H}_{\hat{W}_{em}}]$ and a vector $\delta \boldsymbol{\mathcal{V}}$ with 25 components.

Eventually, it is easy to see the concavity of $\widehat{W}(\boldsymbol{C}, \boldsymbol{G}, C, \boldsymbol{D}_0, \theta)$ in (27) with respect to θ. Therefore, the energy function $\widehat{W}(\boldsymbol{C}, \boldsymbol{G}, C, \boldsymbol{D}_0, \theta)$ in (27) complies with the following two conditions

$$\widehat{W}(\boldsymbol{C}, \boldsymbol{G}, C, \boldsymbol{D}_0, \theta) = \hat{W}(\boldsymbol{\mathcal{V}}, \theta); \qquad \delta\boldsymbol{\mathcal{V}} : [\mathbb{H}_{\hat{W}}] : \delta\boldsymbol{\mathcal{V}} > 0, \ \forall \delta\boldsymbol{\mathcal{V}}; \qquad \partial^2_{\theta\theta}\hat{W} < 0, \qquad (39)$$

provided that $\theta < \theta_{cr}$ in (37). Finally, it is possible to establish the following relationships associated with the energy function $\widehat{W}(\boldsymbol{C}, \boldsymbol{G}, C, \boldsymbol{D}_0, \theta)$ in (27)

$$D\widehat{W}[\delta\boldsymbol{F}] = \boldsymbol{S} : \frac{1}{2}D\boldsymbol{C}[\delta\boldsymbol{F}]; \qquad D\widehat{W}[\delta\boldsymbol{D}_0] = \boldsymbol{E}_0 \cdot \delta\boldsymbol{D}_0; \qquad D\widehat{W}[\delta\theta] = -\eta\delta\theta, \qquad (40)$$

which permit to define $\boldsymbol{S}$, $\boldsymbol{E}_0$ and η as

$$\boldsymbol{S} = 2\partial_{\boldsymbol{C}}\widehat{W} + 2\partial_{\boldsymbol{G}}\widehat{W} \times \boldsymbol{C} + 2\partial_C\widehat{W}\boldsymbol{G}; \qquad \boldsymbol{E}_0 = \partial_{\boldsymbol{D}_0}\widehat{W}; \qquad \eta = -\partial_\theta\widehat{W}. \qquad (41)$$

3.1.4. Satisfaction of convexity/concavity constraints in the enthalpy function

In the previous section we have presented the specific form of the energy function $\widehat{W}(\boldsymbol{C}, \boldsymbol{G}, C, \boldsymbol{D}_0, \theta)$ and its re-expression $\hat{W}(\boldsymbol{\mathcal{V}}, \theta)$, which are recalled for convenience of the reader below

$$\begin{aligned}\widehat{W}(\boldsymbol{C}, \boldsymbol{G}, C, \boldsymbol{D}_0, \theta) &= \widehat{W}_{em}(\boldsymbol{C}, \boldsymbol{G}, C, \boldsymbol{D}_0) + \widehat{W}_{tm}(C, \theta) + \widehat{W}_\theta(\theta); \\ \hat{W}(\boldsymbol{\mathcal{V}}, \theta) &= \hat{W}_{em}(\boldsymbol{\mathcal{V}}, \theta) + \hat{W}_{tm}(J, \theta) + \hat{W}_\theta(\theta).\end{aligned} \qquad (42)$$

where the electro-mechanical, thermo-mechanical and thermal contributions are defined as

$$\begin{aligned}\hat{W}_{em}(\boldsymbol{\mathcal{V}}) &= \frac{\mu_1}{2}II_{\boldsymbol{F}} + \frac{\mu_2}{2}II_{\boldsymbol{H}} - (\mu_1 + 2\mu_2)\log J + \frac{\lambda}{2}(J-1)^2 + \frac{1}{2\varepsilon_1}II_{\boldsymbol{D}_0} + \frac{1}{2\varepsilon_2}J^{-1}II_{\boldsymbol{d}}; \\ \hat{W}_{tm}(J, \theta) &= -3\beta e(J^2 - 1)(\theta - \theta_R); \\ \hat{W}_\theta(\theta) &= c_0\left(\theta - \theta_R - \theta\ln\frac{\theta}{\theta_R}\right),\end{aligned} \qquad (43)$$

We have seen in the previous section that the recalled constitutive model complies with the conditions in equation (39) provided that the critical temperature (37) is never reached. The objective of this section is to prove that the latter are sufficient conditions in order for the enthalpy function $\widehat{\Psi}(\boldsymbol{C}, \boldsymbol{G}, C, \boldsymbol{E}_0, \theta)$ to comply with the constraints in $(14)_{a,b}$. The condition in equation $(14)_c$ has been proven in (22). Proof of this will be carried out through the following two steps:

Step 1: In addition to the energy function $\widehat{W}(\boldsymbol{C}, \boldsymbol{G}, C, \boldsymbol{D}_0, \theta)$ and its polyconvex analogous re-expression $\hat{W}(\boldsymbol{\mathcal{V}}, \boldsymbol{D}_0)$ it is also possible to re-write $\widehat{W}(\boldsymbol{C}, \boldsymbol{G}, C, \boldsymbol{D}_0, \theta)$ in terms of $\{\boldsymbol{F}, \boldsymbol{D}_0, \theta\}$, namely

$$W(\boldsymbol{F}, \boldsymbol{D}_0, \theta) = \widehat{W}(\boldsymbol{C}, \boldsymbol{G}, C, \boldsymbol{D}_0, \theta) = \hat{W}(\boldsymbol{\mathcal{V}}, \theta). \qquad (44)$$

The second directional derivative of $W(\boldsymbol{F}, \boldsymbol{D}_0, \theta)$ with respect to $\boldsymbol{F}$ and $\boldsymbol{D}_0$ can be conveniently written as

$$D^2W[\delta\boldsymbol{F}, \delta\boldsymbol{D}_0; \delta\boldsymbol{F}, \delta\boldsymbol{D}_0] = \delta\boldsymbol{\mathcal{U}} : [\mathbb{H}_W] : \delta\boldsymbol{\mathcal{U}}; \qquad \delta\boldsymbol{\mathcal{U}}^T = \begin{bmatrix}\delta\boldsymbol{F}^T & \delta\boldsymbol{D}_0^T\end{bmatrix}. \qquad (45)$$

Equivalentely, the second directional derivative of $\hat{W}(\boldsymbol{\mathcal{V}}, \theta)$ can be written as

$$\begin{aligned}D^2\hat{W}[D\boldsymbol{\mathcal{V}}[\delta\boldsymbol{F}, \delta\boldsymbol{D}_0]; D\boldsymbol{\mathcal{V}}[\delta\boldsymbol{F}, \delta\boldsymbol{D}_0]] = {}&D\boldsymbol{\mathcal{V}}[\delta\boldsymbol{F}, \delta\boldsymbol{D}_0] : [\mathbb{H}_{\hat{W}}] : D\boldsymbol{\mathcal{V}}[\delta\boldsymbol{F}, \delta\boldsymbol{D}_0] \\ &+ (\partial_{\boldsymbol{H}}W + \partial_JW\boldsymbol{F}) : (\delta\boldsymbol{F} \times \delta\boldsymbol{F}) + \partial_{\boldsymbol{d}}W \cdot (\delta\boldsymbol{F}\delta\boldsymbol{D}_0).\end{aligned} \qquad (46)$$

Consideration of virtual fields of the form $\delta \boldsymbol{F} = \boldsymbol{u} \otimes \boldsymbol{V}$ and $\delta \boldsymbol{D}_0 = \boldsymbol{V}_\perp$, with $\boldsymbol{u}, \boldsymbol{V}, \boldsymbol{V}_\perp \in \mathbb{R}^3$ and $\boldsymbol{V} \cdot \boldsymbol{V}_\perp = 0$, in both (45) and (46) yields

$$
\begin{aligned}
D^2 W \left[\boldsymbol{u} \otimes \boldsymbol{V}, \boldsymbol{V}_\perp; \boldsymbol{u} \otimes \boldsymbol{V}, \boldsymbol{V}_\perp\right] &= \begin{bmatrix} \boldsymbol{u} \otimes \boldsymbol{V} : \\ \boldsymbol{V}_\perp \cdot \end{bmatrix} [\mathbb{H}_W] \begin{bmatrix} : \boldsymbol{u} \otimes \boldsymbol{V} \\ \cdot \boldsymbol{V}_\perp \end{bmatrix}; \\
D^2 \hat{W} \left[\boldsymbol{u} \otimes \boldsymbol{V}, \boldsymbol{V}_\perp; \boldsymbol{u} \otimes \boldsymbol{V}, \boldsymbol{V}_\perp\right] &= D\boldsymbol{\mathcal{V}} \left[\boldsymbol{u} \otimes \boldsymbol{V}, \boldsymbol{V}_\perp\right] : [\mathbb{H}_{\hat{W}}] : D\boldsymbol{\mathcal{V}} \left[\boldsymbol{u} \otimes \boldsymbol{V}, \boldsymbol{V}_\perp\right].
\end{aligned}
\tag{47}
$$

Polyconvexity of $\widehat{W}(\boldsymbol{\mathcal{V}}, \theta)$ in the set $\boldsymbol{\mathcal{V}}$ entails the positive definiteness of $[\mathbb{H}_{\hat{W}}]$ and hence that $D^2\hat{W} \left[\boldsymbol{u} \otimes \boldsymbol{V}, \boldsymbol{V}_\perp; \boldsymbol{u} \otimes \boldsymbol{V}, \boldsymbol{V}_\perp\right] > 0$. Equivalence between $D^2\hat{W} \left[\boldsymbol{u} \otimes \boldsymbol{V}, \boldsymbol{V}_\perp; \boldsymbol{u} \otimes \boldsymbol{V}, \boldsymbol{V}_\perp\right]$ and $D^2 W \left[\boldsymbol{u} \otimes \boldsymbol{V}, \boldsymbol{V}_\perp; \boldsymbol{u} \otimes \boldsymbol{V}, \boldsymbol{V}_\perp\right]$ permits to confirm positiveness of the latter, and hence the rank-one convexity of $W(\boldsymbol{F}, \boldsymbol{D}_0, \theta)$ with respect to the set $\{\boldsymbol{F}, \boldsymbol{D}_0\}$, namely

$$
\begin{bmatrix} \boldsymbol{u} \otimes \boldsymbol{V} : \\ \boldsymbol{V}_\perp \cdot \end{bmatrix} [\mathbb{H}_W] \begin{bmatrix} : \boldsymbol{u} \otimes \boldsymbol{V} \\ \cdot \boldsymbol{V}_\perp \end{bmatrix} > 0.
\tag{48}
$$

Step 2: The rank-one convexity condition (48) is also satisfied individually for the purely mechanical physics and purely electric physics, namely

$$
\begin{aligned}
D^2 W \left[\boldsymbol{u} \otimes \boldsymbol{V}; \boldsymbol{u} \otimes \boldsymbol{V}\right] &:= (\boldsymbol{u} \otimes \boldsymbol{V}) : \partial^2_{\boldsymbol{FF}} W : (\boldsymbol{u} \otimes \boldsymbol{V}) > 0; \\
D^2 W \left[\boldsymbol{V}_\perp; \boldsymbol{V}_\perp\right] &:= \boldsymbol{V}_\perp \cdot \partial^2_{\boldsymbol{D}_0 \boldsymbol{D}_0} W \boldsymbol{V}_\perp > 0.
\end{aligned}
\tag{49}
$$

More generally, the decoupled constraint in equation $(49)_b$, is satisfied for every vector $\boldsymbol{U}$, namely

$$
D^2 W \left[\boldsymbol{U}; \boldsymbol{U}\right] := \boldsymbol{U} \cdot \partial^2_{\boldsymbol{D}_0 \boldsymbol{D}_0} W \boldsymbol{U} > 0.
\tag{50}
$$

It is possible to relate the two tensors $\partial^2_{\boldsymbol{FF}} W$ and $\partial^2_{\boldsymbol{D}_0 \boldsymbol{D}_0} W$ in (49) with the second derivatives of the enthalpy function $\Psi(\boldsymbol{F}, \boldsymbol{E}_0)$ by noting that the latter can be expressed as

$$
\Psi(\boldsymbol{F}, \boldsymbol{E}_0, \theta) = \Psi(\boldsymbol{F}, \boldsymbol{E}_0(\boldsymbol{F}, \boldsymbol{D}_0), \theta).
\tag{51}
$$

Making use of (51), the authors in [19] derived the following relationships

$$
\partial^2_{\boldsymbol{FF}} W = \partial^2_{\boldsymbol{FF}} \Psi + \partial^2_{\boldsymbol{FE}_0} \Psi \left(\partial^2_{\boldsymbol{E}_0 \boldsymbol{E}_0} \Psi\right)^{-1} \partial^2_{\boldsymbol{E}_0 \boldsymbol{F}} \Psi; \qquad \partial^2_{\boldsymbol{D}_0 \boldsymbol{D}_0} W = -\left(\partial^2_{\boldsymbol{E}_0 \boldsymbol{E}_0} \Psi\right)^{-1}.
\tag{52}
$$

Introduction of (52) into $(49)_a$ and (50) yields

$$
\begin{aligned}
D^2 W \left[\boldsymbol{u} \otimes \boldsymbol{V}; \boldsymbol{u} \otimes \boldsymbol{V}\right] &= (\boldsymbol{u} \otimes \boldsymbol{V}) : \left(\partial^2_{\boldsymbol{FF}} \Psi + \partial^2_{\boldsymbol{FE}_0} \Psi \left(\partial^2_{\boldsymbol{E}_0 \boldsymbol{E}_0} \Psi\right)^{-1} \partial^2_{\boldsymbol{E}_0 \boldsymbol{F}} \Psi\right) : (\boldsymbol{u} \otimes \boldsymbol{V}) > 0; \\
D^2 W \left[\boldsymbol{U}; \boldsymbol{U}\right] &= -\boldsymbol{U} \cdot \left(\partial^2_{\boldsymbol{E}_0 \boldsymbol{E}_0} \Psi\right)^{-1} \boldsymbol{U} > 0.
\end{aligned}
\tag{53}
$$

Then, we conveniently choose vectors $\boldsymbol{U}$ in (53) of the following form

$$
\boldsymbol{U} = \partial^2_{\boldsymbol{E}_0 \boldsymbol{F}} \Psi : (\boldsymbol{u} \otimes \boldsymbol{V}).
\tag{54}
$$

Sum of $D^2 W \left[\boldsymbol{u} \otimes \boldsymbol{V}; \boldsymbol{u} \otimes \boldsymbol{V}\right]$ and $D^2 W \left[\boldsymbol{U}; \boldsymbol{U}\right]$ for the particular choice of $\boldsymbol{U}$ in (54) yields

$$
D^2 W[\boldsymbol{u} \otimes \boldsymbol{V}; \boldsymbol{u} \otimes \boldsymbol{V}] + D^2 W[\boldsymbol{U}; \boldsymbol{U}]\big|_{\boldsymbol{U} = \partial^2_{\boldsymbol{E}_0 \boldsymbol{F}} \Psi : (\boldsymbol{u} \otimes \boldsymbol{V})} = (\boldsymbol{u} \otimes \boldsymbol{V}) : \partial^2_{\boldsymbol{FF}} \Psi : (\boldsymbol{u} \otimes \boldsymbol{V}).
\tag{55}
$$

Positiveness of both terms on the left-hand side of (55) entails positiveness of the term on the right-hand side, namely

$$
(\boldsymbol{u} \otimes \boldsymbol{V}) : \partial^2_{\boldsymbol{FF}} \Psi : (\boldsymbol{u} \otimes \boldsymbol{V}) > 0.
\tag{56}
$$

All in all, equations in $(14)_{a,b}$ are fulfilled as can be seen in equations $(53)_b$ and (56).

11

Remark 3. *The constitutive model considered in this work (see equation* (27)*) considers a simplified scenario where interactions between the electro-mechanical contribution* $\widehat{W}_{em}$ *and the temperature field* θ *are not contemplated. For this model, we concluded that the conditions in equation* (14) *that the associated enthalpy density function (related to the internal energy by means of the Legendre transformation in* (28)*) must satisfy are fulfilled provided that:*

- $\widehat{W}(\boldsymbol{C}, \boldsymbol{G}, C, \boldsymbol{D}_0, \theta)$ *is polyconvex, i.e.,* $\widehat{W}(\boldsymbol{C}, \boldsymbol{G}, C, \boldsymbol{D}_0, \theta) = \widehat{W}(\hat{\boldsymbol{\mathcal{V}}}, \theta)$, *with* $\widehat{W}$ *convex with respect to* $\hat{\boldsymbol{\mathcal{V}}}$.

- $\widehat{W}$ *is concave with respect to* θ.

The more realistic scenario where interactions between the termperature field and the thermomechanical energetic contribution are considered can be incorporated by defining the internal energy function as (see for instance [26, 42])

$$\widehat{W}(\boldsymbol{C}, \boldsymbol{G}, C, \boldsymbol{D}_0, \theta) = f(\theta)\widehat{W}_{em}(\boldsymbol{C}, \boldsymbol{G}, C, \boldsymbol{D}_0) + \widehat{W}_{tm}(C, \theta) + \widehat{W}_\theta(\theta). \tag{57}$$

With the aim of permitting a temperature dependence of the heat capacity, the authors in [26] defined the function $f(\theta)$ *as*

$$f(\theta) = \frac{\theta}{\theta_R} + g(\theta) - g(\theta_R) + \partial_\theta g|_{\theta=\theta_R} (\theta - \theta_R), \tag{58}$$

where $g(\theta)$ *is a temperature sensitive scaling function. Following a similar procedure as that throughout the current section, it is possible to conclude that the more generic internal energy energy density function in equation* (57) *complies with the conditions in equation* (14) *provided that, in addition to the previous 2 conditions just listed above, the following two conditions are also satisfied, namely:*

- $f(\theta)$ *in* (58) *is positive* $\forall \theta$.

- $g(\theta)$ *is convex, i.e.* $\partial_{\theta\theta}^2 g(\theta) > 0 \, \forall \theta$.

3.2. Fourier law

Fourier law relates the spatial heat flux $\boldsymbol{q}$ and the spatial gradient of θ by virtue of the following expression

$$\boldsymbol{q} = -\boldsymbol{k}\boldsymbol{\nabla}\theta, \tag{59}$$

where $\boldsymbol{k}$ represents the semi-positive definite second order thermal conductivity tensor in the deformed configuration and $\boldsymbol{\nabla}(\bullet)$ the spatial gradient operator. As customary in continuum mechanics, the relation between $\boldsymbol{q}$ and its material counterpart $\boldsymbol{Q}$ featuring in equation (6) can be carried out by making use of the Gauss' theorem and the Nanson's rule (i.e. $d\boldsymbol{a} = \boldsymbol{H}d\boldsymbol{A}$) as

$$\int_{\mathcal{B}} \mathrm{div}\boldsymbol{q} \, dv = \int_{\partial\mathcal{B}} \boldsymbol{q} \cdot d\boldsymbol{a} = \int_{\partial\mathcal{B}_0} \boldsymbol{Q} \cdot d\boldsymbol{A}, \tag{60}$$

where $\mathrm{div}(\bullet)$ represents the spatial divergence operator and with

$$\boldsymbol{Q} = \boldsymbol{H}^T\boldsymbol{q} = -\boldsymbol{H}^T\boldsymbol{k}\boldsymbol{\nabla}\theta. \tag{61}$$

The spatial gradient of θ in (61) can be conveniently related to its material counterpart as

$$\boldsymbol{\nabla}\theta = \boldsymbol{F}^{-T}\boldsymbol{\nabla}_0\theta = J^{-1}\boldsymbol{H}\boldsymbol{\nabla}_0\theta. \tag{62}$$

Finally, introduction of (62) into (61) yields

$$\boldsymbol{Q} = -\boldsymbol{K}\boldsymbol{\nabla}_0\theta; \qquad \boldsymbol{K} = J^{-1}\boldsymbol{H}^T\boldsymbol{k}\boldsymbol{H}. \tag{63}$$

4. Thermo-electro-elastodynamics

On the basis of Sections 2 and 3 the variational formulation will be introduced in the following.

4.1. Continuum formulation

To facilitate the design of an EM time integrator, we first study the conservation properties of a thermo-electro-elastic continuum given by (2), (3)-(4) and (6). In this connection, we present a formulation in terms of the energy function depending upon the electric displacement field $\boldsymbol{D}_0$, namely $\widehat{W}(\boldsymbol{C}, \boldsymbol{G}, C, \boldsymbol{D}_0, \theta)$ defined as in (42)-(43) in order to satisfy the material stability conditions in (14). In this case, the formulation relies on the following five weak forms:

$$
\begin{aligned}
\mathcal{W}_{\boldsymbol{v}} &= \int_{\mathcal{B}_0} \left(\boldsymbol{v} - \dot{\boldsymbol{\phi}} \right) \cdot \rho_0 \boldsymbol{w_v} \, dV = 0; \\
\mathcal{W}_{\boldsymbol{\phi}} &= \int_{\mathcal{B}_0} \rho_0 \dot{\boldsymbol{v}} \cdot \boldsymbol{w_\phi} \, dV + \int_{\mathcal{B}_0} \boldsymbol{S} : \frac{1}{2} D\boldsymbol{C}[\boldsymbol{w_\phi}] \, dV - \mathcal{W}_{\boldsymbol{\phi}}^{\text{ext}} = 0; \\
\mathcal{W}_{\varphi} &= \int_{\mathcal{B}_0} \boldsymbol{D}_0 \cdot \boldsymbol{\nabla}_0 w_\varphi \, dV - \mathcal{W}_{\varphi}^{\text{ext}} = 0; \\
\mathcal{W}_{\boldsymbol{D}_0} &= \int_{\mathcal{B}_0} \left(\boldsymbol{E}_0 + \boldsymbol{\nabla}_0 \varphi \right) \cdot \boldsymbol{w_{D_0}} \, dV = 0; \\
\mathcal{W}_{\theta} &= \int_{\mathcal{B}_0} \left(\frac{d}{dt} \left(\theta \eta \right) w_\theta - \dot{\theta} \eta w_\theta \right) dV - \int_{\mathcal{B}_0} \boldsymbol{Q} \cdot \boldsymbol{\nabla}_0 w_\theta \, dV - \mathcal{W}_{\theta}^{\text{ext}} = 0,
\end{aligned} \tag{64}
$$

where the external mechanical, electrical and thermal contributions are defined as

$$
\begin{aligned}
\mathcal{W}_{\boldsymbol{\phi}}^{\text{ext}} &= \int_{\mathcal{B}_0} \boldsymbol{f}_0 \cdot \boldsymbol{w_\phi} \, dV + \int_{\partial_t \mathcal{B}_0} \boldsymbol{t}_0 \cdot \boldsymbol{w_\phi} \, dA; \\
\mathcal{W}_{\varphi}^{\text{ext}} &= - \int_{\mathcal{B}_0} \rho_0^e w_\varphi \, dV - \int_{\partial_\omega \mathcal{B}_0} \omega_0^e w_\varphi \, dA \\
\mathcal{W}_{\theta}^{\text{ext}} &= \int_{\mathcal{B}_0} R_\theta w_\theta \, dV + \int_{\partial_Q \mathcal{B}_0} Q_\theta w_\theta \, dA.
\end{aligned} \tag{65}
$$

Furthermore, in (64), $\boldsymbol{S}$, $\boldsymbol{E}_0$ and η are defined in terms of the derivatives of the energy function $\widehat{W}(\boldsymbol{C}, \boldsymbol{G}, C, \boldsymbol{D}_0, \theta)$ as in (41) and with $\{\boldsymbol{v}, \boldsymbol{\phi}, \varphi, \boldsymbol{D}_0, \theta\} \in \{\mathbb{V}^\phi, \mathbb{V}^\phi, \mathbb{V}^\varphi, \mathbb{V}^{D_0}, \mathbb{V}^\theta\}$ and $\{\boldsymbol{w_v}, \boldsymbol{w_\phi}, w_\varphi, \boldsymbol{w_{D_0}}, w_\theta\} \in \{\mathbb{V}^\phi, \mathbb{V}_0^\phi, \mathbb{V}_0^\varphi, \mathbb{V}^{D_0}, \mathbb{V}_0^\theta\}$,

$$
\begin{aligned}
\mathbb{V}^\phi &= \left\{ \boldsymbol{\phi} \in H^1\left(\mathcal{B}_0; \mathbb{R}^3\right) \mid \boldsymbol{\phi} = \bar{\boldsymbol{\phi}} \text{ on } \partial_\phi \mathcal{B}_0 \text{ and } J > 0 \text{ } a.e \right\}; & \mathbb{V}_0^\phi &= \left\{ \boldsymbol{\phi} \in H^1\left(\mathcal{B}_0; \mathbb{R}^3\right) \mid \boldsymbol{\phi} = \boldsymbol{0} \text{ on } \partial_\phi \mathcal{B}_0 \right\}; \\
\mathbb{V}^\varphi &= \left\{ \varphi \in H^1\left(\mathcal{B}_0; \mathbb{R}\right); \mid \varphi = \bar{\varphi} \text{ on } \partial_\varphi \mathcal{B}_0 \right\}; & \mathbb{V}_0^\varphi &= \left\{ \varphi \in H^1\left(\mathcal{B}_0; \mathbb{R}\right); \mid \varphi = 0 \text{ on } \partial_\varphi \mathcal{B}_0 \right\}; \\
\mathbb{V}^\theta &= \left\{ \theta \in H^1\left(\mathcal{B}_0; \mathbb{R}\right) \mid \theta = \bar{\theta} \text{ on } \partial_\theta \mathcal{B}_0 \right\}; & \mathbb{V}_0^\theta &= \left\{ \theta \in H^1\left(\mathcal{B}_0; \mathbb{R}\right) \mid \theta = 0 \text{ on } \partial_\theta \mathcal{B}_0 \right\}; \\
\mathbb{V}^{D_0} &= \left\{ \boldsymbol{D}_0 \in \mathbb{L}_2\left(\mathcal{B}_0; \mathbb{R}^3\right) \right\}.
\end{aligned} \tag{66}
$$

4.2. Balance laws and integrals in thermo-electro-elastodynamics

With the variational formulation in (64) the balance laws for the considered thermo-electro-elastic continuum are examined.

4.2.1. Balance of linear momentum

For a test function $\boldsymbol{w}_\phi = \boldsymbol{\xi}$, with $\mathbb{R}^3 \ni \boldsymbol{\xi} = const.$, the weak form in $(64)_b$ leads to the global form of the conservation of linear momentum, namely

$$\dot{\boldsymbol{L}} = \boldsymbol{F}^{\text{ext}} = \int_{\partial_t \mathcal{B}_0} \boldsymbol{t}_0 \, dA + \int_{\mathcal{B}_0} \boldsymbol{f}_0 \, dV; \qquad \boldsymbol{L} = \int_{\mathcal{B}_0} \rho_0 \boldsymbol{v} \, dV. \tag{67}$$

In the above $\boldsymbol{L}$ represents the total linear momentum and $\boldsymbol{F}^{\text{ext}}$, the total external force. From (67) it is possible to conclude that $\boldsymbol{L}$ is a constant of motion for the case of constant external forces $\boldsymbol{F}^{\text{ext}}$.

4.2.2. Balance of angular momentum

Employing $\boldsymbol{w}_\phi = \boldsymbol{\xi} \times \boldsymbol{\phi}$, where $\mathbb{R}^3 \ni \boldsymbol{\xi} = const.$, the weak form in $(64)_b$ leads to the global form of the balance of angular momentum, i.e.

$$\dot{\boldsymbol{J}} = \boldsymbol{M}^{\text{ext}} = \int_{\partial_t \mathcal{B}_0} \boldsymbol{\phi} \times \boldsymbol{t}_0 \, dA + \int_{\mathcal{B}_0} \boldsymbol{\phi} \times \boldsymbol{f}_0 \, dV; \qquad \boldsymbol{J} = \int_{\mathcal{B}_0} \boldsymbol{\phi} \times \rho_0 \boldsymbol{v} \, dV, \tag{68}$$

where $\boldsymbol{J}$ represents the total angular momentum and $\boldsymbol{M}^{\text{ext}}$, the total external torque. From (68), it is clear that $\boldsymbol{J}$ is a constant of motion for vanishing external torques $\boldsymbol{M}^{\text{ext}}$.

4.2.3. Global form of Gauss's law

Applying $w_\varphi = \xi$, where $\mathbb{R} \ni \xi = const.$, in weak form $(64)_c$ yields the global form of Gauss' law

$$\int_{\mathcal{B}_0} \rho_0^e \, dV + \int_{\partial_\omega \mathcal{B}_0} \omega_0^e \, dA = 0, \tag{69}$$

where assuming time independent volumetric and surface electrical charges ρ_0^e and ω_0^e, equation (69) dictates that the total electric charge of the system is conserved and equal to zero.

4.2.4. Balance of total energy

For the consideration of the balance of totatl energy we replace the test functions $\{\boldsymbol{w}_v, \boldsymbol{w}_\phi\}$ in (64) with $\{\dot{\boldsymbol{v}}, \dot{\boldsymbol{\phi}}\} \in \{\mathbb{V}_0^\phi \times \mathbb{V}_0^\phi\}$ and $\{w_\varphi, \boldsymbol{w}_{\boldsymbol{D}_0}\}$ with $\{\dot{\varphi}, \dot{\boldsymbol{D}}_0\} \in \{\mathbb{V}_0^\varphi, \mathbb{V}^{\boldsymbol{D}_0}\}$ and we choose $w_\theta = 1 \in \mathbb{V}_0^\theta$. Then, summation of the five weak forms and assuming zero contributions $\mathcal{W}_\phi^{\text{ext}}$, $\mathcal{W}_\varphi^{\text{ext}}$ and $\mathcal{W}_\theta^{\text{ext}}$ leads to

$$\int_{\mathcal{B}_0} \left(\rho_0 \dot{\boldsymbol{v}} \cdot \dot{\boldsymbol{\phi}} + \boldsymbol{S} : \frac{1}{2}\dot{\boldsymbol{C}} + \boldsymbol{E}_0 \cdot \dot{\boldsymbol{D}}_0 - \dot{\theta}\eta + \frac{d}{dt}\left(\boldsymbol{D}_0 \cdot \boldsymbol{\nabla}_0 \varphi + \theta\eta\right) \right) dV = 0. \tag{70}$$

With the definition of the kinetic energy $\mathcal{K} = \int_{\mathcal{B}_0} \frac{1}{2}\rho_0 \boldsymbol{v} \cdot \boldsymbol{v} \, dV$ and making use of (41) in (70) we obtain

$$\dot{\mathcal{K}} + \int_{\mathcal{B}_0} \frac{d}{dt}\left(\widehat{W}\left(\boldsymbol{C}, \boldsymbol{G}, C, \boldsymbol{D}_0, \theta\right) + \boldsymbol{D}_0 \cdot \boldsymbol{\nabla}_0 \varphi + \theta\eta \right) dV = 0. \tag{71}$$

For vanishing external mechanical and thermal power, we get

$$\dot{\mathcal{E}} = 0; \qquad \mathcal{E} = \mathcal{K} + \int_{\mathcal{B}_0} \left(\widehat{W}(\boldsymbol{C}, \boldsymbol{G}, C, \boldsymbol{D}_0, \theta) + \boldsymbol{D}_0 \cdot \boldsymbol{\nabla}_0 \varphi + \theta\eta \right) dV. \tag{72}$$

Accordingly, the total energy $\mathcal{E}$ is conserved.

5. Energy-momentum integration scheme for thermo-electro-elastodynamics

For the above weak form (64) we aim at the development of an EM consistent time integration scheme following the publications [6, 7, 16, 17, 20, 29, 32, 35, 40].

14

5.1. Design of the EM scheme

Considering a sequence of time steps $\{t_1, t_2, ..., t_n, t_{n+1}\}$ with t_{n+1} being the current time step, the weak form in (64) is discretized in time yielding the following implicit one-step time integrator

$$(\mathcal{W}_{\boldsymbol{v}})_{\text{algo}} = \int_{\mathcal{B}_0} \left(\boldsymbol{v}_{n+1/2} - \frac{\Delta \boldsymbol{\phi}}{\Delta t}\right) \cdot \rho_0 \boldsymbol{w}_{\boldsymbol{v}} \, dV = 0;$$

$$(\mathcal{W}_{\boldsymbol{\phi}})_{\text{algo}} = \int_{\mathcal{B}_0} \rho_0 \frac{\Delta \boldsymbol{v}}{\Delta t} \cdot \boldsymbol{w}_{\boldsymbol{\phi}} \, dV + \int_{\mathcal{B}_0} \boldsymbol{S}_{\text{algo}} : \frac{1}{2}(D\boldsymbol{C}[\boldsymbol{w}_{\boldsymbol{\phi}}])_{\text{algo}} \, dV - \left(\mathcal{W}_{\boldsymbol{\phi}_{n+1/2}}^{\text{ext}}\right) = 0;$$

$$(\mathcal{W}_{\varphi})_{\text{algo}} = \int_{\mathcal{B}_0} \boldsymbol{D}_{0_{n+1/2}} \cdot \boldsymbol{\nabla}_0 \delta\varphi \, dV + \int_{\mathcal{B}_0} \rho_{0_{n+1/2}}^e \delta\varphi \, dV - \left(\mathcal{W}_{\varphi_{n+1/2}}^{\text{ext}}\right) = 0; \tag{73}$$

$$(\mathcal{W}_{\boldsymbol{D}_0})_{\text{algo}} = \int_{\mathcal{B}_0} \delta\boldsymbol{D}_0 \cdot \left(\boldsymbol{E}_{0\text{algo}} + \boldsymbol{\nabla}_0 \varphi_{n+1/2}\right) \, dV = 0;$$

$$(\mathcal{W}_{\theta})_{\text{algo}} = \int_{\mathcal{B}_0} \left(\frac{\Delta(\theta\eta)}{\Delta t} - \frac{\Delta\theta}{\Delta t}\eta_{\text{algo}}\right) w_{\theta} \, dV - \int_{\mathcal{B}_0} \boldsymbol{Q}_{n+1/2} \cdot \boldsymbol{\nabla}_0 w_{\theta} \, dV - \left(\mathcal{W}_{\theta_{n+1/2}}^{\text{ext}}\right) = 0,$$

where $(\bullet)_{n+1/2} = \frac{1}{2}\left((\bullet)_{n+1} + (\bullet)_n\right)$ and $\Delta(\bullet) = (\bullet)_{n+1} - (\bullet)_n$. In (73) $\{(\mathcal{W}_{\boldsymbol{v}})_{\text{algo}}, (\mathcal{W}_{\boldsymbol{\phi}})_{\text{algo}}, (\mathcal{W}_{\varphi})_{\text{algo}}, (\mathcal{W}_{\boldsymbol{D}_0})_{\text{al}}$ denote the carefully designed algorithmic, time discrete versions of (64). Furthermore, the algorithmic second Piola-Kirchhoff stress tensor $\boldsymbol{S}_{\text{algo}}$, the material electric field $\boldsymbol{E}_{0\text{algo}}$ and the entropy density η_{algo} are related to the five discrete derivatives $\{D_{\boldsymbol{C}}\widetilde{W}, D_{\boldsymbol{G}}\widetilde{W}, D_C\widetilde{W}, D_{\boldsymbol{D}_0}\widetilde{W}, D_\theta\widetilde{W}\}$ (cf. [16, 20, 29, 32]), respectively, which are the algorithmic counterparts of $\{\partial_{\boldsymbol{C}}\widetilde{W}, \partial_{\boldsymbol{G}}\widetilde{W}, \partial_C\widetilde{W}, \partial_{\boldsymbol{D}_0}\widetilde{W}, \partial_\theta\widetilde{W}\}$, respectively, given as

$$\boldsymbol{S}_{\text{algo}} : \frac{1}{2}(D\boldsymbol{C}[\boldsymbol{w}_{\boldsymbol{\phi}}])_{\text{algo}} = D_{\boldsymbol{C}}\widehat{W} : (D\boldsymbol{C}[\boldsymbol{w}_{\boldsymbol{\phi}}])_{\text{algo}} + D_{\boldsymbol{G}}\widehat{W} : (D\boldsymbol{G}[\boldsymbol{w}_{\boldsymbol{\phi}}])_{\text{algo}} + D_C\widehat{W} \, (DC[\boldsymbol{w}_{\boldsymbol{\phi}}])_{\text{algo}};$$

$$\boldsymbol{E}_{0\text{algo}} = D_{\boldsymbol{D}_0}\widehat{W};$$

$$\eta_{\text{algo}} = -D_\theta\widehat{W}, \tag{74}$$

where in the abvoe $\{D_{\boldsymbol{C}}\widehat{W}, D_{\boldsymbol{G}}\widehat{W}, D_C\widehat{W}, D_{\boldsymbol{D}_0}\widehat{W}, D_\theta\widehat{W}\}$ denote the discrete derivatives (cf. [16, 20, 29, 32]) of the function $\widehat{W}(\boldsymbol{C}, \boldsymbol{G}, C, \boldsymbol{D}_0, \theta)$ with respect to $\{\boldsymbol{C}, \boldsymbol{G}, C, \boldsymbol{D}_0, \theta\}$, respectively, which are the algorithmic or time discrete counterparts of $\{\partial_{\boldsymbol{C}}\widehat{W}, \partial_{\boldsymbol{G}}\widehat{W}, \partial_C\widehat{W}, \partial_{\boldsymbol{D}_0}\widehat{W}, \partial_\theta\widehat{W}\}$, respectively. Furthermore in (74) the algorithmic directional derivatives $\{(D\boldsymbol{C}[\boldsymbol{w}_{\boldsymbol{\phi}}])_{\text{algo}}, (D\boldsymbol{G}[\boldsymbol{w}_{\boldsymbol{\phi}}])_{\text{algo}}, (DC[\boldsymbol{w}_{\boldsymbol{\phi}}])_{\text{algo}}\}$ are computed in analogy to [29], such that

$$(D\boldsymbol{C}[\boldsymbol{w}_{\boldsymbol{\phi}}])_{\text{algo}} = \left((\boldsymbol{\nabla}_0\boldsymbol{w}_{\boldsymbol{\phi}})^T \boldsymbol{F}_{n+1/2} + \boldsymbol{F}_{n+1/2}^T \boldsymbol{\nabla}_0\boldsymbol{w}_{\boldsymbol{\phi}}\right);$$

$$(D\boldsymbol{G}[\boldsymbol{w}_{\boldsymbol{\phi}}])_{\text{algo}} = \boldsymbol{C}_{\text{algo}} \times (D\boldsymbol{C}[\boldsymbol{w}_{\boldsymbol{\phi}}])_{\text{algo}}; \qquad \boldsymbol{C}_{\text{algo}} = \boldsymbol{C}_{n+1/2};$$

$$(DC[\boldsymbol{w}_{\boldsymbol{\phi}}])_{\text{algo}} = \boldsymbol{G}_{\text{algo}} : (D\boldsymbol{C}[\boldsymbol{w}_{\boldsymbol{\phi}}])_{\text{algo}}; \qquad \boldsymbol{G}_{\text{algo}} = \frac{1}{3}\left(\boldsymbol{C}_{n+1/2} \times \boldsymbol{C}_{n+1/2} + \boldsymbol{G}_{n+1/2}\right). \tag{75}$$

Finally, introduction of (75) into (74) permits to conveniently re-write (74) as

$$\boldsymbol{S}_{\text{algo}} = 2D_{\boldsymbol{C}}\widehat{W} + 2D_{\boldsymbol{G}}\widehat{W} \times \boldsymbol{C}_{\text{algo}} + 2D_C\widehat{W}\boldsymbol{G}_{\text{algo}}. \tag{76}$$

The definition of the discrete derivatives, which are presented in detail in Appendix A, must satisfy two crucial properties for the design of EM time integrators, namely:

- They fulfil the so called *directionality property* [16, 20],

$$D_{\boldsymbol{C}}\widehat{W} : \Delta\boldsymbol{C} + D_{\boldsymbol{G}}\widehat{W} : \Delta\boldsymbol{G} + D_C\widehat{W}\Delta C + D_{\boldsymbol{D}_0}\widehat{W} \cdot \Delta\boldsymbol{D}_0 + D_\theta\widehat{W}\Delta\theta = \Delta\widehat{W}. \tag{77}$$

- They are well defined in the limit as $||\Delta\boldsymbol{C}|| \to 0$, $||\Delta\boldsymbol{D}_0|| \to 0$ and $\Delta\theta \to 0$.

15

The first property is critical for the algorithm in (73) to preserve the balance of power in (71) in the discrete setting. Furthermore, the EM time integrator is second order accurate with necessary condition

$$D_{\boldsymbol{\mathcal{U}}_i}\widehat{W} = \partial_{\boldsymbol{\mathcal{U}}_i}\widehat{W}\left(\boldsymbol{\mathcal{U}}_{in+1/2}\right) + \mathcal{O}\left(\Delta t^2\right); \qquad \boldsymbol{\mathcal{U}} = \{\mathcal{U}_1,\mathcal{U}_2,\mathcal{U}_3,\mathcal{U}_4,\mathcal{U}_5\} = \{\boldsymbol{C},\boldsymbol{G},C,\boldsymbol{D}_0,\theta\}. \tag{78}$$

5.2. Semi-discrete balance laws and integrals in thermo-electro-elastodynamics

In the following we show the conservation properties of the balance laws and integrals for the semi-discrete thermo-electro-elastodynamical system with proposed EM scheme (73).

5.2.1. Semi-discrete balance of linear momentum

In analogy to Section 4.2.1 we apply $\boldsymbol{w}_\phi = \boldsymbol{\xi}$, where $\mathbb{R}^3 \ni \boldsymbol{\xi} = const.$ in weak form $(73)_b$ which gives

$$\frac{\Delta\boldsymbol{L}}{\Delta t} = \boldsymbol{F}_{n+1/2}^{\text{ext}} = \int_{\partial_t\mathcal{B}_0} \boldsymbol{t}_{0_{n+1/2}}\, dA + \int_{\mathcal{B}_0} \boldsymbol{f}_{0_{n+1/2}}\, dV. \tag{79}$$

I.e. for employing constant external forces $\boldsymbol{F}_{n+1/2}^{\text{ext}}$ the balance of total linear momentum is conserved.

5.2.2. Semi-discrete balance of angular momentum

In analogy to Section 4.2.2 we apply $\boldsymbol{w}_\phi = \boldsymbol{\xi} \times \boldsymbol{\phi}_{n+1/2}$, where $\mathbb{R}^3 \ni \boldsymbol{\xi} = const.$ in weak form $(73)_b$ which finally leads to

$$\frac{\Delta\boldsymbol{J}}{\Delta t} = \boldsymbol{M}_{n+1/2}^{\text{ext}} = \int_{\partial_t\mathcal{B}_0} \boldsymbol{\phi}_{n+1/2} \times \boldsymbol{t}_{0_{n+1/2}}\, dA + \int_{\mathcal{B}_0} \boldsymbol{\phi}_{n+1/2} \times \boldsymbol{f}_{0_{n+1/2}}\, dV. \tag{80}$$

Accordingly, for employing constant external torques $\boldsymbol{M}_{n+1/2}^{\text{ext}}$ the balance of angular momentum is conserved.

5.2.3. Semi-discrete global form of the Gauss law

In analogy to Section 4.2.3 we apply $w_\varphi = \xi$, where $\mathbb{R} \ni \xi = const.$ in weak form (73) which yields

$$\int_{\mathcal{B}_0} \rho_{0_{n+1/2}}^e\, dV + \int_{\partial_\omega\mathcal{B}_0} \omega_{0_{n+1/2}}^e\, dA = 0. \tag{81}$$

From the above (81) it becomes obvious that for time independent volumetric and surface electrical charges ρ_0^e and ω_0^e the total electrical charge vanishes.

5.2.4. Semi-discrete balance of total energy

In analogy to Section (4.2.4) we apply the test functions $\{\boldsymbol{w}_v, \boldsymbol{w}_\phi, w_\varphi, \boldsymbol{w}_{D_0}, \boldsymbol{w}_\theta\}$ where $\{\Delta\boldsymbol{v}/\Delta t, \Delta\boldsymbol{\phi}/\Delta t, \Delta\varphi/\Delta t, \Delta\boldsymbol{D}_0, 1\} \in \{\mathbb{V}_0^\phi, \mathbb{V}_0^\phi, \mathbb{V}_0^\varphi, \mathbb{V}_0^{D_0}, \mathbb{V}_0^\theta\}$ in (73). Furthermore neglecting the external contributions $\left(\mathcal{W}_{\phi_{n+1/2}}^{\text{ext}}\right)$, $\left(\mathcal{W}_{\varphi_{n+1/2}}^{\text{ext}}\right)$ and $\left(\mathcal{W}_{\theta_{n+1/2}}^{\text{ext}}\right)$ we get

$$\frac{\Delta\mathcal{K}}{\Delta t} + \int_{\mathcal{B}_0} \frac{1}{\Delta t}\left(\boldsymbol{S}_{\text{algo}} : \frac{1}{2}(D\boldsymbol{C}[\Delta\boldsymbol{\phi}])_{\text{algo}} + \boldsymbol{E}_{0_{\text{algo}}} \cdot \Delta\boldsymbol{D}_0 - \Delta\theta\eta_{\text{algo}} + \Delta\left(\theta\eta + \boldsymbol{D}_0 \cdot \boldsymbol{\nabla}_0\varphi\right)\right) dV = 0. \tag{82}$$

With (75) and (74) equation (82) can be stated as

$$\begin{aligned} \boldsymbol{S}_{\text{algo}} : \frac{1}{2}(D\boldsymbol{C}[\Delta\boldsymbol{\phi}])_{\text{algo}} + \boldsymbol{E}_{0_{\text{algo}}} \cdot \Delta\boldsymbol{D}_0 - \Delta\theta\eta_{\text{algo}} = {}&D_{\boldsymbol{C}}\widehat{W} : \Delta\boldsymbol{C} + D_{\boldsymbol{G}}\widehat{W} : \Delta\boldsymbol{G} + D_C\widehat{W}\Delta C \\ &+ D_{\boldsymbol{D}_0}\widehat{W} \cdot \Delta\boldsymbol{D}_0 + D_\theta\widehat{W}\Delta\theta. \end{aligned} \tag{83}$$

Furthermore inserting (83) into (82) yields

$$\Delta \mathcal{K} + \int_{\mathcal{B}_0} \left(D_{\boldsymbol{C}}\widetilde{W} : \Delta \boldsymbol{C} + D_{\boldsymbol{G}}\widetilde{W} : \Delta \boldsymbol{G} + D_C\widetilde{W} : \Delta C + \right.$$
$$\left. D_{\boldsymbol{D}_0}\widetilde{W} \cdot \Delta \boldsymbol{D}_0 + D_\theta \widetilde{W} \Delta \theta + \Delta \left(\boldsymbol{D}_0 \cdot \boldsymbol{\nabla}_0 \varphi + \theta \eta \right) \right) dV = 0. \tag{84}$$

Appyling the directionality property (77) for the discrete derivatives $\{D_{\boldsymbol{C}}\widehat{W}, D_{\boldsymbol{G}}\widehat{W}, D_C\widehat{W}, D_{\boldsymbol{D}_0}\widehat{W}, D_\theta \widehat{W}\}$ the above equation (84) yields the desired form

$$\Delta \left(\underbrace{\mathcal{K} + \int_{\mathcal{B}_0} (\widehat{W}(\boldsymbol{C}, \boldsymbol{G}, C, \boldsymbol{D}_0, \theta) + \boldsymbol{D}_0 \cdot \boldsymbol{\nabla}_0 \varphi + \theta \eta) \, dV}_{\mathcal{E}} \right) = 0. \tag{85}$$

Accordingly, neglecting external mechanical, electrical and thermal contributions the total energy $\mathcal{E}$ (72) of the nonlinear coupled system is conserved which is a primary goal of the proposed EM scheme.

6. Space discretization via the finite element method

For space discretization the finite element method is employed. Therfore the domain $\mathcal{B}_0$ described in Section 2.1 and represents a thermo-elastic continuum is sub-divided into a finite set of non-overlapping elements $e \in \mathbb{E}$ such that

$$\mathcal{B}_0 \approx \mathcal{B}_0^h = \bigcup_{e \in \mathbb{E}} \mathcal{B}_0^e. \tag{86}$$

The unknown fields $\{\boldsymbol{v}, \boldsymbol{\phi}, \varphi, \boldsymbol{D}_0, \theta\}$ in (73) are discretised employing the function spaces $\mathbb{V}^{\boldsymbol{\phi}^h} \times \mathbb{V}^{\boldsymbol{\phi}^h} \times \mathbb{V}^{\varphi^h} \times \mathbb{V}^{\boldsymbol{D}_0^h} \times \mathbb{V}^{\theta^h}$ given by

$$\mathbb{V}^{\boldsymbol{\phi}^h} = \{\boldsymbol{\phi} \in \mathbb{V}^{\boldsymbol{\phi}}; \quad \boldsymbol{\phi}^h\big|_{\mathcal{B}_0^e} = \sum_{a=1}^{n_{\text{node}}^{\boldsymbol{\phi}}} N_a^{\boldsymbol{\phi}} \boldsymbol{\phi}_a\}; \qquad \mathbb{V}^{\varphi^h} = \{\varphi \in \mathbb{V}^{\varphi}; \quad \varphi^h\big|_{\mathcal{B}_0^e} = \sum_{a=1}^{n_{\text{node}}^{\varphi}} N_a^{\varphi} \varphi_a\};$$

$$\mathbb{V}^{\boldsymbol{D}_0^h} = \{\boldsymbol{D}_0 \in \mathbb{V}^{\boldsymbol{D}_0}; \quad \boldsymbol{D}_0^h\big|_{\mathcal{B}_0^e} = \sum_{a=1}^{n_{\text{node}}^{\boldsymbol{D}_0}} N_a^{\boldsymbol{D}_0} \boldsymbol{D}_{0a}\}; \qquad \mathbb{V}^{\theta^h} = \{\theta \in \mathbb{V}^{\theta}; \quad \theta^h\big|_{\mathcal{B}_0^e} = \sum_{a=1}^{n_{\text{node}}^{\theta}} N_a^{\theta} \theta_a\}. \tag{87}$$

In the above for any field $n_{\text{node}}^{\boldsymbol{\mathcal{Y}}}$ denotes the number of nodes per element of the discretisation associated with associated field $\boldsymbol{\mathcal{Y}} \in \{\boldsymbol{\phi}, \varphi, \boldsymbol{D}_0, \theta\}$. Furthermore, the ath shape function $N_a^{\boldsymbol{\mathcal{Y}}} : \mathcal{B}_0^e \to \mathbb{R}$ is employed for the interpolation of fields $\boldsymbol{\mathcal{Y}}$ where $\boldsymbol{\mathcal{Y}}_a$ denotes the value of the field $\boldsymbol{\mathcal{Y}}$ at the ath node of a considered finite element. Employing a Bubnov-Galerkin approach, the function spaces for the test functions $\{\boldsymbol{w_v}, \boldsymbol{w_\phi}, w_\varphi, \boldsymbol{w_{D_0}}, w_\theta\} \in \mathbb{V}_0^{\boldsymbol{\phi}^h} \times \mathbb{V}_0^{\boldsymbol{\phi}^h} \times \mathbb{V}_0^{\varphi^h} \times \mathbb{V}_0^{\boldsymbol{D}_0^h} \times \mathbb{V}_0^{\theta^h}$ are provided by

$$\mathbb{V}_0^{\boldsymbol{\phi}^h} = \left\{ \forall \boldsymbol{\phi} \in \mathbb{V}^{\boldsymbol{\phi}^h}; \quad \boldsymbol{\phi}^h = \boldsymbol{0} \text{ on } \partial_\phi \mathcal{B}_0 \right\}; \qquad \mathbb{V}_0^{\varphi^h} = \left\{ \forall \varphi \in \mathbb{V}^{\varphi^h}; \quad \varphi^h = 0 \text{ on } \partial_\varphi \mathcal{B}_0 \right\};$$
$$\mathbb{V}_0^{\theta^h} = \left\{ \forall \theta \in \mathbb{V}^{\theta^h}; \quad \theta^h = 0 \text{ on } \partial_\theta \mathcal{B}_0 \right\}. \tag{88}$$

Although the time derivative of $\boldsymbol{\phi}$ and the velocity field $\boldsymbol{v}$ are imposed in a weak sense due to $(73)_a$, the consideration of equal function spaces for both fields, i.e. $\boldsymbol{\phi} \in \mathbb{V}^{\boldsymbol{\phi}}$ and $\boldsymbol{v} \in \mathbb{V}^{\boldsymbol{\phi}}$ enables the strong relation

$$\frac{\Delta \boldsymbol{\phi}}{\Delta t} = \boldsymbol{v}_{n+1/2}. \tag{89}$$

17

Applying the function spaces for $\boldsymbol{\mathcal{Y}}$ and $\boldsymbol{w_{\mathcal{Y}}}$ in (87) and (88) in (73) we obtain

$$
\begin{aligned}
(\mathcal{W}_{\boldsymbol{\phi}})_{\text{algo}} &= \sum_{e=1}^{N} \boldsymbol{w}_{\boldsymbol{\phi}_a} \cdot \boldsymbol{R}_{a,e}^{\boldsymbol{\phi}}; & (\mathcal{W}_{\varphi})_{\text{algo}} &= \sum_{e=1}^{N} w_{\varphi_a} R_{a,e}^{\varphi}; \\
(\mathcal{W}_{\boldsymbol{D}_0})_{\text{algo}} &= \sum_{e=1}^{N} \boldsymbol{w}_{\boldsymbol{D}_0 a} \cdot \boldsymbol{R}_{a,e}^{\boldsymbol{D}_0}; & (\mathcal{W}_{\theta})_{\text{algo}} &= \sum_{e=1}^{N} w_{\theta_a} R_{a,e}^{\theta},
\end{aligned}
\tag{90}
$$

where N is the total number of elements for the space discretisation and $\boldsymbol{R}_{a,e}^{\boldsymbol{\mathcal{Y}}}$ denote the residual contribution for field $\boldsymbol{\mathcal{Y}}$ given as[9]

$$
\begin{aligned}
\boldsymbol{R}_{a,e}^{\boldsymbol{\phi}} &= \int_{\mathcal{B}_0^e} \rho_0 N_{\boldsymbol{\phi}}^a \left(2\frac{\Delta\boldsymbol{\phi}}{\Delta t^2} - 2\frac{\boldsymbol{v}_n}{\Delta t} \right) dV + \int_{\mathcal{B}_0^e} \left(\boldsymbol{F}_{n+1/2} \boldsymbol{S}_{\text{algo}} \right) \boldsymbol{\nabla}_0 N_a^{\boldsymbol{\phi}} \, dV + \int_{\mathcal{B}_0^e} N_a^{\boldsymbol{\phi}} \boldsymbol{f}_{0_{n+1/2}} \, dV; \\
R_{a,e}^{\varphi} &= \int_{\mathcal{B}_0} \boldsymbol{D}_{0_{n+1/2}} \cdot \boldsymbol{\nabla}_0 N_a^{\varphi} \, dV + \int_{\mathcal{B}_0} \rho_{0_{n+1/2}}^e N_a^{\varphi} \, dV; \\
\boldsymbol{R}_{a,e}^{\boldsymbol{D}_0} &= \int_{\mathcal{B}_0} \left(\boldsymbol{E}_{0\text{algo}} + \boldsymbol{\nabla}_0 \varphi_{n+1/2} \right) N_a^{\boldsymbol{D}_0} \, dV; \\
R_{a,e}^{\theta} &= \int_{\mathcal{B}_0} \frac{\Delta(\theta\eta)}{\Delta t} N_a^{\theta} \, dV - \int_{\mathcal{B}_0} \frac{\Delta\theta}{\Delta t} \eta_{\text{algo}} N_a^{\theta} \, dV - \int_{\mathcal{B}_0} \boldsymbol{Q}_{n+1/2} \cdot \boldsymbol{\nabla}_0 N_a^{\theta} \, dV - \int_{\mathcal{B}_0} R_{\theta n+1/2} N_a^{\theta} \, dV.
\end{aligned}
\tag{91}
$$

In the above equation $(91)_a$ use has been made of (89) for the inertia term of the residual. For the whole system (91) a consistent linearisation has been carried out in order to compute the following examples properly in Section 7.

7. Numerical examples

In this section, the robustness and stability properties of the EM time integration scheme presented in Section 5 will be investigated in a variety of numerical examples. In particular, the long-term stability of the EM time integrator will be compared against that of the mid point time integrator, denoted as MP in the sequel.

In all the examples, the thermo-electro-mechanical constitutive model defined by means of the energy function $\widehat{W}(\boldsymbol{C}, \boldsymbol{G}, C, \boldsymbol{D}_0, \theta)$ in equations (42)-(43) will be used. Furthermore, the upper bound for the temperature field θ in equation (37) which compromises the stability conditions for the dual function $\Psi(\boldsymbol{F}, \boldsymbol{E}_0, \theta)$ in (14) will be computed and its possible violation will be monitored. With regards to the spatial discretisation, the following three families of Finite Elements will be employed throughout the examples section:

1 $H1^c H0^d$: continuous trilinear hexahedral elements (8 nodes) for $\{\boldsymbol{\phi}, \varphi, \theta\}$ and discontinuous constant hexahedral elements (1 node) for $\boldsymbol{D}_0$, see Fig. 2_a.

2 $P2^c P1^d$: continuous triquadratic tetrahedron elements (10 nodes) for $\{\boldsymbol{\phi}, \varphi, \theta\}$ and discontinuous trilinear tetrahedron elements (4 nodes) for $\boldsymbol{D}_0$, see Fig. 2_b.

3 $H2^c H1^d$: continuous triquadratic serenpedity-type hexahedral elements (20 nodes) for $\{\boldsymbol{\phi}, \varphi, \theta\}$ and discontinuous trilinear hexahedral elements (8 nodes) for $\boldsymbol{D}_0$, see Fig. 2_c.

---

[9]For the sake of simplicity, the external contributions on the boundary of the continuum have not been included in (91).
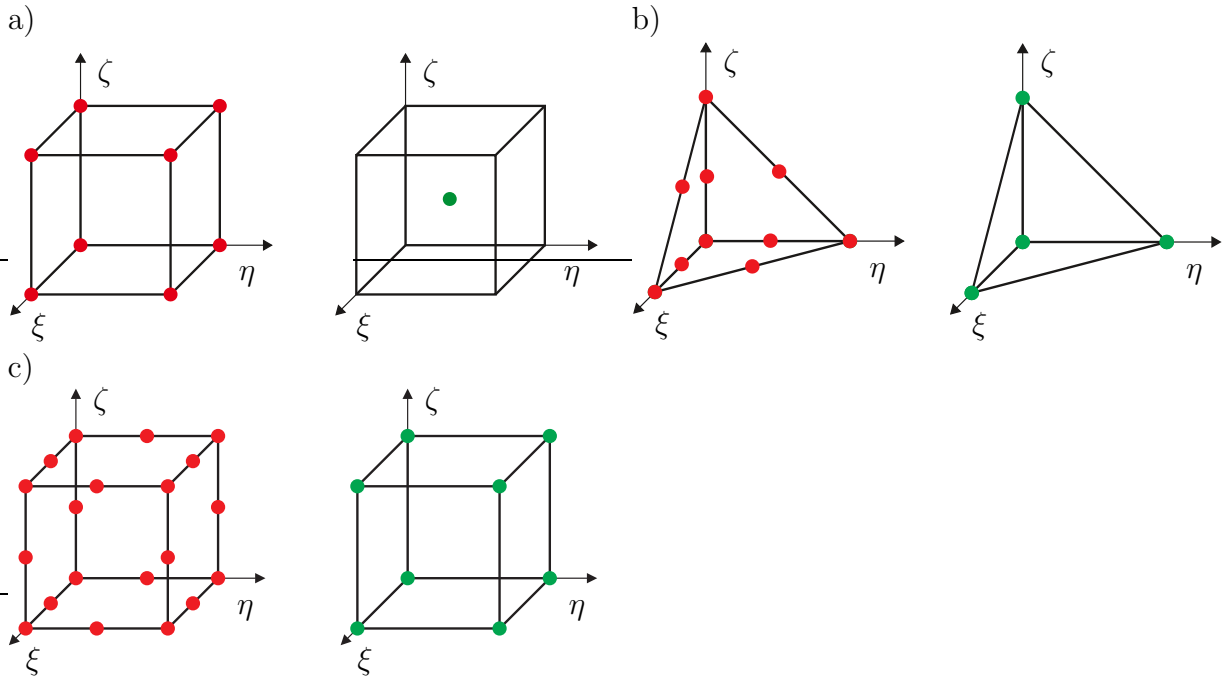
Figure 2: a) nodal points for the $H1^c H0^d$ element. b) nodal points for the $P2^c P1^d$ element. c) nodal points for the $H2^c H1^d$ element. Red bullets represent the nodes of the continuous fields and the green bullets represent the nodes of the discontinuous mixed field (cf. [17]).

Remark 4. *Note that the $H1^c H0^d$ element is not appropriate for modeling nearly incompressible materials. This can be addressed with a mixed formulation, e.g. employing a Hu-Washizu type formulation by augmenting the formulation via the fields $\{\mathbf{C}, \mathbf{G}, C\}$ and corresponding Lagrange multipliers $\{\boldsymbol{\Lambda}_{\mathbf{C}}, \boldsymbol{\Lambda}_{\mathbf{G}}, \Lambda_C\}$ (cf. [7, 17]) and will be dealt with in a follow up paper.*

First two static examples are introduced in order to show the element behavior of the three families described. Next, two dynamic examples are investigated.

7.1. Static examples

7.1.1. Patch test

The objective of this example is:

O1.I To verify the spatial discretisation/element formulation by means of the well-known three-dimensional patch test (see [16 **?** , 17]).

With the patch test, the ability to reproduce homogeneous states of stress of the mixed element formulation, electrical potential and temperature is examined. A cubic domain $\mathcal{B}_0$ with dimensions $(0,1)[\mathrm{m}] \times (0,1)[\mathrm{m}] \times (0,1)[\mathrm{m}]$ is considered (see Fig. 3). Dirichlet boundary conditions on the displacement field are employed on the faces at $x_i = 0$ where $i = 1, 2, 3$ and are fixed in the respective $\mathbf{e}_i$-directions such that only expansions into the $\mathbf{e}_1$-$\mathbf{e}_2$-plane are permitted. An incremental Dirichlet boundary condition is applied on the top face (face at $x_3 = 1$, see Fig. 3 left) in order to reduce the initial length of the $\mathbf{e}_3$-dimension by a factor of two. Zero Dirichlet boundary conditions are imposed on the face $x_1 = 0$. The full list of the employed simulation parameters is provided by Tab. 1[10]. The von Mises stress distribution is computed via

$$\sigma_{vM} = \sqrt{\sigma_{11}^2 + \sigma_{22}^2 + \sigma_{33}^2 - \sigma_{11}\,\sigma_{22} - \sigma_{11}\,\sigma_{33} - \sigma_{22}\,\sigma_{33} + 3\,(\sigma_{12}^2 + \sigma_{13}^2 + \sigma_{23}^2)}, \tag{92}$$

---

[10]Note that we use $\epsilon_1 = 10^5\,\epsilon_2$ and $\epsilon_2 = \epsilon_r\,\epsilon_0$. This results in an almost vanishing effect of the invariant associated with ϵ_1 in equation $(43)_1$.

where σ_{ij}, $i,j = 1,2,3$. The electrical potential and the temperature distribution are shown in Fig. 4 for the regular mesh and for the initially distorted mesh, respectively. As depicted in Fig. 4, homogeneous states of von Mises stress, electrical potential and temperature distribution are obtained, e.g. patch test requirement is achieved by the proposed element formulation. Identical results as shown in Fig. 4 are obtained for an *H1H0* mesh but are not shown here for the sake of overview.

mechanical parameters	μ_1	1662.5	Pa	geometry
	μ_2	332.5	Pa	
	λ	10000	Pa	
	e	5209	Pa	
specific heat capacity	κ	100	$\text{JK}^{-1}\text{m}^{-3}$	
coupling coefficient	β	$2.233 \cdot 10^{-4}$	K^{-1}	
thermal conductivity	k_0	10	$\text{WK}^{-1}\text{m}^{-1}$	
reference Temperature	θ_R	293.15	K	
Electrical parameters	ϵ_0	8.854×10^{-12}	$\text{A}^2\,\text{s}^4\,\text{kg}^{-1}\,\text{m}^{-3}$	
	ϵ_r	4	$-$	
Ref. potential	φ_0	0	V	
Mass density	ρ_0	0	kgm^{-3}	
Newton tolerance	ϵ	$1 \cdot 10^{-6}$	-	
simulation duration	T	1	s	
timestep/increment size	Δt	0.1	s	

Table 1: Patch test: Material and simulation parameters.

With regards to the upper bound θ_{cr} in equation (37), for the material parameters in Table 1 we obtain an estimate (assuming $J \approx 1$) of

$$\theta_{cr} = \theta_R \left(1 + \frac{\frac{\mu_1 + 2\mu_2}{J^2} + \lambda}{6\beta e \theta_R} \right) \approx 779\,K, \tag{93}$$

which is well above the values of θ obtained in this numerical example.
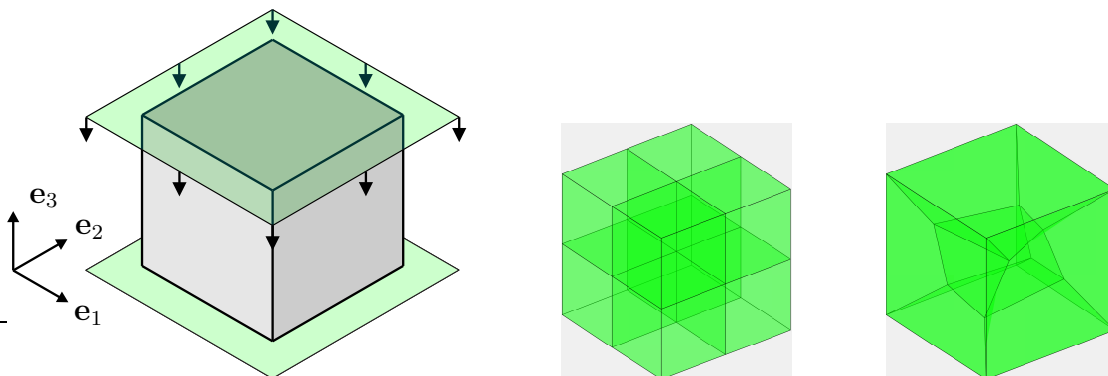
Figure 3: Patch test: Boundary conditions (left), initial regular mesh (middle) and initial distorted mesh (right).
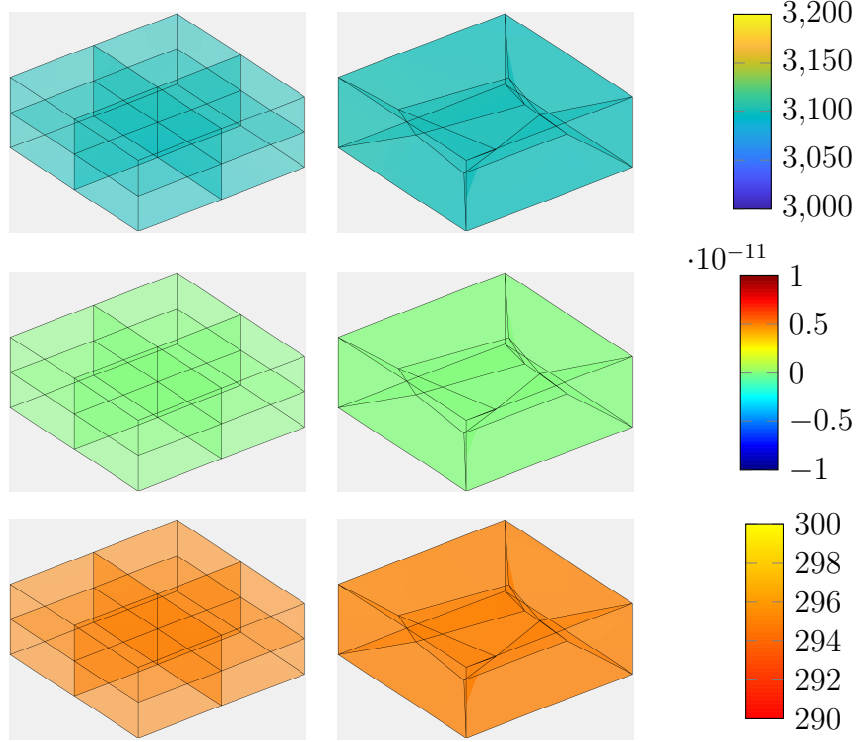
Figure 4: Patch test: Von Mises stress distribution σ_{vM} [Pa] (top), electrical potential distribution φ [V] (mid) and temperature distribution θ [K] (bottom) with regular (left) and initially distorted (right) meshes.

7.1.2. Analytical convergence analysis

The objective of this example is:

O2.I To verify the p-order of the accuracy of the various families of Finite Elements considering, namely the $P2^cP1^d$, $H1^cH0^d$ and $H2^cH1^d$ elements (see [17?] for more details).

mechanical parameters	μ_1, μ_2	2	Pa	geometry
mechanical parameters	c, e	1	Pa	
specific heat capacity	κ	1	$JK^{-1}m^{-3}$	
coupling coefficient	β	$2.233 \cdot 10^{-4}$	K^{-1}	
thermal conductivity	k_0	0.1	$WK^{-1}m^{-1}$	
reference Temperature	θ_R	293.15	K	
Electrical parameters	ϵ_0	8.854×10^{-12}	$A^2\,s^4\,kg^{-1}\,m^{-3}$	
	ϵ_r	4	$-$	
Ref. potential	φ_0	0	V	
Mass density	ρ_0	0	kgm^{-3}	
Newton tolerance	ϵ	$1 \cdot 10^{-6}$	-	
simulation duration	T	1	s	
timestep/increment size	Δt	0.05	s	

Table 2: Analytical convergence analysis: Material and simulation parameters for patch tests.
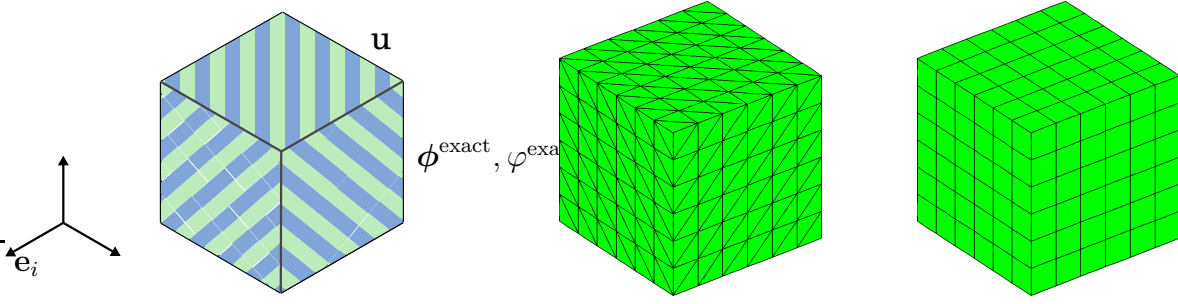
Figure 5: Analytical convergence analysis: Outer faces (patterned surfaces) are imposed with Dirichlet boundary conditions for ϕ^{exact}, φ^{exact} and θ^{exact} given in (95) (left). Typical $P2^cP1^d$ (centred) and $H2^cH1^d$ (right) meshes are shown, respectively.

The convergence analysis of an *ad-hoc* manufactured problem is carried out next (cf. [17?]) where time dependent effects are neglected, i.e. stationary heat conduction and no inertia effects[11]. For this, the cubic domain $\mathcal{B}_0$ of dimensions $(0,1)[\text{m}] \times (0,1)[\text{m}] \times (0,1)[\text{m}]$ shown in Fig. 5 is considered. In particular, geometry, boundary conditions and material parameters are provided in Tab. 2 and Fig. 5. The following exact fields associated with the deformed configuration ϕ^{exact}, the electrical potential φ^{exact} and the thermal field θ^{exact} are defined as

$$\phi^{\text{exact}} = \mathbf{X} + \gamma_1 \sin(X)\,\mathbf{E}_1 + \gamma_2 \cos(Y)\,\mathbf{E}_2 + \gamma_3 (\sin(Z) + \cos(Z))\,\mathbf{E}_3; \tag{94}$$

$$\varphi^{\text{exact}} = \tilde{\varphi}_0\,X; \tag{95}$$

$$\theta^{\text{exact}} = \tilde{\theta}_0\,Y, \tag{96}$$

where $\gamma_i = \frac{i}{2}\,10^{-1}$, $i = 1, 2, 3$, $\tilde{\varphi}_0 = 100$ and $\tilde{\theta}_0 = 10$ (cf. [17]). Based on $\{\phi^{\text{exact}}, \varphi^{\text{exact}}, \theta^{\text{exact}}\}$, it is now possible to derive:

- the (exact) deformation gradient tensor ($\boldsymbol{F}^{\text{exact}} := \boldsymbol{\nabla}_0 \phi^{\text{exact}}$)

$$\boldsymbol{F}^{\text{exact}} = (1 + \gamma_1 \cos(X))\,\mathbf{E}_1 \otimes \mathbf{E}_1 + (1 - \gamma_2 \sin(Y))\,\mathbf{E}_2 \otimes \mathbf{E}_2 + (1 + \gamma_3 (\cos(Z) - \sin(Z)))\,\mathbf{E}_3 \otimes \mathbf{E}_3,$$

- the co-factor and determinant of $\boldsymbol{F}^{exact}$

$$\boldsymbol{H}^{\text{exact}} = \frac{1}{2}\,\boldsymbol{F}^{\text{exact}} \times \boldsymbol{F}^{\text{exact}}; \quad J^{\text{exact}} = \frac{1}{3}\,\boldsymbol{H}^{\text{exact}} : \boldsymbol{F}^{\text{exact}}$$

- the Cauchy-Green tensor, its co-factor and its determinant

$$\boldsymbol{C}^{\text{exact}} = \boldsymbol{F}^{\text{exact}\,T} \boldsymbol{F}^{\text{exact}}; \quad \boldsymbol{G}^{\text{exact}} = \frac{1}{2}\,\boldsymbol{C}^{\text{exact}} \times \boldsymbol{C}^{\text{exact}}; \quad C^{\text{exact}} = \frac{1}{3}\,\boldsymbol{G}^{\text{exact}} : \boldsymbol{C}^{\text{exact}}$$

- the (exact) electric field and electric displacement field

$$\boldsymbol{E}_0^{\text{exact}} = -\boldsymbol{\nabla}_0 \varphi^{\text{exact}} = -\varphi_0 \cos(X)\,\boldsymbol{E}_1;$$

$$\boldsymbol{E}_0^{\text{exact}} = \partial_{\boldsymbol{D}_0} \widehat{W}^{\text{exact}} = \frac{1}{\varepsilon_r \varepsilon_0 (C^{\text{exact}})^{1/2}} \boldsymbol{C}^{\text{exact}} \boldsymbol{D}_0^{\text{exact}} \Rightarrow \quad \boldsymbol{D}_0^{\text{exact}} = \varepsilon_r\,\varepsilon_0\,(C^{\text{exact}})^{1/2}\,(\boldsymbol{C}^{\text{exact}})^{-1}\,\boldsymbol{E}_0^{\text{exact}},$$

$$\tag{97}$$

- the material heat flux $\boldsymbol{Q}^{\text{exact}}$ in (63), namely

$$\boldsymbol{Q}^{\text{exact}} = -J^{\text{exact}} \boldsymbol{H}^{\text{exact}} \boldsymbol{k} \left(\boldsymbol{H}^{\text{exact}}\right)^T \boldsymbol{\nabla}_0 \theta^{\text{exact}}, \tag{98}$$

---

[11]In contrast to the patch test example 7.1.1, the proposed integrator cannot be used within this full static example.

- the second Piola-Kirchhoff stress tensor is computed via

$$\boldsymbol{S}^{\text{exact}} = 2(\partial_{\boldsymbol{C}}\widehat{W}^{\text{exact}} + \partial_{\boldsymbol{G}}\widehat{W}^{\text{exact}} \times \boldsymbol{C}^{\text{exact}} + \partial_C\widehat{W}^{\text{exact}}\,\boldsymbol{G}^{\text{exact}}), \tag{99}$$

With the above exact quantities we are able to compute from the static/time independent version of $(2)_a$, $(3)_a$ and $(6)_a$ the body force $\boldsymbol{f}_0^{\text{exact}}$, the volume density charge $(\rho_0^e)^{\text{exact}}$ and the heat source R_θ^{exact} as follows

$$\boldsymbol{f}_0^{\text{exat}} = -\text{DIV}(\boldsymbol{F}^{\text{exact}}\,\boldsymbol{S}^{\text{exact}}); \quad (\rho_0^e)^{\text{exact}} = \text{DIV}(\boldsymbol{D}_0^{\text{exact}}); \quad R_\theta^{\text{exact}} = \text{DIV}(\boldsymbol{Q}^{\text{exact}}). \tag{100}$$

The exact solutions (94)-(96) are imposed as a Dirichlet boundary at the surfaces of the body (see Fig. 5). Furthermore the above analytically computed volumetric load $\boldsymbol{f}_0^{\text{exat}}$, charge density $(\rho_0^e)^{\text{exact}}$ and heat source R_θ^{exact} are imposed within the body. Finally, exact solutions (94)-(96) are compared against the numerical solutions obtained by imposing the analytically computed Dirichlet boundaries and volume influences. In particular, the h-convergence rate for displacement $\boldsymbol{\phi}$, electrical potential φ, thermal field θ and electrical displacement $\mathbf{D}_0$ is computed by employing the L^2 norm of the error, i.e.

$$\|e_\bullet\|_{L^2} = \frac{\|(\bullet) - (\bullet)^{\text{exact}}\|_{L^2}}{\|(\bullet)^{\text{exact}}\|_{L^2}}, \tag{101}$$

where $(\bullet)$ denotes the numerically computed variable and $(\bullet^{\text{exact}})$ its analytical counterpart. A numerical solution with von Mises stress, electrical potential distribution and thermal field is depicted in Fig. 6 for the $P2^cP1^d$ and $H2^cH1^d$ elements. Fig. 7 shows the convergence results for all variables.
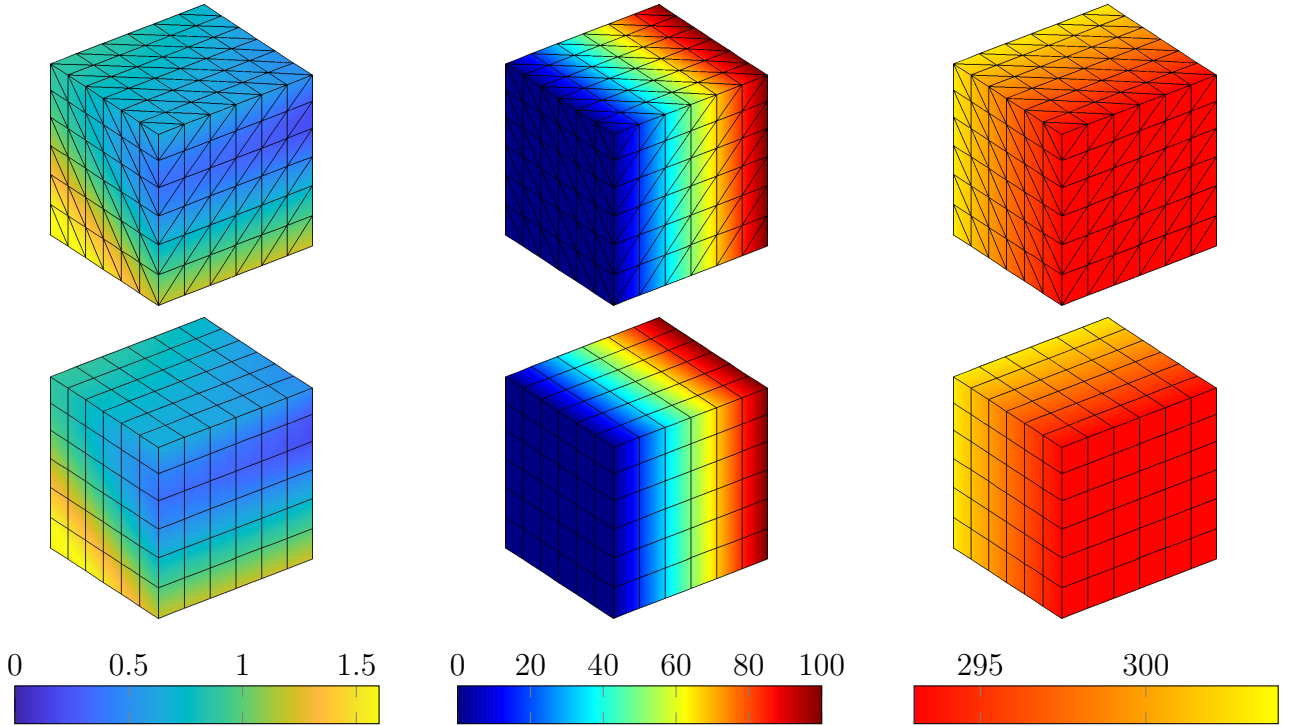
Figure 6: Static convergence analysis: Von Mises stress σ_{vM} [Pa] (left), electrical potential distribution φ [V] (mid) and thermal field θ [K] (right) for $P2^cP1^d$ (top) and $H2^cH1^d$ (bottom) meshes, respectively.

As expected $p+1$ convergence is observed for all the fields for the $P2^cP1^d$ elements, since the convergence is optimal for this element (see Fig. 7). For the primary fields $\boldsymbol{\phi}$ and φ the convergence observed for the $H2^cH1^d$ elements is even slightly better. Expected p-order convergence is also observed for all the fields in the $H1^cH0^d$ element.
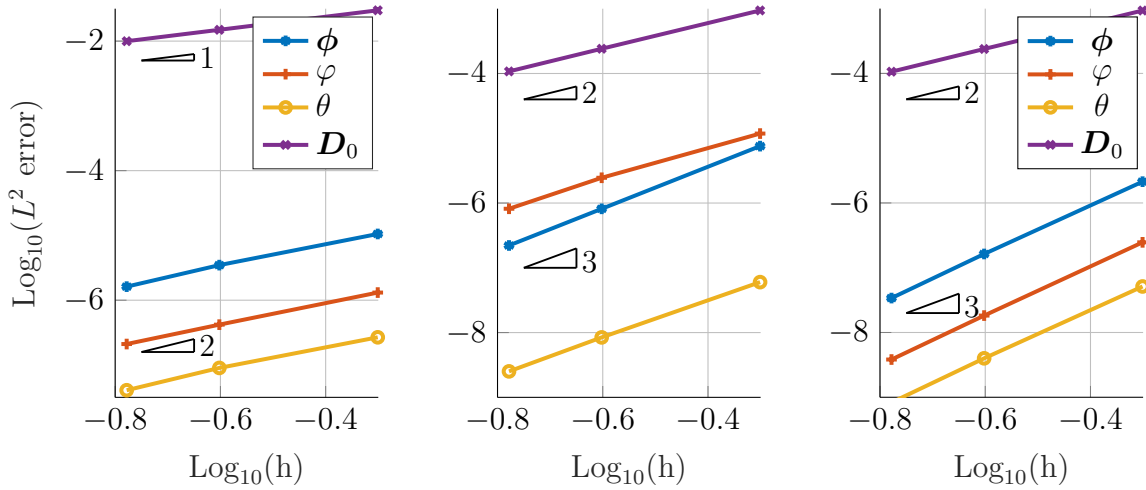
Figure 7: Spatial convergence analysis for $H1^c H0^d$ (left), $P2^c P1^d$ (mid) and $H2^c H1^d$ (right) elements.

With regard to the upper bound θ_{cr} in equation (37), for the material parameters in Table 1 we obtain an estimate (assuming $J \approx 1$) of

$$\theta_{cr} = \theta_0 \left(1 + \frac{\frac{\mu_1 + 2\mu_2}{J^2} + \lambda}{6\beta e \theta_0} \right) \approx 5517\,K, \tag{102}$$

which is well above the values of θ obtained in this numerical example.

7.2. Transient examples

Full transient simulations are investigated in the following. In particular the performance and robustness properties of the newly proposed integrator are investigated when compared to a standard midpoint integration scheme.

7.2.1. Flying L-shaped block

The objectives of this example are:

O4.I Show the conserving properties of the EM integrator.

O4.II Show the second order accuracy the the EM integrator.

O4.III Compare the robustness and long-term stability of the EM integrator against that of the MP time integrator.

In this example, the L-shaped body depicted in Fig. 8 is considered. Note this example is inspired by the third example given in [16]. The body is free in space and the geometry of the body is specified in Tab. 3. Time-dependent electrical Dirichlet boundaries and pressure loads are applied as shown in Fig. 8 (left).
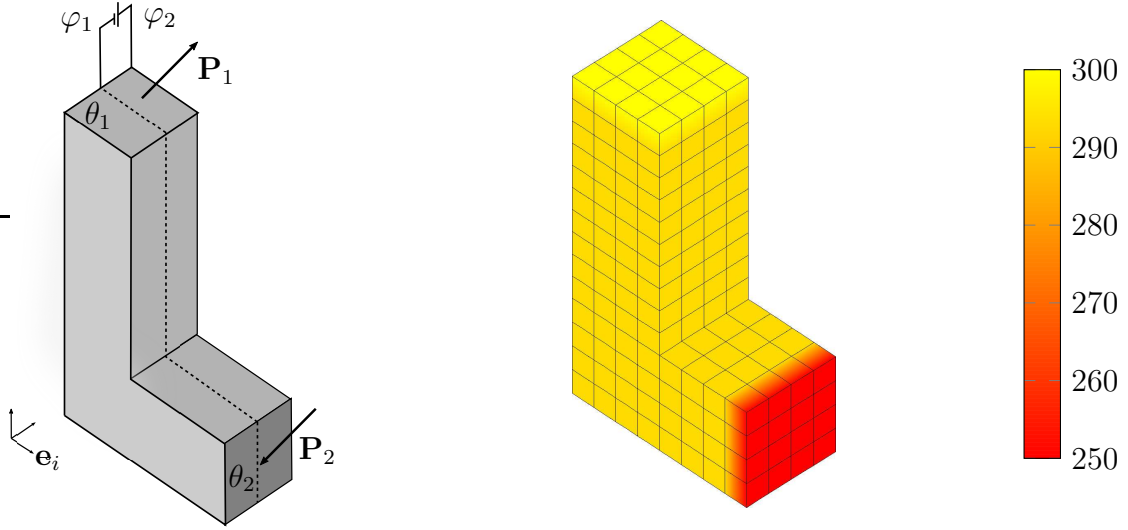
Figure 8: Flying L-shaped block: Mechanical boundary conditions (left), initial temperature conditions θ [K] (right), and discretisation (right).

In particular the time-dependent electrical Dirichlet boundaries are prescribed by

$$\varphi_1(X, Y = -1.5, Z) = 0, \quad \varphi_2(X, Y = 0, Z) = \begin{cases} 6\,e6\,\sin(\frac{\pi}{2}\frac{t}{5}) & \text{for} \quad t \leq 5\text{s} \\ 6\,e6 & \text{for} \quad t > 5\text{s} \end{cases}.$$

Furthermore the dead load pressures are given by

$$\mathbf{P}_1(t) = -\mathbf{P}_2(t) = f(t) \begin{pmatrix} 256/9 \\ 512/9 \\ 768/9 \end{pmatrix} \frac{\text{N}}{\text{m}^2}, \quad \text{with} \quad f(t) = \begin{cases} t & \text{for} \quad t \leq 2.5\text{s} \\ 5 - t & \text{for} \quad 2.5 \leq t \leq 5\text{s} \\ 0 & \text{for} \quad t > 5\text{s} \end{cases} \tag{103}$$

As indicated in Fig. 8 (right) two faces of the block are subjected to initial temperature conditions. The temperature of these faces deviates from the initially homogeneous temperature distribution of the solid. It is important to remark that for the applied $H2^c H1^d$ elements a linear temperature distribution is assumed within the first face elements in direction of the bulk as can be observed in Fig. 8 (right). For the discretisation of the L-shaped block $H2^c H1^d$ elements with in total 89440 degrees of freedom are applied (see Fig. 8). The material parameters and simulation parameter for this example are summarized in Tab. 3.

Table 3: Flying L-shaped block: thermo-electro-elastic compressible Mooney-Rivlin material data, simulation parameters and geometry.

				geometry
mechanical parameters	μ_1	1662.5	Pa	
	μ_2	332.5	Pa	
	λ	0	Pa	
	e	1000	Pa	
specific heat capacity	κ	100	$\mathrm{JK^{-1}m^{-3}}$	
coupling coefficient	β	$2.233 \cdot 10^{-4}$	$\mathrm{K^{-1}}$	
thermal conductivity	k_0	10	$\mathrm{WK^{-1}m^{-1}}$	
reference temperature	θ_R	293.15	K	
Electrical parameters	ϵ_0	8.854×10^{-12}	$\mathrm{A^2\,s^4\,kg^{-1}\,m^{-3}}$	
	ϵ_r	4	$-$	
Ref. potential	φ_0	0	V	
density	ρ_0	100	$\mathrm{kgm^{-3}}$	
initial temperature	θ_1	300	K	
	θ_2	250	K	
Newton tolerance	ϵ	10^{-4}	-	
simulation duration	T	100	s	
timestep size	Δt	0.8	s	

Due the chosen material parameters and boundary conditions, the L-shaped block undergoes large deformations, rotations, translations, temperature and electrical potential evolutions. After the loading phase only a constant electrical potential field is applied, such that for this isolated system with $t > 5$s the total linear momentum, angular momentum and energy are conserving quantities, respectively. In Figures 9 and 10, the evolution of the angular momentum for the EM consistent and the MP integrator is shown, illustrating how the EM integrator conserves angular momentum throughout the entire simulation. In Fig. 11 the energy evolution of the EM consistent and the MP integrator is shown. The EM scheme correctly reproduces conservation of energy and is numerically stable during the simulation. In contrast to that the MP integrator becomes unstable accompanied by an energy blow-up. In Fig. 12 the change of energy of the EM scheme is shown. As can be observed the change of the energy is (nearly) bounded by the chosen Newton tolerance (see Tab. 3).
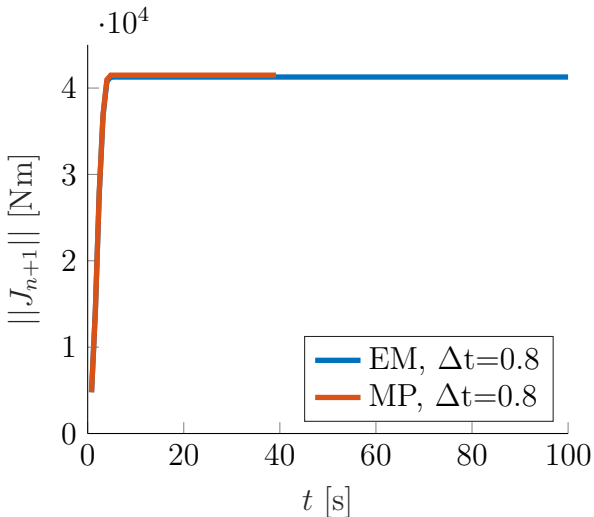
Figure 9: Total angular momentum evolution.
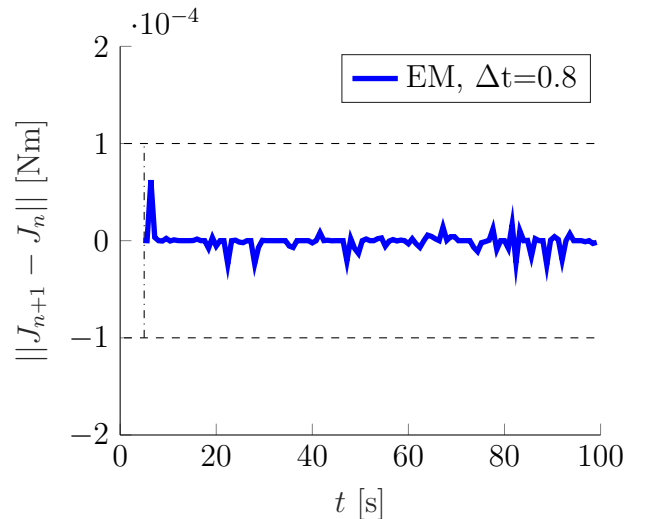
Figure 10: Discrete angular momentum difference.
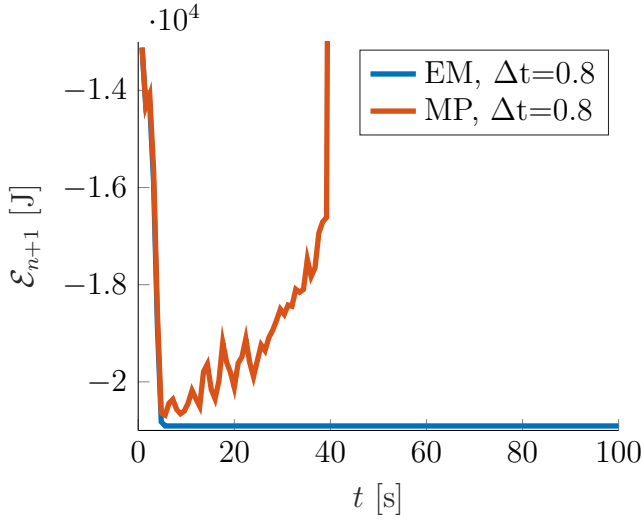
Figure 11: Total energy evolution.
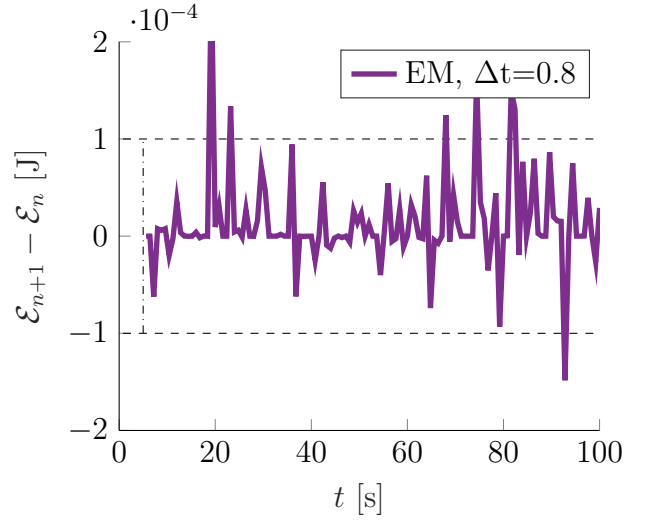
Figure 12: Discrete energy difference.

Furthermore, the order of accuracy of the EM integration scheme is shown which is expected to be of second-order. In this gard the L_2 norm of the error of quantity $(\bullet)$ can be computed with

$$||\mathbf{e}||_{L_2} = \frac{||(\bullet) - (\bullet)_r||_{L_2}}{||(\bullet)_r||_{L_2}}, \tag{104}$$

where

$$||(\bullet)||_{L_2} = \left[\int_{\mathcal{B}_r} ((\bullet) : (\bullet)) \, dV \right]^{\frac{1}{2}}. \tag{105}$$

In the above, $(\bullet)_r$ denote the reference solution of $\{\boldsymbol{\phi}, \varphi, \theta, \boldsymbol{D}_0\}$, respectively computed by a very small time-step size. For this the time interval after the loading phase, i.e. $5 \leq t \leq 5.1$ is taken into account. In Fig. 13 second order accuracy in time (specific slopes are $\{\boldsymbol{\phi}, \varphi, \theta, \boldsymbol{D}_0\} = \{1.8557, 1.8684, 2.0118, 1.8432\}$) of the proposed integration scheme is shown.
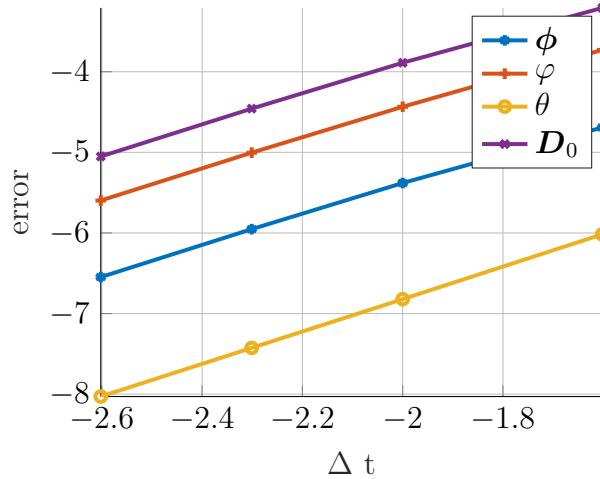
Figure 13: Study of convergence of the error.

The motion of the L-shaped block and its contour plot temperature distribution are shown in Fig. 14, whilst the von Mises stress distribution is shown in Fig. 15.

With regards to the upper bound θ_{cr} in equation (37), for the material parameters in Table 1, we obtained an estimate (we monitored J all over the Gauss points and time steps and obtained that $0.8 \leq J \leq 1.2$) of

$$\theta_{cr} = \theta_R \left(1 + \frac{\frac{\mu_1 + 2\mu_2}{1.2^2} + \lambda}{6\beta e \theta_R} \right) \approx 1329.29 \, K, \tag{106}$$

27
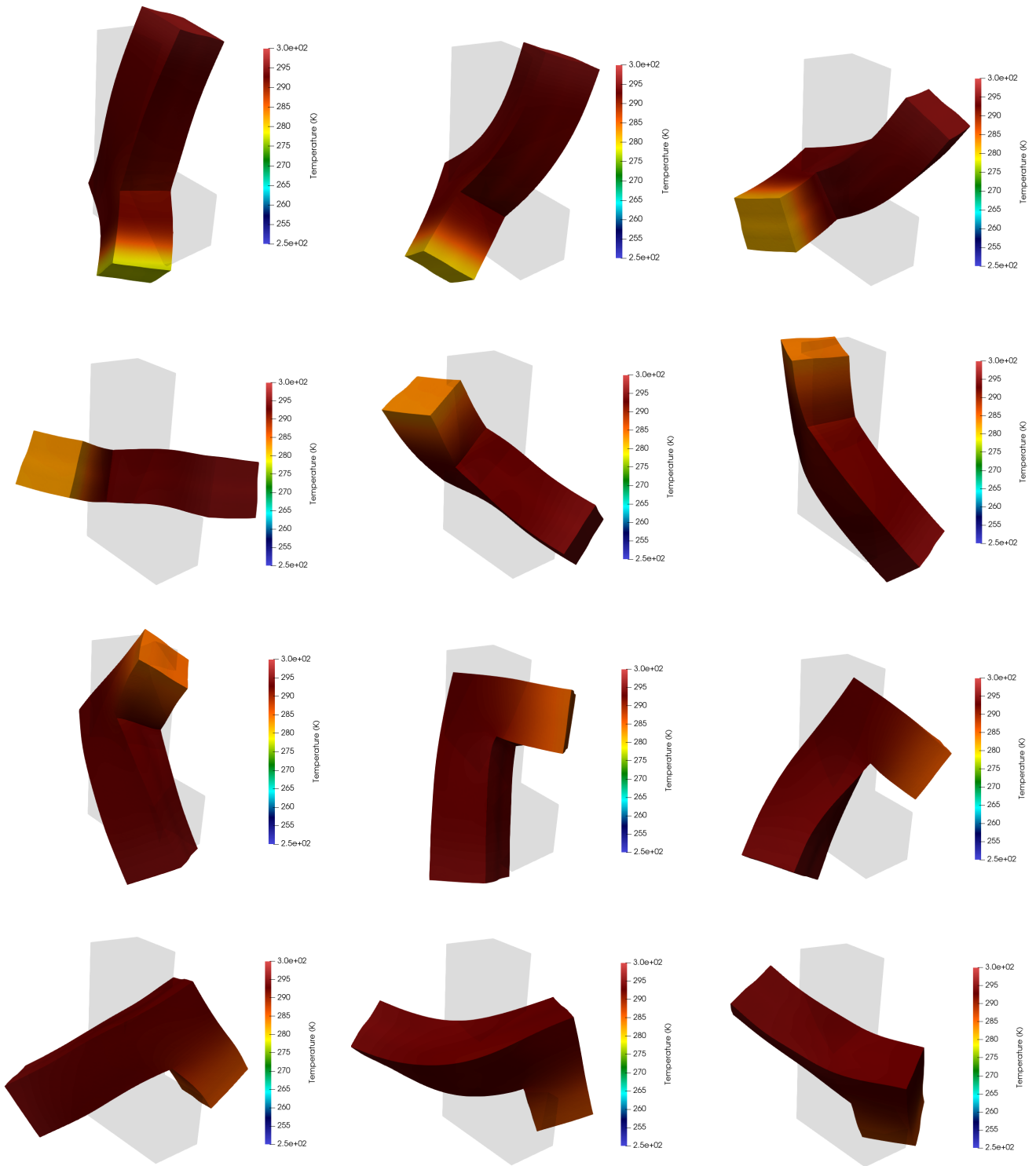
Figure 14: Flying L-shaped block: temperature field T for different configurations corresponding to (left to right-top to bottom): (a) $t = \{1.6, 3.2, 4.8, 6.4, 8, 9.6, 11.2, 12.8, 14.4, 16, 17.8, 19.4\}\ s$.
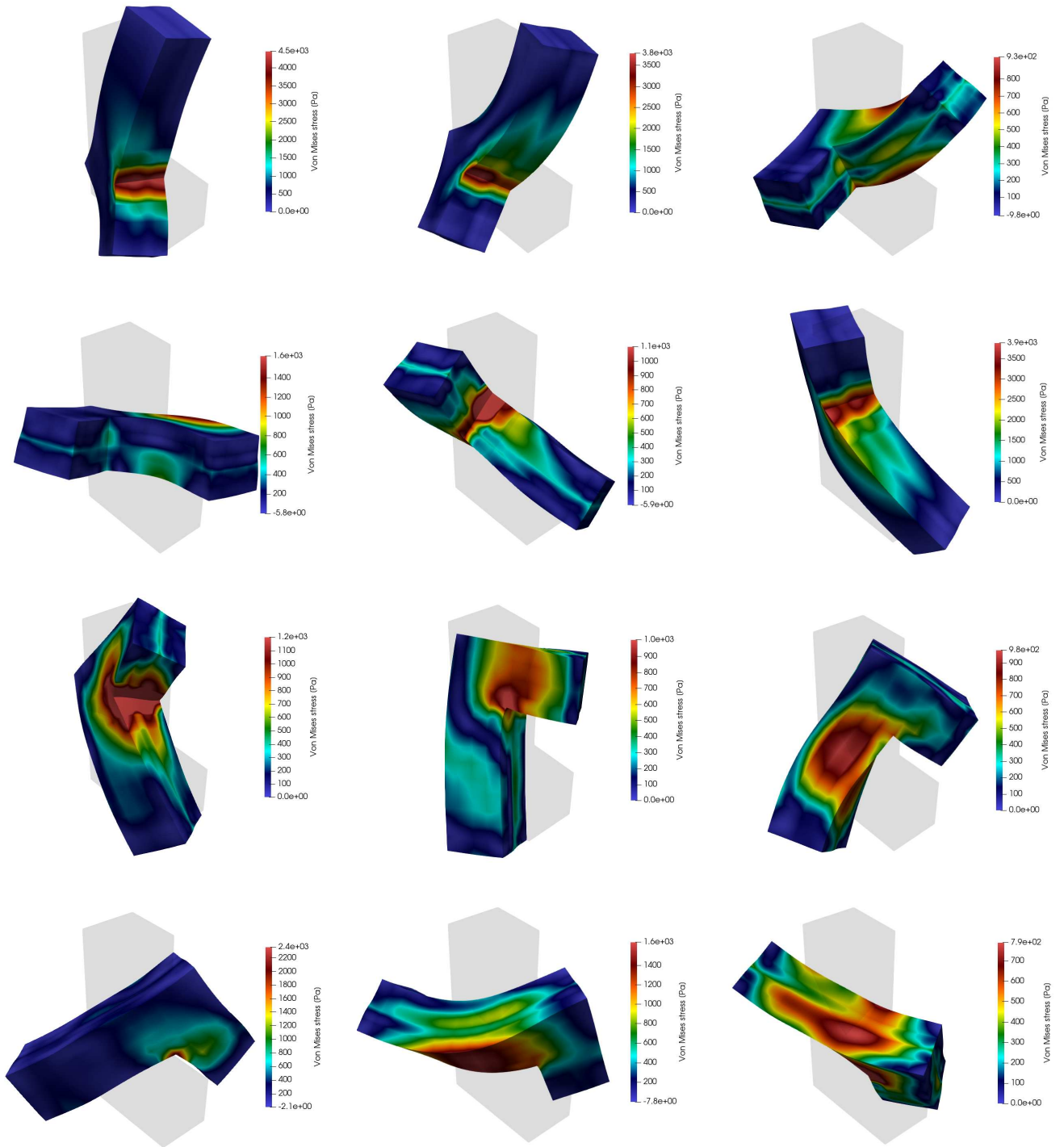
Figure 15: Flying L-shaped block: vom Mises stress σ_{vM} for different configurations corresponding to (left to right-top to bottom): $t = \{1.6, 3.2, 4.8, 6.4, 8, 9.6, 11.2, 12.8, 14.4, 16, 17.8, 19.4\}\, s$.

which is well above the values of θ obtained in this numerical example.

7.2.2. Dielectric plate with heating spot

The objective of this example is:

O4.I Comparison of the robustness between the proposed EM time integrator and the MP rule time integrator in scenarios with more sophisticated electrical and thermal induced configurations which can represent a challenge from the robustness standpoint of the algorithm.

mechanical parameters	μ_1	2e5	Pa	geometry
	μ_2	2e5	Pa	
	λ	10000	Pa	
	e	5209	Pa	
specific heat capacity	κ	100	$JK^{-1}m^{-3}$	
coupling coefficient	β	$2.233 \cdot 10^{-4}$	K^{-1}	
thermal conductivity	k_0	10	$WK^{-1}m^{-1}$	
reference temperature	θ_R	293.15	K	
Electrical parameters	ϵ_0	8.854×10^{-12}	$A^2 s^4 kg^{-1} m^{-3}$	
	ϵ_r	4	$-$	
Ref. potential	φ_0	0	V	
density	ρ_0	1	kgm^{-3}	
Newton tolerance	ϵ	10^{-3}	-	
simulation duration	T	3	s	
timestep size	Δt	0.05	s	

Table 4: Dielectric plate with heating spot: Material parameters, simulation parameters and geometry.
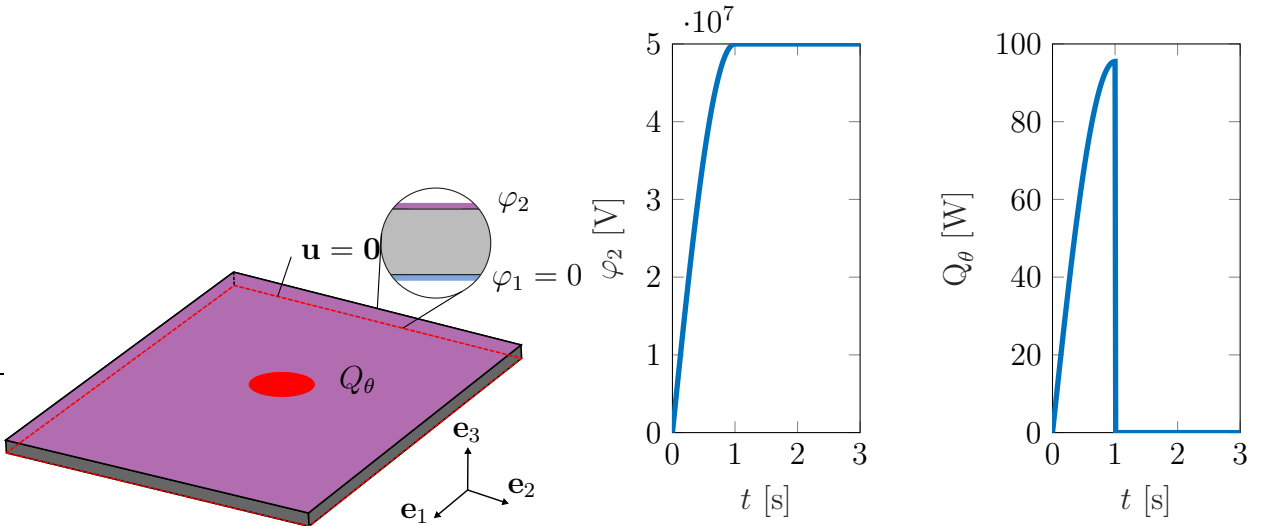
Figure 16: Dielectric plate with heating spot: Mechanical boundary conditions (left) where $\mathbf{u}(X_1 = 0, X_2, X_3 = 0) = \mathbf{u}(X_1 = 100, X_2, X_3 = 0) = \mathbf{u}(X_1, X_2 = 0, X_3 = 0) = \mathbf{u}(X_1, X_2 = 100, X_3 = 0) = \mathbf{0}$ and applied electric potentials φ_1, φ_2 (mid) corresponding to (107) and heat flow Q_θ (right) corresponding to (108).

The geometry, boundary conditions, material and simulation parameters of the dielectric plate with heating spot are depicted in Tab. 4 and Fig. 16. Note that this example is inspired by [**?**

, Sect. 4.6.4.] and the seventh example in [17]. The applied mesh (see Fig. 18) with $H2^cH1^d$ elements consists in total of 8425 (condensed) degrees of freedom. The following time dependent electric potential Dirichlet boundaries according to Fig. 16 are employed

$$\varphi_1 = 0 \; ; \quad \varphi_2 = \left(5 \times 10^7\right) \times \begin{cases} \sin(\frac{\pi}{2} \frac{t}{1}) & \text{for } t \leq 1\,\text{s} \\ 1 & \text{for } t > 1\,\text{s} \end{cases} \; [V]. \tag{107}$$

Furthermore a sinusoidal heat flow Q_θ into the system given by

$$Q_\theta = \frac{7.5e3}{A_0} f(t), \quad f(t) = \begin{cases} \sin(\frac{\pi}{2} \frac{t}{1}) & \text{for } t \leq 1\,\text{s} \\ 0 & \text{for } t > 1\,\text{s} \end{cases} \; [W], \tag{108}$$

where $A_0 = \pi\,r^2$, $r = 2.5$ heats up the center of the plate. Fig. 17 (left) shows that the midpoint-rule time integrator exhibits an energy blow-up and becomes unstable. In contrast, the newly proposed EM time integrator conserves the total energy after the loading phase and remains stable for the whole simulation for the same fixed time step size of $\Delta t = 0.05\,s$. Furthermore, Fig. 17 (right) shows that the energy difference $(\mathcal{E}_{n+1} - \mathcal{E}_n)$ is perfectly bounded to the applied Newton tolerance (see Tab. 4). Snapshots of the motion with the von Mises stress distribution are shown in Fig. 18 and Fig. 19, respectively. In addition, Figure 20 shows the temperature distribution for different time snapshots. These figures illustrate the wrinkling pattern that unfolds over the surface of the Dielectric Elastomer. These wrinkles develop as a result of the specific boundary conditions considered. Similar wrinkling pattern with the same boundary conditions but in a quasistatic scenario has also been obtained numerically in Reference [?].
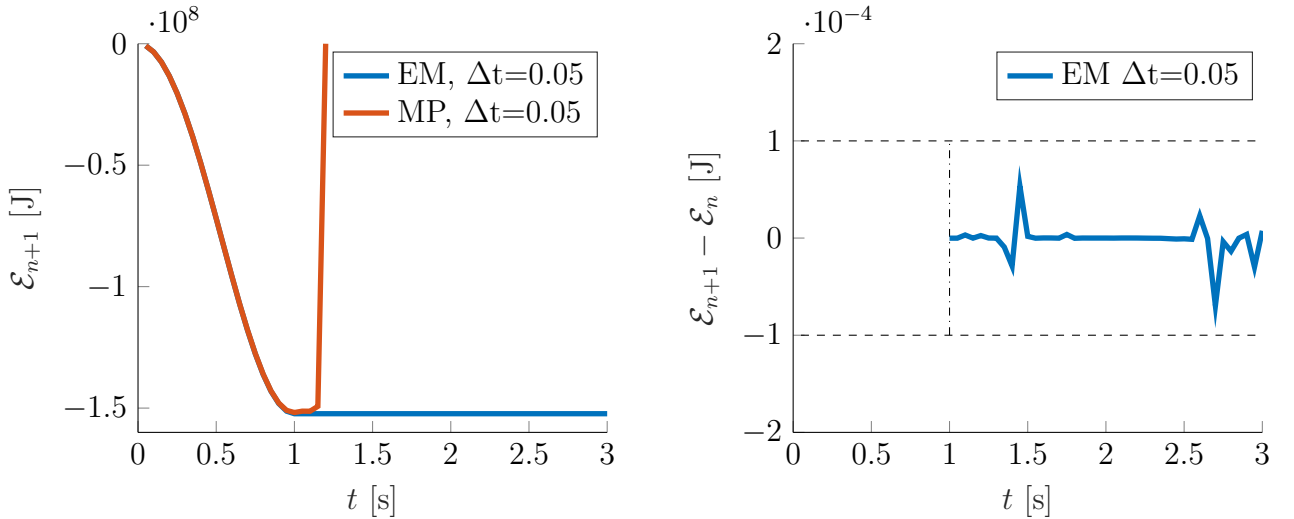
Figure 17: Dielectric plate with heating spot: Energy evolution for the proposed EM scheme. Left: Time evolution of $\mathcal{E}_{\widetilde{W}}$ for proposed scheme. Right: Time evolution of $\Delta\mathcal{E}_{\widetilde{W}}$ in the time interval $[1,3]$.

Finally, with regards to the upper bound θ_{cr} in equation (37), for the material parameters in Table 1 we obtain an estimate (assuming $J \approx 1$) of

$$\theta_{cr} = \theta_R \left(1 + \frac{\frac{\mu_1 + 2\mu_2}{J^2} + \lambda}{6\beta e\theta_R}\right) \approx 8770\,K, \tag{109}$$

which is well above the values of θ obtained in this numerical example.
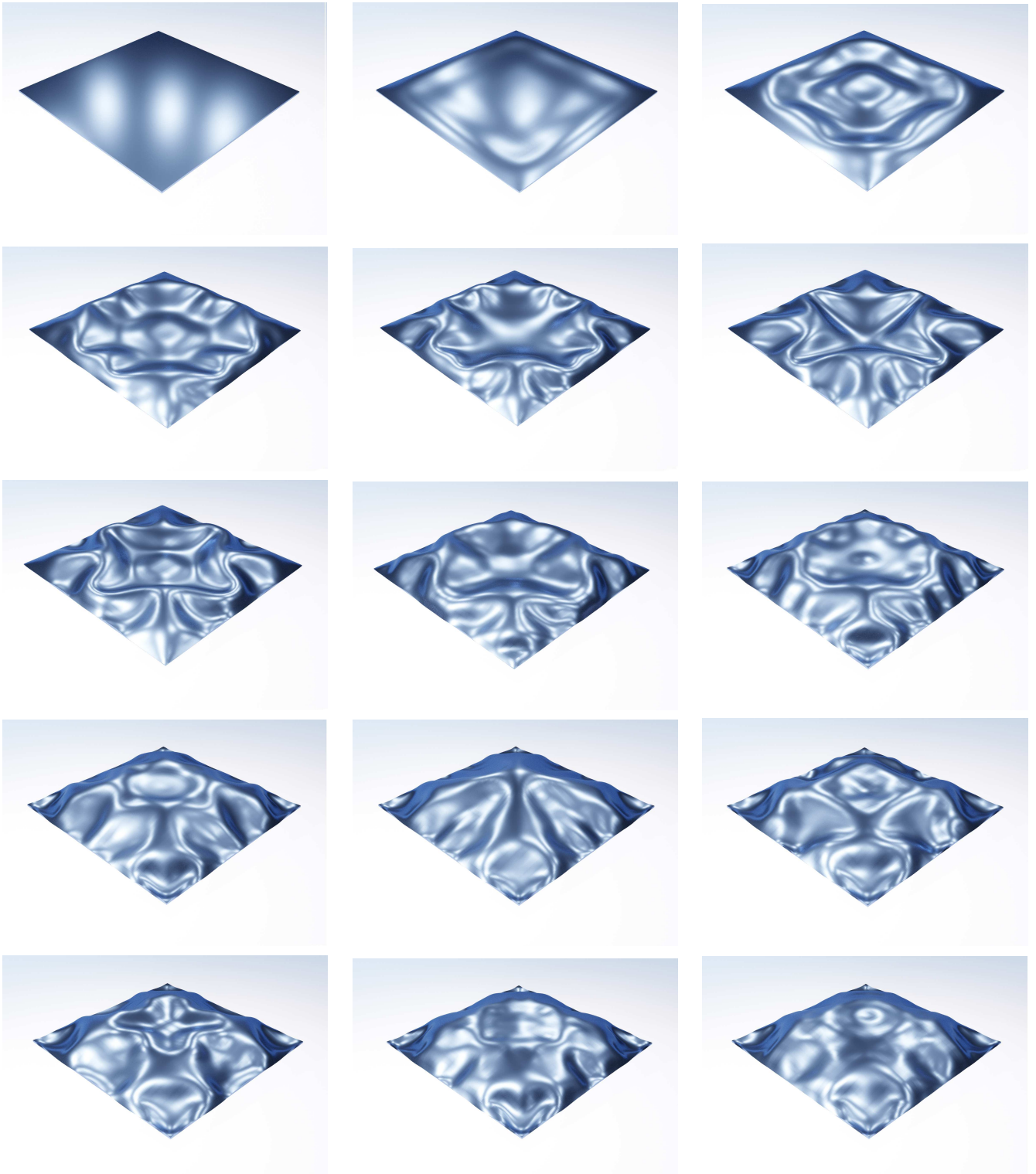
Figure 18: Dielectric plate with heating spot: Wrinkling patterns for different configurations corresponding to (left to right-top to bottom): $t = \{0.1, 0.3, 0.5, 0.7, 0.9, 1.1, 1.3, 1.5, 1.7, 1.9, 2.1, 2.3, 2.5, 2.7, 2.9\}\,s$.
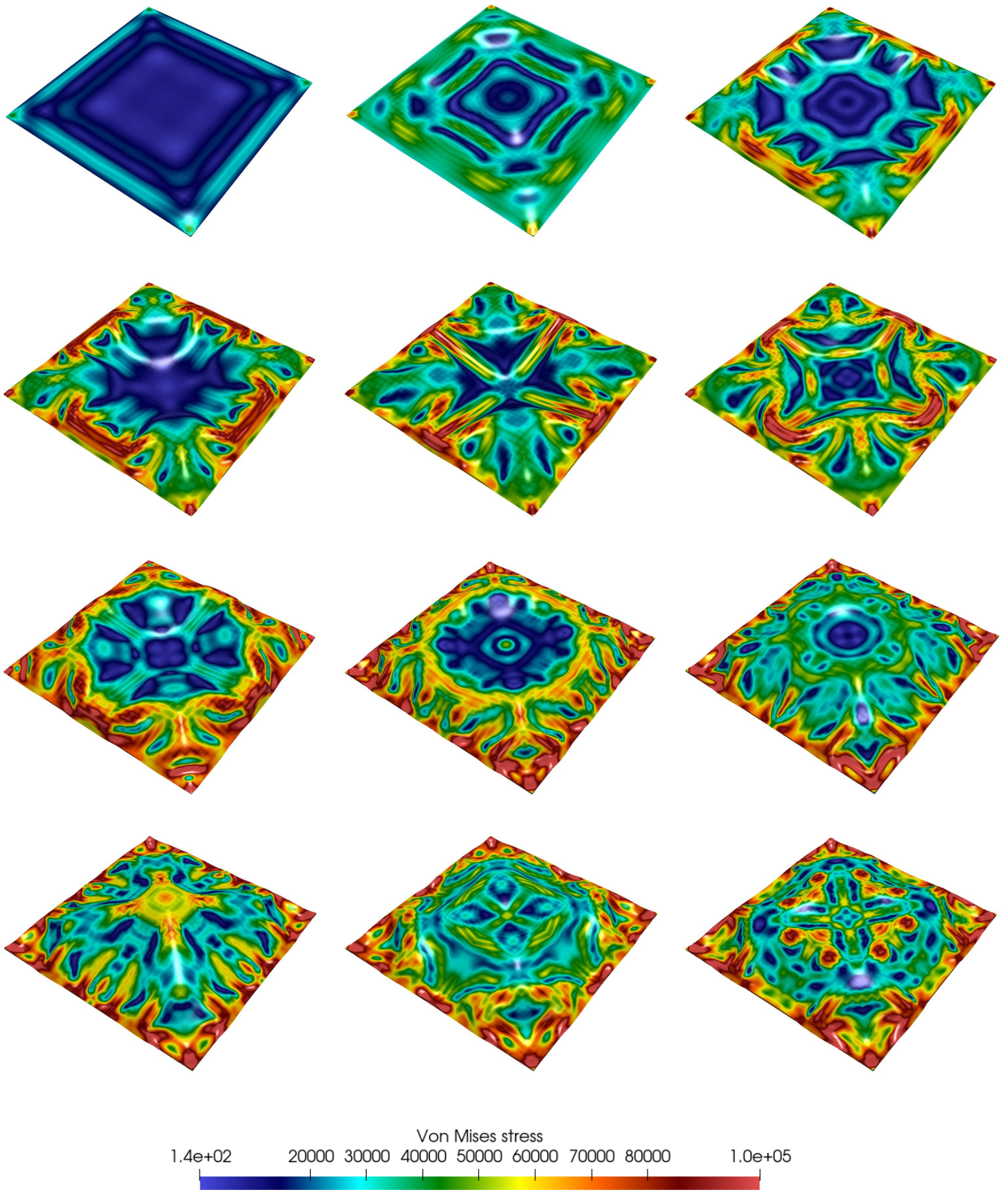
Figure 19: Dielectric plate with heating spot: Snapshots of von Mises stress σ_{vM} [Pa] for different configurations corresponding to (left to right-top to bottom): $t = \{0.1, 0.3, 0.5, 0.7, 0.9, 1.1, 1.3, 1.5, 1.7, 2.1, 2.3, 2.7\}\, s$.
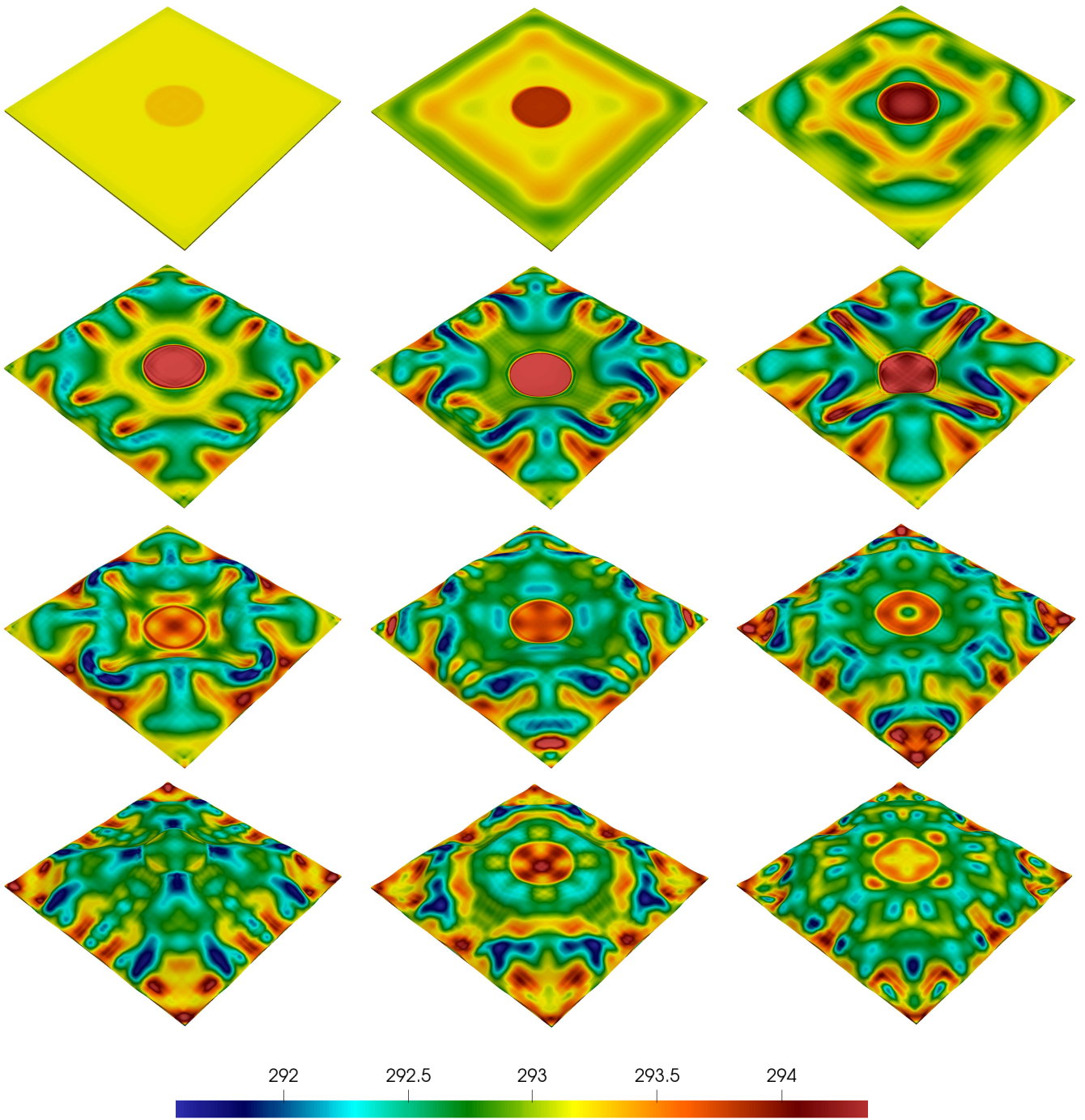
Figure 20: Dielectric plate with heating spot: Snapshots of temperature T [K] for different configurations corresponding to (left to right-top to bottom): $t = \{0.1, 0.3, 0.5, 0.7, 0.9, 1.1, 1.3, 1.5, 1.7, 2.1, 2.3, 2.7\}\,s$.

8. Conclusions

The aim of this paper is the design of a new one-step implicit and thermodynamically consistent Energy-Momentum (EM) preserving time integration scheme for the simulation of thermo-electro-elastic processes undergoing large deformations. The time integration scheme takes advantage of the notion of polyconvexity and of a new tensor cross product algebra, which are shown to be crucial in order to derive the discrete derivatives, fundamental for the construction of the algorithmic derived variables, namely the second Piola-Kirchhoff stress tensor, the entropy and the electric field. These two ingredients, namely polyconvexity and the tensor cross product, enable the derivation of very simple discrete derivatives, circumventing one of the main downsides of EM time integration schemes. The proposed scheme inherits the advantages of new EM schemes recently published in the context of thermo-elasticity [32] and electro-mechanics [17, 29], whilst extending those previous works to the more generic case of nonlinear thermo-electro-mechanics. A thorough study on suitable convexity/concavity restrictions that the thermo-electro-mechanical strain energy functions must comply with has been presented in this paper, where we have finally advocated for polyconvex functions in the electro-mechanics physics whilst concave with respect to the temperature field. Furthermore, a series of numerical examples have been presented in order to investigate the robustness and stability properties of the new EM scheme.

9. Acknowledgements

Appendix A. Computation of the discrete derivatives

By introducing the following notation $\{\mathcal{V}_1, \mathcal{V}_2, \mathcal{V}_3, \mathcal{V}_4, \mathcal{V}_5\} = \{\boldsymbol{C}, \boldsymbol{G}, C, \boldsymbol{D}_0, \theta\}$ we are able to define the discrete derivatives $D_{\widehat{\mathcal{V}}_1}\widehat{W} = D_{\boldsymbol{C}}\widehat{W}$, $D_{\widehat{\mathcal{V}}_2}\widehat{W} = D_{\boldsymbol{G}}\widehat{W}$, $D_{\widehat{\mathcal{V}}_3}\widehat{W} = D_C\widehat{W}$, $D_{\widehat{\mathcal{V}}_4}\widehat{W} = D_{\boldsymbol{D}_0}\widehat{W}$ and $D_{\widehat{\mathcal{V}}_5}\widehat{W} = D_\theta\widehat{W}$ in $(73)_d$. These are defined as

$$D_{\widehat{\mathcal{V}}_i}\widehat{W} = \frac{1}{2}\left(D_{\widehat{\mathcal{V}}_{i_{n+1,n}}}\widehat{W} + D_{\widehat{\mathcal{V}}_{i_{n,n+1}}}\widehat{W}\right); \qquad i \in Y = \{1,2,3,4,5\};$$

$$D_{\widehat{\mathcal{V}}_{i_{n+1,n}}}\widehat{W} = \left.D_{\widehat{\mathcal{V}}_i}\widehat{W}\left(\widehat{\mathcal{V}}_{i_{n+1}}, \widehat{\mathcal{V}}_{i_n}\right)\right|_{\widehat{\mathcal{V}}_{j_{n+1}}, \widehat{\mathcal{V}}_{k_n}}; \qquad \forall j \in Y : j < i; \ \forall k \in Y : k > i; \qquad \text{(A.1)}$$

$$D_{\widehat{\mathcal{V}}_{i_{n,n+1}}}\widehat{W} = \left.D_{\widehat{\mathcal{V}}_i}\widehat{W}\left(\widehat{\mathcal{V}}_{i_n}, \widehat{\mathcal{V}}_{i_{n+1}}\right)\right|_{\widehat{\mathcal{V}}_{j_n}, \widehat{\mathcal{V}}_{k_{n+1}}}; \qquad \forall j \in Y : j < i; \ \forall k \in Y : k > i.$$

In the above equation the discrete operators $\left.D_{\widehat{\mathcal{V}}_i}\widehat{W}\right|_{\widehat{\mathcal{V}}_{j_{n+1}}, \widehat{\mathcal{V}}_{k_n}}$ and $\left.D_{\widehat{\mathcal{V}}_i}\widehat{W}\right|_{\widehat{\mathcal{V}}_{j_n}, \widehat{\mathcal{V}}_{k_{n+1}}}$ can be computed with

$$\left.D_{\widehat{\mathcal{V}}_i}\widehat{W}\right|_{\widehat{\mathcal{V}}_{j_{n+1}}, \widehat{\mathcal{V}}_{k_n}} = \left.\partial_{\widehat{\mathcal{V}}_i}\widehat{W}\left(\widehat{\mathcal{V}}_{n+1/2}\right)\right|_{\widehat{\mathcal{V}}_{j_{n+1}}, \widehat{\mathcal{V}}_{k_n}}$$
$$+ \frac{\left.\widehat{W}\left(\widehat{\mathcal{V}}_{n+1}\right)\right|_{\widehat{\mathcal{V}}_{j_{n+1}}, \widehat{\mathcal{V}}_{k_n}} - \left.\widehat{W}\left(\widehat{\mathcal{V}}_n\right)\right|_{\widehat{\mathcal{V}}_{j_{n+1}}, \widehat{\mathcal{V}}_{k_n}} - \left.\partial_{\widehat{\mathcal{V}}_i}\widehat{W}\left(\widehat{\mathcal{V}}_{n+1/2}\right)\right|_{\widehat{\mathcal{V}}_{j_{n+1}}, \widehat{\mathcal{V}}_{k_n}} : \Delta\widehat{\mathcal{V}}_i}{||\Delta\widehat{\mathcal{V}}_i||^2}\Delta\widehat{\mathcal{V}}_i;$$

$$\left.D_{\widehat{\mathcal{V}}_i}\widehat{W}\right|_{\widehat{\mathcal{V}}_{j_n}, \widehat{\mathcal{V}}_{k_{n+1}}} = \left.\partial_{\widehat{\mathcal{V}}_i}\widehat{W}\left(\widehat{\mathcal{V}}_{n+1/2}\right)\right|_{\widehat{\mathcal{V}}_{j_n}, \widehat{\mathcal{V}}_{k_{n+1}}}$$
$$+ \frac{\left.\widehat{W}\left(\widehat{\mathcal{V}}_{n+1}\right)\right|_{\widehat{\mathcal{V}}_{j_n}, \widehat{\mathcal{V}}_{k_{n+1}}} - \left.\widehat{W}\left(\widehat{\mathcal{V}}_n\right)\right|_{\widehat{\mathcal{V}}_{j_n}, \widehat{\mathcal{V}}_{k_{n+1}}} - \left.\partial_{\widehat{\mathcal{V}}_i}\widehat{W}\left(\widehat{\mathcal{V}}_{n+1/2}\right)\right|_{\widehat{\mathcal{V}}_{j_n}, \widehat{\mathcal{V}}_{k_{n+1}}} : \Delta\widehat{\mathcal{V}}_i}{||\Delta\widehat{\mathcal{V}}_i||^2}\Delta\widehat{\mathcal{V}}_i.$$

$$\text{(A.2)}$$

Employing the set $\widehat{\mathcal{V}}_{\boldsymbol{C}} = \widehat{\mathcal{V}} \setminus \{\boldsymbol{C}\}$, i.e. $\mathcal{V}_{\boldsymbol{C}} = \{\boldsymbol{G}, C, \boldsymbol{D}_0, \theta\}$ we are able to compute the directional derivative $D_{\boldsymbol{C}}\widehat{W}$ from equations (A.1) and (A.2) as

$$D_{\boldsymbol{C}}\widehat{W} = \frac{1}{2}\left(\partial_{\boldsymbol{C}}\widehat{W}\left(\boldsymbol{C}_{n+1/2}, \widehat{\mathcal{V}}_{1_{n+1}}\right) + \partial_{\boldsymbol{C}}\widehat{W}\left(\boldsymbol{C}_{n+1/2}, \widehat{\mathcal{V}}_{\boldsymbol{C}_n}\right)\right)$$
$$+ \frac{1}{2}\frac{\widehat{W}\left(\boldsymbol{C}_{n+1}, \widehat{\mathcal{V}}_{1_{n+1}}\right) - \widehat{W}\left(\boldsymbol{C}_n, \widehat{\mathcal{V}}_{1_{n+1}}\right)}{||\Delta\boldsymbol{C}||^2}\Delta\boldsymbol{C} + \frac{1}{2}\frac{\widehat{W}\left(\boldsymbol{C}_{n+1}, \widehat{\mathcal{V}}_{\boldsymbol{C}_n}\right) - \widehat{W}\left(\boldsymbol{C}_n, \widehat{\mathcal{V}}_{\boldsymbol{C}_n}\right)}{||\Delta\boldsymbol{C}||^2}\Delta\boldsymbol{C}$$
$$- \frac{1}{2}\frac{\partial_{\boldsymbol{C}}\widehat{W}\left(\boldsymbol{C}_{n+1/2}, \widehat{\mathcal{V}}_{1_{n+1}}\right) : \Delta\boldsymbol{C}}{||\Delta\boldsymbol{C}||^2}\Delta\boldsymbol{C} - \frac{1}{2}\frac{\partial_{\boldsymbol{C}}\widehat{W}\left(\boldsymbol{C}_{n+1/2}, \widehat{\mathcal{V}}_{\boldsymbol{C}_n}\right) : \Delta\boldsymbol{C}}{||\Delta\boldsymbol{C}||^2}\Delta\boldsymbol{C}.$$

$$\text{(A.3)}$$

For the above equation, the discrete derivatives with respect to $\boldsymbol{C}$ with $\widehat{\mathcal{V}}_{\boldsymbol{C}_{n+1}}$ and $\widehat{\mathcal{V}}_{\boldsymbol{C}_n}$ are kept fixed, accordingly

$$D_{\boldsymbol{C}}\widehat{W}(\bullet, \widehat{\mathcal{V}}_{\boldsymbol{C}_{n+1}}) := \partial_{\boldsymbol{C}}\widehat{W}\left(\boldsymbol{C}_{n+1/2}, \widehat{\mathcal{V}}_{\boldsymbol{C}_{n+1}}\right)$$
$$+ \frac{\widehat{W}\left(\boldsymbol{C}_{n+1}, \widehat{\mathcal{V}}_{\boldsymbol{C}_{n+1}}\right) - \widehat{W}\left(\boldsymbol{C}_n, \widehat{\mathcal{V}}_{\boldsymbol{C}_{n+1}}\right) - \partial_{\boldsymbol{C}}\widehat{W}\left(\boldsymbol{C}_{n+1/2}, \widehat{\mathcal{V}}_{\boldsymbol{C}_{n+1}}\right) : \Delta\boldsymbol{C}}{||\Delta\boldsymbol{C}||^2}\Delta\boldsymbol{C};$$

$$D_{\boldsymbol{C}}\widehat{W}(\bullet, \widehat{\mathcal{V}}_{\boldsymbol{C}_n}) := \partial_{\boldsymbol{C}}\widehat{W}\left(\boldsymbol{C}_{n+1/2}, \widehat{\mathcal{V}}_{\boldsymbol{C}_n}\right)$$
$$+ \frac{\widehat{W}\left(\boldsymbol{C}_{n+1}, \widehat{\mathcal{V}}_{\boldsymbol{C}_n}\right) - \widehat{W}\left(\boldsymbol{C}_n, \widehat{\mathcal{V}}_{\boldsymbol{C}_n}\right) - \partial_{\boldsymbol{C}}\widehat{W}\left(\boldsymbol{C}_{n+1/2}, \widehat{\mathcal{V}}_{\boldsymbol{C}_n}\right) : \Delta\boldsymbol{C}}{||\Delta\boldsymbol{C}||^2}\Delta\boldsymbol{C}.$$

$$\text{(A.4)}$$

Finally (A.3) can be written in a convenient manner as

$$D_{\boldsymbol{C}}\widehat{W} = \frac{1}{2}\left(D_{\boldsymbol{C}}\widehat{W}(\bullet, \widehat{\mathcal{V}}_{\boldsymbol{C}_{n+1}}) + D_{\boldsymbol{C}}\widehat{W}(\bullet, \widehat{\mathcal{V}}_{\boldsymbol{C}_n})\right). \tag{A.5}$$

In analogy to the above the following sets $\widehat{\mathcal{V}}_{\boldsymbol{G}} = \widehat{\mathcal{V}} \setminus \{\boldsymbol{G}\}$, $\widehat{\mathcal{V}}_C = \widehat{\mathcal{V}} \setminus \{C\}$, $\widehat{\mathcal{V}}_{\boldsymbol{D}_0} = \widehat{\mathcal{V}} \setminus \{\boldsymbol{D}_0\}$ and $\widehat{\mathcal{V}}_\theta = \widehat{\mathcal{V}} \setminus \{\theta\}$ are defined. With that it is possible to compute the following directional derivatives as

$$\begin{aligned}
D_{\boldsymbol{G}}\widehat{W} &= \frac{1}{2}\left(D_{\boldsymbol{G}}\widehat{W}(\bullet, \mathcal{V}_{\boldsymbol{G}_{n+1}}) + D_{\boldsymbol{G}}\widehat{W}(\bullet, \mathcal{V}_{\boldsymbol{G}_n})\right); \\
D_C\widehat{W} &= \frac{1}{2}\left(D_C\widehat{W}(\bullet, \mathcal{V}_{C_{n+1}}) + D_C\widehat{W}(\bullet, \mathcal{V}_{C_n})\right); \\
D_{\boldsymbol{D}_0}\widehat{W} &= \frac{1}{2}\left(D_{\boldsymbol{D}_0}\widehat{W}(\bullet, \mathcal{V}_{\boldsymbol{D}_{0,n+1}}) + D_{\boldsymbol{D}_0}\widehat{W}(\bullet, \mathcal{V}_{\boldsymbol{D}_{0,n}})\right); \\
D_\theta\widehat{W} &= \frac{1}{2}\left(D_\theta\widehat{W}(\bullet, \mathcal{V}_{\theta_{n+1}}) + D_\theta\widehat{W}(\bullet, \mathcal{V}_{\theta_n})\right).
\end{aligned} \tag{A.6}$$

Appendix B. Proof of directionality property

In the following the definition of the discrete derivatives of the internal energy $\widehat{W}(\boldsymbol{C}, \boldsymbol{G}, C, \boldsymbol{D}_0, \theta)$ in (A.1) and (A.2) is validated for satisfying the directionality property in (77). Therefore the expression on the left-hand side of the directionality property in (77) is given by

$$\mathcal{T} = D_{\boldsymbol{C}}W : \Delta\boldsymbol{C} + D_{\boldsymbol{G}}W : \Delta\boldsymbol{G} + D_CW\Delta C + D_{\boldsymbol{D}_0}W \cdot \Delta\boldsymbol{D}_0 + D_\theta W \cdot \Delta\theta. \tag{B.1}$$

Inserting (A.3), (A.6)$_{a-d}$ into (B.1) yields

$$\begin{aligned}
\mathcal{T} = &\frac{1}{2}\widehat{W}(\boldsymbol{C}_{n+1}, \boldsymbol{G}_{n+1}, C_{n+1}, \boldsymbol{D}_{0,n+1}, \theta_{n+1}) - \frac{1}{2}\widehat{W}(\boldsymbol{C}_n, \boldsymbol{G}_{n+1}, C_{n+1}, \boldsymbol{D}_{0,n+1}, \theta_{n+1}) \\
&+ \frac{1}{2}\widehat{W}(\boldsymbol{C}_{n+1}, \boldsymbol{G}_n, C_n, \boldsymbol{D}_{0,n}, \theta_n) - \frac{1}{2}\widehat{W}(\boldsymbol{C}_n, \boldsymbol{G}_n, C_n, \boldsymbol{D}_{0,n}, \theta_n) \\
&+ \frac{1}{2}\widehat{W}(\boldsymbol{C}_n, \boldsymbol{G}_{n+1}, C_{n+1}, \boldsymbol{D}_{0,n+1}, \theta_{n+1}) - \frac{1}{2}\widehat{W}(\boldsymbol{C}_n, \boldsymbol{G}_n, C_{n+1}, \boldsymbol{D}_{0,n+1}, \theta_{n+1}) \\
&+ \frac{1}{2}\widehat{W}(\boldsymbol{C}_{n+1}, \boldsymbol{G}_{n+1}, C_n, \boldsymbol{D}_{0,n}, \theta_n) - \frac{1}{2}\widehat{W}(\boldsymbol{C}_{n+1}, \boldsymbol{G}_n, C_n, \boldsymbol{D}_{0,n}, \theta_n) \\
&+ \frac{1}{2}\widehat{W}(\boldsymbol{C}_n, \boldsymbol{G}_n, C_{n+1}, \boldsymbol{D}_{0,n+1}, \theta_{n+1}) - \frac{1}{2}\widehat{W}(\boldsymbol{C}_n, \boldsymbol{G}_n, C_n, \boldsymbol{D}_{0,n+1}, \theta_{n+1}) \\
&+ \frac{1}{2}\widehat{W}(\boldsymbol{C}_{n+1}, \boldsymbol{G}_{n+1}, C_{n+1}, \boldsymbol{D}_{0,n}, \theta_n) - \frac{1}{2}\widehat{W}(\boldsymbol{C}_{n+1}, \boldsymbol{G}_{n+1}, C_n, \boldsymbol{D}_{0,n}, \theta_n) \\
&+ \frac{1}{2}\widehat{W}(\boldsymbol{C}_n, \boldsymbol{G}_n, C_n, \boldsymbol{D}_{0,n+1}, \theta_{n+1}) - \frac{1}{2}\widehat{W}(\boldsymbol{C}_n, \boldsymbol{G}_n, C_n, \boldsymbol{D}_{0,n}, \theta_{n+1}) \\
&+ \frac{1}{2}\widehat{W}(\boldsymbol{C}_{n+1}, \boldsymbol{G}_{n+1}, C_{n+1}, \boldsymbol{D}_{0,n+1}, \theta_n) - \frac{1}{2}\widehat{W}(\boldsymbol{C}_{n+1}, \boldsymbol{G}_{n+1}, C_{n+1}, \boldsymbol{D}_{0,n}, \theta_n) \\
&+ \frac{1}{2}\widehat{W}(\boldsymbol{C}_n, \boldsymbol{G}_n, C_n, \boldsymbol{D}_{0,n}, \theta_{n+1}) - \frac{1}{2}\widehat{W}(\boldsymbol{C}_n, \boldsymbol{G}_n, C_n, \boldsymbol{D}_{0,n}, \theta_n) \\
&+ \frac{1}{2}\widehat{W}(\boldsymbol{C}_{n+1}, \boldsymbol{G}_{n+1}, C_{n+1}, \boldsymbol{D}_{0,n+1}, \theta_n) - \frac{1}{2}\widehat{W}(\boldsymbol{C}_{n+1}, \boldsymbol{G}_{n+1}, C_{n+1}, \boldsymbol{D}_{0,n+1}, \theta_n) \\
= &\Delta\widehat{W}.
\end{aligned} \tag{B.2}$$

Accordingly, as provided by the above equation the definition of the discrete derivatives satisfy the directionality property.

Appendix C. The discrete derivatives in the limit

The objective is to prove that the directional derivatives in equations (A.1) and (A.2) satisfy the second condition stated in (78). Accordingly we want to show that the directional derivatives are well defined in the limit $||\Delta\boldsymbol{C}|| \to 0$, $||\Delta\boldsymbol{G}|| \to 0$, $||\Delta C|| \to 0$, $||\Delta\boldsymbol{D}_0|| \to 0$ and $||\Delta\theta|| \to 0$. Accordingly, we show that the directional derivatives are well defined in the limit, such that

$$D_{\widehat{\mathcal{V}}_i}\widehat{W} = \partial_{\widehat{\mathcal{V}}_i}\widehat{W}\left(\widehat{\mathcal{V}}_{n+1/2}\right) + \sum_{i=1}^{5} O\left(||\Delta\widehat{\mathcal{V}}_i||^2\right) + \sum_{j=1,j\neq i}^{5}\sum_{k=j+1,k\neq 1}^{5} O\left(||\Delta\widehat{\mathcal{V}}_j||||\Delta\widehat{\mathcal{V}}_k||\right), \qquad \text{(C.1)}$$

In so doing, a Taylor series expansion is carried out for the four different evaluations of the internal energy $\widehat{W}$ in equation (A.3) around $\boldsymbol{C}_{n+1/2}$, which gives

$$
\begin{aligned}
\widehat{W}\left(\boldsymbol{C}_{n+1}, \widehat{\mathcal{V}}_{\boldsymbol{C}_{n+1}}\right) &= \widehat{W}\left(\boldsymbol{C}_{n+1/2}, \widehat{\mathcal{V}}_{\boldsymbol{C}_{n+1}}\right) + \partial_{\boldsymbol{C}}\widehat{W}\left(\boldsymbol{C}_{n+1/2}, \widehat{\mathcal{V}}_{\boldsymbol{C}_{n+1}}\right) : \left(\frac{1}{2}\Delta\boldsymbol{C}\right) \\
&\quad + \left(\frac{1}{2}\Delta\boldsymbol{C}\right) : \partial_{\boldsymbol{C}\boldsymbol{C}}^2\widehat{W}\left(\boldsymbol{C}_{n+1/2}, \widehat{\mathcal{V}}_{\boldsymbol{C}_{n+1}}\right) : \left(\frac{1}{2}\Delta\boldsymbol{C}\right) + O\left(||\Delta\boldsymbol{C}||^3\right); \\
\widehat{W}\left(\boldsymbol{C}_n, \widehat{\mathcal{V}}_{\boldsymbol{C}_{n+1}}\right) &= \widehat{W}\left(\boldsymbol{C}_{n+1/2}, \widehat{\mathcal{V}}_{\boldsymbol{C}_{n+1}}\right) - \partial_{\boldsymbol{C}}\widehat{W}\left(\boldsymbol{C}_{n+1/2}, \widehat{\mathcal{V}}_{\boldsymbol{C}_{n+1}}\right) : \left(\frac{1}{2}\Delta\boldsymbol{C}\right) \\
&\quad + \left(\frac{1}{2}\Delta\boldsymbol{C}\right) : \partial_{\boldsymbol{C}\boldsymbol{C}}^2\widehat{W}\left(\boldsymbol{C}_{n+1/2}, \widehat{\mathcal{V}}_{\boldsymbol{C}_{n+1}}\right) : \left(\frac{1}{2}\Delta\boldsymbol{C}\right) + O\left(||\Delta\boldsymbol{C}||^3\right); \\
\widehat{W}\left(\boldsymbol{C}_{n+1}, \widehat{\mathcal{V}}_{\boldsymbol{C}_n}\right) &= \widehat{W}\left(\boldsymbol{C}_{n+1/2}, \widehat{\mathcal{V}}_{\boldsymbol{C}_n}\right) + \partial_{\boldsymbol{C}}\widehat{W}\left(\boldsymbol{C}_{n+1/2}, \widehat{\mathcal{V}}_{\boldsymbol{C}_n}\right) : \left(\frac{1}{2}\Delta\boldsymbol{C}\right) \\
&\quad + \left(\frac{1}{2}\Delta\boldsymbol{C}\right) : \partial_{\boldsymbol{C}\boldsymbol{C}}^2\widehat{W}\left(\boldsymbol{C}_{n+1/2}, \widehat{\mathcal{V}}_{\boldsymbol{C}_n}\right) : \left(\frac{1}{2}\Delta\boldsymbol{C}\right) + O\left(||\Delta\boldsymbol{C}||^3\right); \\
\widehat{W}\left(\boldsymbol{C}_n, \widehat{\mathcal{V}}_{\boldsymbol{C}_n}\right) &= \widehat{W}\left(\boldsymbol{C}_{n+1/2}, \widehat{\mathcal{V}}_{\boldsymbol{C}_n}\right) - \partial_{\boldsymbol{C}}\widehat{W}\left(\boldsymbol{C}_{n+1/2}, \widehat{\mathcal{V}}_{\boldsymbol{C}_n}\right) : \left(\frac{1}{2}\Delta\boldsymbol{C}\right) \\
&\quad + \left(\frac{1}{2}\Delta\boldsymbol{C}\right) : \partial_{\boldsymbol{C}\boldsymbol{C}}^2\widehat{W}\left(\boldsymbol{C}_{n+1/2}, \widehat{\mathcal{V}}_{\boldsymbol{C}_n}\right) : \left(\frac{1}{2}\Delta\boldsymbol{C}\right) + O\left(||\Delta\boldsymbol{C}||^3\right).
\end{aligned}
\qquad \text{(C.2)}
$$

Inserting the above equations (C.2) in (A.3) yields

$$
\begin{aligned}
&\frac{1}{2}\frac{\widehat{W}\left(\boldsymbol{C}_{n+1}, \widehat{\mathcal{V}}_{\boldsymbol{C}_{n+1}}\right) - \widehat{W}\left(\boldsymbol{C}_n, \widehat{\mathcal{V}}_{\boldsymbol{C}_{n+1}}\right)}{||\Delta\boldsymbol{C}||^2}\Delta\boldsymbol{C} + \frac{1}{2}\frac{\widehat{W}\left(\boldsymbol{C}_{n+1}, \widehat{\mathcal{V}}_{\boldsymbol{C}_n}\right) - \widehat{W}\left(\boldsymbol{C}_n, \widehat{\mathcal{V}}_{\boldsymbol{C}_n}\right)}{||\Delta\boldsymbol{C}||^2}\Delta\boldsymbol{C} \\
&\quad - \frac{1}{2}\frac{\partial_{\boldsymbol{C}}\widehat{W}\left(\boldsymbol{C}_{n+1/2}, \widehat{\mathcal{V}}_{\boldsymbol{C}_{n+1}}\right) : \Delta\boldsymbol{C}}{||\Delta\boldsymbol{C}||^2}\Delta\boldsymbol{C} - \frac{1}{2}\frac{\partial_{\boldsymbol{C}}\widehat{W}\left(\boldsymbol{C}_{n+1/2}, \widehat{\mathcal{V}}_{\boldsymbol{C}_n}\right) : \Delta\boldsymbol{C}}{||\Delta\boldsymbol{C}||^2}\Delta\boldsymbol{C} = O\left(||\Delta\boldsymbol{C}||^2\right).
\end{aligned}
\qquad \text{(C.3)}
$$

Introduction of the result in (C.3) into the expression for the directional derivative $D_{\boldsymbol{C}}\widehat{W}$ in (A.5) leads to

$$D_{\boldsymbol{C}}\widehat{W} = \frac{1}{2}\left(\partial_{\boldsymbol{C}}\widehat{W}\left(\boldsymbol{C}_{n+1/2}, \widehat{\mathcal{V}}_{\boldsymbol{C}_{n+1}}\right) + \partial_{\boldsymbol{C}}\widehat{W}\left(\boldsymbol{C}_{n+1/2}, \widehat{\mathcal{V}}_{\boldsymbol{C}_n}\right)\right) + O\left(||\Delta\boldsymbol{C}||^2\right). \qquad \text{(C.4)}$$

For the two first terms on the right-hand side of the above equation (C.4) a Taylor series expansion

is developed which yields

$$
\begin{aligned}
\partial_{\boldsymbol{C}}\widehat{W}\left(\boldsymbol{C}_{n+1/2},\widehat{\mathcal{V}}_{\boldsymbol{C}_{n+1}}\right) = {} & \partial_{\boldsymbol{C}}\widehat{W}\left(\boldsymbol{C}_{n+1/2},\widehat{\mathcal{V}}_{\boldsymbol{C}_{n+1/2}}\right) \\
& + \partial_{\boldsymbol{CG}}^{2}\widehat{W}\left(\boldsymbol{C}_{n+1/2},\widehat{\mathcal{V}}_{\boldsymbol{C}_{n+1/2}}\right):\left(\frac{1}{2}\Delta\boldsymbol{G}\right) \\
& + \partial_{\boldsymbol{CC}}^{2}\widehat{W}\left(\boldsymbol{C}_{n+1/2},\widehat{\mathcal{V}}_{\boldsymbol{C}_{n+1/2}}\right)\left(\frac{1}{2}\Delta C\right) \\
& + \partial_{\boldsymbol{CD}_{0}}^{2}\widehat{W}\left(\boldsymbol{C}_{n+1/2},\widehat{\mathcal{V}}_{\boldsymbol{C}_{n+1/2}}\right):\left(\frac{1}{2}\Delta\boldsymbol{D}_{0}\right) \\
& + \partial_{\boldsymbol{C\theta}}^{2}\widehat{W}\left(\boldsymbol{C}_{n+1/2},\widehat{\mathcal{V}}_{\boldsymbol{C}_{n+1/2}}\right):\left(\frac{1}{2}\Delta\theta\right) \\
& + O\left(||\Delta\boldsymbol{G}||^{2}\right) + O\left(\Delta C^{2}\right) + O\left(||\Delta\boldsymbol{D}_{0}||^{2}\right) + O\left(\Delta\theta^{2}\right) \\
& + O\left(||\Delta\boldsymbol{G}||\Delta C\right) + O\left(||\Delta\boldsymbol{G}||||\Delta\boldsymbol{D}_{0}||\right) + O\left(||\Delta\boldsymbol{G}||\Delta\theta\right) \\
& + O\left(||\Delta C||||\Delta\boldsymbol{D}_{0}||\right) + O\left(\Delta C||\Delta\theta||\right) + O\left(||\Delta\boldsymbol{D}_{0}||\Delta\theta\right);; \\
\partial_{\boldsymbol{C}}\widehat{W}\left(\boldsymbol{C}_{n+1/2},\widehat{\mathcal{V}}_{\boldsymbol{C}_{n}}\right) = {} & \partial_{\boldsymbol{C}}\widehat{W}\left(\boldsymbol{C}_{n+1/2},\widehat{\mathcal{V}}_{\boldsymbol{C}_{n+1/2}}\right) \\
& - \partial_{\boldsymbol{CG}}^{2}\widehat{W}\left(\boldsymbol{C}_{n+1/2},\widehat{\mathcal{V}}_{\boldsymbol{C}_{n+1/2}}\right):\left(\frac{1}{2}\Delta\boldsymbol{G}\right) \\
& - \partial_{\boldsymbol{CC}}^{2}\widehat{W}\left(\boldsymbol{C}_{n+1/2},\widehat{\mathcal{V}}_{\boldsymbol{C}_{n+1/2}}\right)\left(\frac{1}{2}\Delta C\right) \\
& - \partial_{\boldsymbol{CD}_{0}}^{2}\widehat{W}\left(\boldsymbol{C}_{n+1/2},\widehat{\mathcal{V}}_{\boldsymbol{C}_{n+1/2}}\right):\left(\frac{1}{2}\Delta\boldsymbol{D}_{0}\right) \\
& - \partial_{\boldsymbol{C\theta}}^{2}\widehat{W}\left(\boldsymbol{C}_{n+1/2},\widehat{\mathcal{V}}_{\boldsymbol{C}_{n+1/2}}\right):\left(\frac{1}{2}\Delta\theta\right) \\
& + O\left(||\Delta\boldsymbol{G}||^{2}\right) + O\left(\Delta C^{2}\right) + O\left(||\Delta\boldsymbol{D}_{0}||^{2}\right) + O\left(\Delta\theta^{2}\right) \\
& + O\left(||\Delta\boldsymbol{G}||\Delta C\right) + O\left(||\Delta\boldsymbol{G}||||\Delta\boldsymbol{D}_{0}||\right) + O\left(||\Delta\boldsymbol{G}||\Delta\theta\right) \\
& + O\left(||\Delta C||||\Delta\boldsymbol{D}_{0}||\right) + O\left(\Delta C||\Delta\theta||\right) + O\left(||\Delta\boldsymbol{D}_{0}||\Delta\theta\right).
\end{aligned}
\tag{C.5}
$$

Inserting (C.5) into (C.4) yields the desired result

$$
\begin{aligned}
D_{\boldsymbol{C}}\widehat{W} = {} & \partial_{\boldsymbol{C}}\widehat{W}\left(\boldsymbol{C}_{n+1/2},\widehat{\mathcal{V}}_{\boldsymbol{C}_{n+1/2}}\right) \\
& + + O\left(||\Delta\boldsymbol{G}||^{2}\right) + O\left(\Delta C^{2}\right) + O\left(||\Delta\boldsymbol{D}_{0}||^{2}\right) + O\left(\Delta\theta^{2}\right) \\
& + O\left(||\Delta\boldsymbol{G}||\Delta C\right) + O\left(||\Delta\boldsymbol{G}||||\Delta\boldsymbol{D}_{0}||\right) + O\left(||\Delta\boldsymbol{G}||\Delta\theta\right) \\
& + O\left(||\Delta C||||\Delta\boldsymbol{D}_{0}||\right) + O\left(\Delta C||\Delta\theta||\right) + O\left(||\Delta\boldsymbol{D}_{0}||\Delta\theta\right),
\end{aligned}
\tag{C.6}
$$

An analogous result is obtained for the remaining discrete derivatives $\{D_{\boldsymbol{G}}\widehat{W}, D_{C}\widehat{W}, D_{\boldsymbol{D}_{0}}\widehat{W}, D_{\theta}\widehat{W}\}$.

References

[1] J. M. Ball. Convexity conditions and existence theorems in nonlinear elasticity. *Archive for Rational Mechanics and Analysis*, 63(4):337–403, 1976.

[2] J. M. Ball. Energy-minimising configurations in nonlinear elasticity. *Archive for Rational Mechanics and Analysis*, 63(4):337–403, 1976.

[3] J. M. Ball. *Geometry, Mechanics and Dynamics*, chapter Some open problems in Elasticity, pages 3–59. Springer, 2002.

[4] J. M. Ball and F. Murat. $W^{1,p}$-quasiconvexity and variational problems for multiple integrals. *Journal of Functional Analysis*, 58(3):225–253, 1984.

[5] K. Bertoldi and M. Gei. Instabilities in multilayered soft dielectrics. *Journal of the Mechanics and Physics of Solids*, 59(1):18–42, 2011.

[6] P. Betsch and A. Janz. An energy-momentum consistent method for transient simulations with mixed finite elements developed in the framework of geometrically exact shells. *Int. J. Numer. Meth. Engng*, 108(5):423–455, 2016.

[7] Peter Betsch, Alexander Janz, and Christian Hesch. A mixed variational framework for the design of energy–momentum schemes inspired by the structure of polyconvex stored energy functions. *Computer Methods in Applied Mechanics and Engineering*, 335:660–696, 2018.

[8] J. Bonet, A. J. Gil, C. H. Lee, M. Aguirre, and R. Ortigosa. A first order hyperbolic framework for large strain computational solid dynamics - Part I: Total Lagrangian isothermal elasticity. *Computer Methods in Applied Mechanics and Engineering*, 283(0):689–732, 2015.

[9] J. Bonet, A. J. Gil, and R. Ortigosa. A computational framework for polyconvex large strain elasticity. *Computer Methods in Applied Mechanics and Engineering*, 283:1061–1094, 2015.

[10] J. Bonet, A. J. Gil, and R. Ortigosa. On a tensor cross product based formulation of large strain solid mechanics. *International Journal of Solids and Structures*, 84:49–63, 2016.

[11] Javier Bonet, Chun Hean Lee, Antonio J. Gil, and Ataollah Ghavamian. A first order hyperbolic framework for large strain computational solid dynamics. Part III: Thermo-elasticity. *Computer Methods in Applied Mechanics and Engineering*, 373:113505, 2021.

[12] F. Brezzi and M. Fortin. *Mixed and Hybrid Finite Element Methods*. Springer-Verlag New York, Inc., New York, NY, USA, 1991.

[13] R. Bustamante, A. Dorfmann, and R.W. Ogden. On electric body forces and Maxwell stresses in nonlinearly electroelastic solids. *International Journal of Engineering Science*, 47(11-12):1131–1141, 2009.

[14] R. de Boer. *Vektor- und Tensorrechnung für Ingenieure*. Springer-Verlag, 1982.

[15] A. Dorfmann and R. W. Ogden. Nonlinear electroelasticity. *Acta Mechanica*, 174(3-4):167–183, 2005.

[16] M. Franke, A. Janz, M. Schiebl, and P. Betsch. An energy momentum consistent integration scheme using a polyconvexity-based framework for nonlinear thermo-elastodynamics. *International Journal for Numerical Methods in Engineering*, 115(5):549–577, 2018.

[17] M. Franke, R. Ortigosa, A. Janz, A.J. Gil, and P. Betsch. A mixed variational framework for the design of energy–momentum integration schemes based on convex multi-variable electro-elastodynamics. *Computer Methods in Applied Mechanics and Engineering*, 351:109–152, 2019.

[18] A. Ghavamian, C. H. Lee, A. J. Gil, J. Bonet, T. Heuzé, and L. Stainier. An entropy-stable smooth particle hydrodynamics algorithm for large strain thermo-elasticity. *Computer Methods in Applied Mechanics and Engineering*, 379:113736, 2021.

[19] A. J. Gil and R. Ortigosa. A new framework for large strain electromechanics based on convex multi-variable strain energies: variational formulation and material characterisation. *Computer Methods in Applied Mechanics and Engineering*, 302:293–328, 2016.

[20] O. Gonzalez. Exact energy and momentum conserving algorithms for general models in nonlinear elasticity. *Comput. Methods Appl. Mech. Engrg.*, 190:1763–1783, 2000.

[21] M. Groß and P. Betsch. Energy-momentum consistent finite element discretization of dynamic finite viscoelasticity. *Int. J. Numer. Meth. Engng*, 81(11):1341–1386, 2010.

[22] G. Kofod, P. Sommer-Larsen, R. Kornbluh, and R. Pelrine. Actuation response of polyacrylate dielectric elastomers. *Journal of Intelligent Material Systems and Structures*, 14(12):787–793, 2003.

[23] T. Li, C. Keplinger, R. Baumgartner, S. Bauer, W. Yang, and Z. Suo. Giant voltage-induced deformation in dielectric elastomers near the verge of snap-through instability. *Journal of the Mechanics and Physics of Solids*, 61(2):611–628, 2013.

[24] J. E. Marsden and T. J. R. Hughes. *Mathematical foundations of elasticity*. 1994.

[25] S. C. Martín and J. C. García Orden. On energy-entropy-momentum integration methods for discrete thermo-visco-elastodynamics. *Computers & Structures*, 181:3–20, 2017. UK Association of Computational Mechanics.

[26] M. Mehnert, M. Hossain, and P. Steinmann. Numerical modeling of thermo-electro-viscoelasticity with field-dependent material parameters. *International Journal of Non-Linear Mechanics*, 106:13–24, 2018.

[27] Markus Mehnert, Mokarram Hossain, and Paul Steinmann. A complete thermo-electro-viscoelastic characterization of dielectric elastomers -part ii: Continuum modelling approach. *Journal of the Mechanics and Physics of Solids*, 08 2021.

[28] C. Miehe, D. Vallicotti, and S. Teichtmeister. Homogenization and multiscale stability analysis in finite magneto-electro-elasticity. application to soft matter ee, me and mee composites. *Computer Methods in Applied Mechanics and Engineering*, 300:294–346, 2016.

[29] R. Ortigosa, M. Franke, A. Janz, A.J. Gil, and P. Betsch. An energy–momentum time integration scheme based on a convex multi-variable framework for non-linear electro-elastodynamics. *Computer Methods in Applied Mechanics and Engineering*, 339:1–35, 2018.

[30] R. Ortigosa and A. J. Gil. A new framework for large strain electromechanics based on convex multi-variable strain energies: Conservation laws, hyperbolicity and extension to electro-magneto-mechanics. *Computer Methods in Applied Mechanics and Engineering*, 309:202–242, 2016.

[31] R. Ortigosa and A. J. Gil. A new framework for large strain electromechanics based on convex multi-variable strain energies: Finite element discretisation and computational implementation. *Computer Methods in Applied Mechanics and Engineering*, 302:329–360, 2016.

[32] R. Ortigosa, A.J. Gil, J. Martínez-Frutos, M. Franke, and J. Bonet. A new energy–momentum time integration scheme for non-linear thermo-mechanics. *Computer Methods in Applied Mechanics and Engineering*, 372:113395, 2020.

[33] R. Pelrine, R. Kornbluh, Q. Pei, and J. Joseph. High-speed electrically actuated elastomers with strain greater than 100 %. *Science*, 287(5454):836–839, 2000.

[34] R. E. Pelrine, R. D. Kornbluh, and J. P. Joseph. Electrostriction of polymer dielectrics with compliant electrodes as a means of actuation. *Sensors and Actuators A: Physical*, 64(1):77–85, 1998.

[35] I. Romero. An analysis of the stress formula for energy-momentum methods in nonlinear elastodynamics. *Computational Mechanics*, 50(5):603–610, Nov 2012.

[36] M. Schiebl and I. Romero. Energy-momentum conserving integration schemes for molecular dynamics. *Computational Mechanics*, 67(3):915–935, 2021.

[37] J. Schröder. Anisotropic polyconvex energies. In J. Schröder and P. Neff, editors, *Poly-, quasi- and rank-one convexity in Applied Mechanics, volume 516 of CISM Courses and Lectures*, volume 516 of CISM Courses and Lectures, pages 53–105. Springer-Verlag, 2010.

[38] J. Schröder, P. Neff, and D. Balzani. A variational approach for materially stable anisotropic hyperelasticity. *International Journal of Solids and Structures*, 42:4352–4371, 2005.

[39] M. Shilhavy. *The Mechanics and Thermodynamics of Continuous Media.* Springer-Verlag Berlin Heidelberg, 1982.

[40] J. C. Simo and N. Tarnow. The discrete energy-momentum method. Conserving algorithms for nonlinear elastodynamics. *Zeitschrift für angewandte Mathematik und Physik ZAMP*, 43(5):757–792, Sep 1992.

[41] S. Skatulla, C. Sansour, and A. Arockiarajan. A multiplicative approach for nonlinear electro-elasticity. *Computer Methods in Applied Mechanics and Engineering*, 245-246(0):243–255, 2012.

[42] R. Vertechy, G. Berselli, V. P. Castelli, and M. Bergamasco. Continuum thermo-electro-mechanical model for electrostrictive elastomers. *Journal of Intelligent Material Systems and Structures*, 24(6):761–778, 2013.

[43] N. Viebahn, P.M. Pimenta, and J. Schröder. A simple triangular finite element for nonlinear thin shells: statics, dynamics and anisotropy. *Computational Mechanics*, 59(2):281–297, 2017.

[44] D. K. Vu and P. Steinmann. A 2-D coupled BEM-FEM simulation of electro-elastostatics at large strain. *Computer Methods in Applied Mechanics and Engineering*, 199(17-20):1124–1133, 2010.

[45] D. K. Vu and P. Steinmann. On 3-D coupled BEM-FEM simulation of nonlinear electro-elastostatics. *Computer Methods in Applied Mechanics and Engineering*, 201-204(0):82–90, 2012.

[46] D. K. Vu, P. Steinmann, and G. Possart. Numerical modelling of non-linear electroelasticity. *International Journal for Numerical Methods in Engineering*, 70(6):685–704, 2007.